ParisTech
INSTITUT DES SCIENCES ET TECHNOLOGIES
PARIS INSTITUTE OF TECHNOLOGY

AgroParisTech
INSTITUT DES SCIENCES ET INDUSTRIES DU VIVANT ET DE L'ENVIRONNEMENT
PARIS INSTITUTE OF TECHNOLOGY FOR LIFE, FOOD AND ENVIRONMENTAL SCIENCES

Ecole Doctorale SIBAGHE

Doctorat ParisTech

THÈSE

pour obtenir le grade de docteur délivré par

L'Institut des Sciences et Industries du Vivant et de l'Environnement

(AgroParisTech)

Spécialité : Eaux Continentales et Société

présentée et soutenue publiquement par

Rouba Ziade

le 30 septembre, 2014

L'impact potentiel des incendies de forêt sur l'apparition de mouvements en masse dans le bassin versant de Damour sous variations climatiques et changement d'utilisation des sols

Directeur de thèse : Nicolas BAGHDADI
Co-Directeur de thèse : Chadi ABDALLAH

Jury

M. Jean CHOROWICZ, Professeur Emerite, Pierre and Marie Curie University - Paris 6	Rapporteur
M. Philip ROCHE, Directeur de recherche, IRSTEA	Rapporteur
M. Jean-Paul DEROIN, Professeur, Université de Reims Champagne-Ardenne	Examinateur
M. Olivier CERDAN, Directeur de recherche, BRGM	Examinateur
M. Nicolas BAGHDADI, Directeur de recherche, IRSTEA	Directeur de thèse
M. Chadi ABDALLAH, Directeur de recherche, CNRS Liban	Co-Directeur de thèse
M. Pierre-Yves VION, AgroParisTech, Representant de l'ED	Invité

ACKNOWLEGMENTS

First of all, I am grateful for my family who has put up with me for last four years especially my husband Georges.

I wish to express my thanks to Dr. Nicolas Baghdadi for welcoming me in the Maison de la Teledetection in Montpellier and providing me with all the necessary facilities during my stay there as a student in co-advisory.

I place on record my gratitude to Dr. Chadi Abdallah for signing me up for this PhD and for his assistance and guidance throughout this thesis.

I would also like to thank the members of my steering committees (Dr. Dr. Jean-Stéphane Bailly, Dr. Frederic Berger, Dr. Olivier Cerdan, Dr. Yves Lebissonet, Dr. Roger Moussa) for their constructive remarks and suggestions.

And to Mr. Pierre-Yves Vion, thank you for the help in all the administrative paperwork and processes, your assistance was very indispensable.

DEDICATION

I dedicate this thesis to my daughter Yasmine and my husband Georges. May this thesis be a new start for us.

Résumé de thèse en Français

Les Mouvements en Masse (MM) présentent un risque naturel majeur menaçant les milieux naturels et humains au Liban. Survenant sous diverses formes et requérant un large éventail de techniques de télédétection, de modélisation et de zonage pour leur analyse et suivi, l'occurrence des MM est surtout influencée par des facteurs de pré-conditionnement et induisant tels que les incendies de forêt (IF) qui ont dû contribuer à la destruction de plus de 22% des forêts du Liban en moins de 50 ans. Cette thèse étudie l'impact des IF sur l'occurrence des MM dans un contexte de changement climatique et de conversion accrue des modes d'occupation des sols. Après la normalisation des facteurs de pré-conditionnement, la gravité des brûlures des IF est représentée par le Rapport de Brulure Normalisé (RBN) à l'aide du système d'information géographique (SIG). Le facteur de pondération (FP) de chaque couche est évalué en utilisant la méthode InfoVal modifiée. Une Carte de Susceptibilité aux MM (CSMM) est générée et validée par un groupe indépendant de MM. Précédé seulement par le type de sol, la gravité des brûlures des IF a obtenu le deuxième plus haut FP. Une enquête plus approfondie sur les facteurs de génération des IF a aussi été réalisée. Les facteurs climatiques provoquant la prolongation de la sécheresse ont été analysés à travers de l'Index de Reconnaissance de de Sécheresse (IRS), et l'utilisation des sols a été évaluée via l'Indice de Végétation Normalisée par Différence (IVND). Les associations entre RBN et IRS et RBN et IVND indiquent que le RNB est le résultat de l'interaction entre le climat et l'utilisation des sols.

Titre de la Thèse en Anglais

The potential impact of Forest Fire on the occurrence of Mass Movements in Damour watershed under climatic variations and land-use change

Résumé de thèse en Anglais

Mass movement (MM) is a major natural hazard that threatens natural and human environments in Lebanon. It comes under various forms needing a wide range of MM detection, modeling and zoning techniques. MM occurrence is influenced by preconditioning factors and inducing factors such as forest fires. Since the latter has emerged as another hazard destroying over 22% of Lebanon's forests in less than 50 years, this thesis investigates impact of forest fire on MM occurrence under climatic variations and land-use change. Following the standardization of the preconditioning factors in addition to the forest fire burn severity out of the Normalized Burn Ratio (NBR) into layers using geographic information systems (GIS), the Weight factor (Wf) of each was evaluated using the modified InfoVal method. A MM susceptibility map (MMSM) was

generated and validated by an independent set of MM. Preceded only by soil type; forest fire burn severity obtained the second-highest Wf. Further investigation into forest fire generating factors was performed. Climatic factors causing prolonged droughts were observed using a meteorological Reconnaissance Drought Index (RDI) and land-use was assessed using Normalized Difference Vegetation index (NDVI) .The associations between NBR and RDI and NBR and NDVI indicate that NBR is a result of the interaction between climate and land-use.

Abstract

Mass movements such as landslides, earth flows, block falls and erosion are among the most invasive hazards in the Mediterranean basin, causing surface instability favorable to land degradation threatening the natural and human environments. In Lebanon, the occurrence of MM has increased by almost 60% between 1956- 2008. Similarly, forest fire has emerged as another hazard and has destroyed over 25% of Lebanon's forests in less than 40 years. Although both hazards affect vast areas of the Lebanese territories, the impact of forest fire on MM occurrence has not been studied yet and corresponding MM susceptibility maps are still lacking. This research deals with the use of remote sensing and GIS in assessing the impact of Forest fire burn severity on MM occurrence in Damour watershed.

In this context, the first part reviews existing knowledge on the topic of MM and defines research gaps. It displays MM classifications, preconditioning and inducing factors and their corresponding impact on MM. Furthermore, the efficiency of land stability detection and zonation remote sensing methods were compared pointing out possible ways of research

The second part studies in depth the study area of Damour watershed. Geomorphology, geology, soil and land use characteristics were explained as well as natural hazards that are already occurring in the study area. The study area, extending from the Mediterranean coast to around 2000m of elevation covering almost 3.7% of the total area of Lebanon.

The third part investigates the potential effect of forest fire on the occurrence of mass movement in the Damour watershed. Mass movement and forest fire inventory maps were produced through remote sensing (RS) using aerial and satellite images. Forest fire was introduced as the inducing factor whose effect was extracted from Landsat images through the normalized burn ratio (NBR) index. A field study was conducted to substantiate the mass movement inventory and Normalized Burn Ratio maps. Following the standaRDIstzation of the effect factors into layers using geographic information systems (GIS), the weight factor of each layer for inducing mass movement was evaluated using the modified InfoVal method, and an mass movement susceptibility map (MMSM) was generated. Preceded only by changes in land use, the NBR obtained the highest weight, making forest fire burn severity the second-highest impacting factor on mass movement occurrence in the study areas.

The fourth part is dedicated to conclude whether forest fire burn severity; one of the main MM occurrence inducing factors, is driven by climatic variations or land use changes. Climatic factors causing prolonged droughts are observed using the Standardized Reconnaissance Drought Index

(RDI_{st}). On the other hand, understanding the role of land use in shaping wildfire regimes was achieved using Normalized Difference Vegetation Index (NDVI). The spatiotemporal changes in forest fire burn severity tracing the yearly burned severity patterns was compared with corresponding climatic and land use patterns respectively in order to establish a individual correlations. It was synthesized that the association indicates that climatic variables and anthropogenic factors simultaneously affect forest fire burn severity rather than it being the product of a sole factor.

The fifth part displays a general conclusion of the research findings in addition to stating the study setbacks which can be furetheron addressed to enhance results accuracy. Furthermore, recommendations for MM and forest fire adaptive measurements have been suggested in oreder to improve study area resilience to these destructive natural hazards .

Keywords: Mass Movement (MM), Forest fire, LANDSAT satellite images, Normalized Burn Ratio (NBR), Information Value Method (InfoVal), Mass Movement Susceptibility Map (MMSM), Standardized Reconnaissance drought Index (RDI_{st}), Normalized Difference Vegetation Index (NDVI).

Résumé

Les mouvements en masse (MM) tels que les glissements de terrain, coulées de boue, chutes de blocs et érosion du sol sont parmi les dangers les plus répandus dans le bassin méditerranéen, entraînant une instabilité de surface favorable à la dégradation des sols et menaçant les environnements naturels et humains. Au Liban, la fréquence des MM a augmenté de près de 60% entre 1956 et 2008 engendrant entre autre des incendies de forêts (IF) - danger supplémentaire qui a dû détruire plus de 25% des forêts du Liban en moins de 40 ans. Bien que les deux risques affectent de vastes zones du territoire Libanais, l'impact des IF sur l'occurrence des MM n'a pas encore été analysé préalablement et les cartes de sensibilité aux MM demeurent toujours en défaut. Cette recherche utilise la télédétection et les techniques de système d'information géographique (SIG) dans l'évaluation de l'impact de la gravité des brûlures des IF sur la fréquence des MM dans le bassin versant du Damour.

Dans ce contexte, la première partie passe en revue sur les connaissances actuelles autour du sujet de MM et identifie les lacunes de la recherche. Elle définit les classifications des MM, leurs facteurs de pré-conditionnant et induisant, et leur impact sur les MM. En outre, l'efficacité de détection de la stabilité des sols et le zonage des méthodes de télédétection sont comparées, indiquant les voies possibles de recherche.

La deuxième partie évalue en profondeur les caractéristiques de la géomorphologie, la géologie, et l'utilisation des sols de la zone d'étude. Les catastrophes naturelles qui se produisent dans la zone d'étude qui s'étend de la côte méditerranéenne à environ 2000 m d'altitude couvrant près de 3,7% de la superficie totale du Liban sont aussi expliquées.

La troisième partie examine l'effet potentiel des incendies de forêt sur la fréquence des MM. Une carte d'inventaire des MM et des incendies de forêt sont produites par télédétection (RS) en utilisant des images satellitaires et aériennes. Les IF sont présentés comme facteur induisant dont l'effet a été extrait à partir d'images Landsat par le Rapport de Brûlure Normalisée (RBN). Une étude de terrain est menée à l'appui de cartes d'inventaires de MM et RBN. Après la normalisation des facteurs pré-conditionnant et induisant en couches à l'aide du SIG, le facteur de pondération (FP) de chaque couche pour induire un MM a été évalué en utilisant la méthode InfoVal modifié, et une Carte de Sensibilité de MM (CSMM) est générée. Précédé seulement par des changements du type de sol; la RBN a obtenu le deuxième plus haut FP qui impacte l'apparition de MM dans la zone d'étude.

La quatrième partie est consacrée à déterminer si la gravité des brûlures des incendies de forêt, l'un des principaux facteurs induisant l'occurrence MM, est entraînée par les variations

climatiques ou le changement des modes d'utilisation des sols. Les facteurs climatiques qui provoquent la prolongation de la sécheresse sont observés en utilisant l'Indice de Reconnaissance météorologique de Sécheresse (IRS). D'autre part, la compréhension du rôle de l'utilisation des sols dans l'élaboration des régimes des IF est réalisée via l'Indice Normalisée de Végétation par Différence (INVD). Les changements spatio-temporels dans la gravité des brûlures des IF retraçant les motifs de gravité de brulure annuelle ont été comparés respectivement avec les modèles du climat et d'utilisation des sols afin d'établir des corrélations individuelles. La gravité des brûlures des IF est jusqu'à présent impactée par l'interaction entre le climat et l'utilisation des terres, plutôt qu'elle soit la conséquence d'un seul facteur.

La cinquième partie présente une conclusion générale des résultats de la recherche en indiquant les perspectives et les revers de l'étude qui peuvent encore être traités pour améliorer la précision des résultats. Des recommandations pour les mesures d'adaptation aux MM et IF sont proposées afin d'améliorer la résilience de la zone d'étude à ces risques naturels destructeurs.

Mots-Clés: **Mouvements en Masse (MM), Incendie de Forêt (IF), Images satellite Landsat, Rapport de Brûlure Normalisée (RBN), InfoVal, Carte de Sensibilité de mouvement de masse (CSMM), l'Indice de Reconnaissance de Sécheresse (IRS), l'Indice Normalisée de Végétation par Différence (INVD).**

Table of Contents

List of Tables 13

List of Figures 14

List of Annexes 16

GENERAL INTRODUCTION 17

CHAPTER 1 A review of Mass Movement Classification, Detection and Susceptibility Analysis 20

1.1 Introduction to Mass Movement 20

1.2 Mass Movement Classification 21

1.2.1 Falls 24

1.2.2 Slides 24

1.2.3 Flows 25

1.3 Factors Influencing the Occurrence of Mass Movement 26

1.3.1 Preconditioning Factors 26

1.3.1.1 Topography 26

1.3.1.2 Lithology 27

1.3.1.3 Soil 27

1.3.1.4 Land use 28

1.3.2 Inducing Factors 28

1.3.2.1 Neotectonics 28

1.3.2.2 Intensity Rainfall 29

1.3.2.3 Forest fires 30

1.3.2.4 Manmade excavation, road construction, unplanned urbanism 31

1.3.2.5 Climatic Variations 31

Temperature 32

Precipitation 32

1.4 Land Instability Detection and Zonation Methods and Techniques 33

1.4.1 Geotechnical Methods 34

1.4.2 Remote Sensing in MM interpretation and analysis 35
1.4.2.1 Aerial photography 35
1.4.2.2 Optical Satellite Imagery 36
Automatic and Semi Automatic Methods 37
1.4.2.3 RADAR Satellite Imagery 38
1.4.2.4 LiDAR 39
1.5 Guidelines for Mass Movement Zoning and Mapping 41
1.6 Mass Movement Susceptibility Assessment Methods and Mapping 43
CHAPTER 2 Detailed Description of the Study Area 48
2.1 Geographic Location 48
2.2 Geomorphology 50
2.3 Geology 50
2.4 Soils 53
2.5 Land use 54
2.6 Climate 55
CHAPTER 3 Analysis of the potential effect of Forest fire on Mass Movement in the study area 59
3.1 Introduction 59
3.2 Mass Movement Inventory Map Production 60
3.2.1 Visual Interpretation of Mass Movement and Forest Fire Mapping 60
3.3 Burn Severity Estimation Using Remotely Sensed Data 65
3.3.1 Gap-Filling LANDSAT 7 SLC-off Single Scenes 67
3.3.2 Radiometric Calibration of LANDSAT images 68
3.3.3 Change detection of Normalized Burn Ratio Maps 71
3.3.4 Cumulative NBR map 72
3.4 Mass Movement Field Investigation 72
3.5 Forest Fire Burn Severity Field Investigation 74
3.5.1 The Mini-Disk Infiltrometer (MDI) 74
3.6 Selection and Acquisition of Thematic Database Using GIS 77

3.7 Statistical Correlation Using Information Value Method (InfoVal) 79
3.8 Mass Movement Susceptibility Assessment and Validation of Result 81
3.8.1 Establishing relationship between impacting factors and Mass Movement 81
3.8.1.1 Rock Type 81
3.8.1.2 Soil 81
3.8.1.3 Land use 82
3.8.1.4 Slope Aspect 82
3.8.1.5 Slope Degree 82
3.8.1.6 Mean Annual Precipitation (MAP) 83
3.8.1.7 Normalized Burn Ratio 83
3.9 Soil Water Repellency Status by Means of Infiltration Rate 84
3.10 Mass Movement Susceptibility Map and Model Validation 85
3.11 Major constraints in Evaluation Mass Movement Susceptibility Maps 91
CHAPTER 4 Comparative correlation of Forest Fire burn severity with climatic fluctuations and land use change 93
4.1 Introduction 93
4.2 Climatic variability Detection Utilizing Evpotranspiration and Drought Indices 96
4.2.1 Potential Evapotranspiration 96
4.2.2 Drought Indices 97
4.3 Evaluating Land Use Change Using Normalized Difference Vegetation Index 99
4.3.1 Drought as a major Forest Fire driver 100
4.3.2 Monitoring land use variation using NDVI 103
4.3.3 Analysis results of forest fire burn severity variation through Normalized burn ratio 106
4.4 Correlation between Forest fire burn severity and impacting factors 108
Conclusion 112
References 116
ANNEX 161

List of Tables

Chapter 1: A review of Mass Movement Classification, Detection and Susceptibility Analysis

Table 1.1 Classification of most common mass movements in the Mediterranean

Table 1.2 Type and quantity of MM occurring in selected regions of the Mediterranean area over the last two decades

Table 1.3 Overview of techniques for the collection of MM information H= Highly Relevance; M=Medium Relevance; L= Low Relevance)

Chapter 3: Analysis of the potential effect of Forest fire on Mass Movement in the study area

Table 3.1 Number and percentage of Mass Movement delineated between 1956 and 2012

Table 3.2 Aerial and satellite images that were used in the process of mass movement (MM) and forest fire (FF) detection and delineation for GIS database compilation.

Table 3.3 Mini-Disk infiltrometer (MDI) test values interpretation as suggested by the field guide for mapping post-fire soil burn severity which was developed by Parsons et al 2010 for the United States Department of Agriculture (USDA)-Forest Service reference

Table 3.4 Environmental attributes used for the preparation of mass movement susceptibility zonation

Table 3.5 Weight of each parameter defining its contribution to mass movement occurrence in our study areas as well as the percentage of impact of each parameter on the Mass Movement Susceptibility Map (MMSM) Damour (D)

Table 3.6 Highlighting the impact of Normalized burn ratio (NBR) on the mass movement susceptibity map through demonstrating the shift in area distribution of the susceptibility classes when NBR was induced and deduced from the (MMSM) equation

Chapter 4: Comparative correlation of Forest Fire burn severity with climatic fluctuations and land use change

Table 4.1 Standardized Reconnaissance Drought Index (RDIst) values which are similar to SPI Values

Table 4.2 Comparison of Land cover maps of 1984 and 2012

List of Figures

Chapter 1: A review of Mass Movement Classification, Detection and Susceptibility Analysis

Figure 1.1 Movement and material type as classified by Cruden & Varnes (1996)

Chapter 2: Detailed Description of Study Area

Figure 2.1 Study Area and its geomorphologic unit

Figure 2.2 Simplified Geologic Map of the study area

Figure 2.3 Soil Map of the study area

Figure 2.4 Land use map of the study area based on CORINE classification of Level 1 description

Figure 2.5 Rainfall map of the study area

Figure 2.6 Average Monthly Temperature of Damour Watershed for the years 1984-2012

Figure 2.7 Average Monthly Precipitation of Damour Watershed for the years 1984-2012

Chapter 3: Analysis of the potential effect of Forest fire on Mass Movement in the study area

Figure 3.1 Orthorectification of Aerial Photos using ERDAS LPS

Figure 3.2 Mass Movement delineation using IKONOS satellite images

Figure 3.3 Google Earth 3D terrain for enhanced visual interpretation of Mass Movement

Figure 3.4 Damour Watershed pre gap filling (a) and post gap filling (b) LANDSAT image

Figure 3.5 Comparison of pixel mean distribution and standard deviation of pre and post gap filling

Figure 3.6 Normalized burn ratio (NBR) variation maps in Damour watershed showing the progression of burn severity from 1986-2012

Figure 3.7 Mass Movement inventory field investigation

Figure 3.8 Mass Movement delineation using Google Earth (on the right) vs. field investigation (on the left)

Figure 3.9 Forest fire field investigation using the Mini Disk Infiltrometer (MDI)

Figure 3.10 Relationship of mass movement (MM) frequency with Rock Type, Slope Degree, Mean Annual Rainfall, Normalized Burn ratio, Land Cover, Soil Type and Slope Aspect in Damour

Figure 3.11 Mini disk infiltrometer (MDI) measurement points distribution over the cumulative Normalized burn ratio (NBR) map. Water repellency (WR) interpretation used accoRDIstng to Parsons et al 2010 for the United States Department of Agriculture (USDA)

Figure 3.12 Workflow Diagram in order to obtain the Mass Movement Susceptibility Map

Figure 3.13 Impact of Normalized Burn Ratio (NBR) as an inducing factor on Mass Movement Susceptibility Map (MMSM) observed through Shifts in Mass Movement (MM) potential occurrence from High and Moderate to Low and No susceptibility in Damour (D) watershed

Figure 3.14 InfoVAL susceptibility model maps validated through an independent mass movement validation set extracted from MM inventory and NBR weight factor removed from MMSM equation

Chapter 4: Comparative correlation of Forest Fire burn severity with climatic fluctuations and land use change

Figure 4.1 US National Oceanic and Atmospheric Administration (NOAA) study on Mediterranean changing precipitation trends

Figure 4.2 Fluctuation precipitation trend between 1986 and 2012 in Damour

Figure 4.3 Increasing Potential Evapotranspiration (PET) of Damour watershed from year 1985 to 2012

Figure 4.4 Decreasing Standardized Reconnaissance Drought Index (RDIst) trendline (in red) implying a tendency towards increased drought severity

Figure 4.5 Normalized Difference Vegetation Index (NDVI) variation maps in Damour watershed showing the progression of burn severity from 1984-2012

Figure 4.6 Normalized Difference Vegetation Index maximum (NDVImax) and minimum (NDVImin) values showing an increasing trendline in NDVImax values insinuating a decreased vegetation cover and increased NDVImin

Figure 4.7 Overlay Analysis between Remotely Sensed NDVI and NCSR Land Use Map 2010

Figure 4.8 Normalized Burn Ratio maximum (NBRmax) and minimum (NBRmin) values showing an increasing trendline in NBRmax values insinuating an increased burn severity

Figure 4.9 Comparing Normalized Burn Ratio (NBR) to Normalized Difference Vegetation Index (NDVI)

Figure 4.10 Comparing Normalized Burn Ratio (NBR) to Standardized Reconnaissance Drought Index (RDIst) trendline showing negative correlation

List of Annexes

Annex 1 Preconditioning and inducing parameters affecting MM Occurrence (3:Restricted to this technique, 2=Mainly from this technique, 1:Spplementary).

Annex 2 Optical satellite images used in MM detection and delineation.

Annex 3 Radar satellite images used in MM detection and delineation.

Annex 4 Mass Movement susceptibility assessment methods.

Annex 5 Mass Movement and Forest fire field survey sheet.

GENERAL INTRODUCTION

Mass movements (MM) such as mass movements, earth flows, block falls and erosion are among the most invasive hazards causing surface instability favorable to land degradation (Poesen and Hooke, 1997; Atkinson and Massari, 1998; Duman et al., 2005; Bou Kheir et al., 2008; Goswami et al., 2011). They are severe natural hazards because of the extent of their damages and difficulty to control.

According to the database of the Research Center on the Epidemiology of Disasters, MM and related processes killed approximately 61000 people in the world over the period 1900–2009 (EM-DAT, 2010). This trend is expected to continue in the next decades due to increased urbanization and development, continued deforestation and increased regional precipitation in MM-prone areas due to changing climatic patterns (Yilmaz, 2010).

The occurrence of mass movement is influenced by many preconditioning factors conveyed through terrain parameters, including geology, slope gradient, soil, mean annual rainfall, and land use (Zinck et al., 2001; Abdallah et al., 2005; Kamp et al. 2008 ; Hadji et al., 2013). Mass movement is generally triggered by events or factors, such as abundant rainfall, earthquakes, and land use changes (Rodriguez et al., 1999; Huang et al., 2012; Mugagga et al., 2012). Fire is unquestionably a key factor in shaping the current forest landscape of the Mediterranean Basin (Trabaud, 1987; Pausas et al., 2008). It is considered a significant, if not the primary, foundation of geomorphologic and hydrological modification in fire-prone areas over both short and long time scales.

The consequence of fire on Mediterranean ecosystems varies and depends on the intensity, recurrence and location of the event (Tsitsoni, 1997; Broncano and Retana, 2004; Paula and Ojeda, 2006). In the last decades, fire system in the Mediterranean has altered, becoming larger and more intense (Lloret et al., 2009; Moreira et al., 2011). Lebanon being a small country of almost 10452 km^2, forest fires are generally small in their area if compared to other countries. Burned areas can stretch over accumulative area of 40km^2/year whereas in other Mediterranean countries such as Spain, Italy and Greece, total burned forest and wooded area can reach 2080km^2, 1180km^2 and 390km^2 respectively (Alexandrian et al., 1999). Nevertheless, Forest areas have decreased from 35% of the country's land area in 1960 to 13% in 2010. A total of 70,600 forest fire events took place between 1994 and 2004. The impact of climatic variations on forest fire is obtaining an increased attention. It is widely recognized that weather plays a key role in shaping extreme fire potential (Fried et al., 2004; Westerling and Bryant, 2008; Wastl et al., 2012).

Even though forest fire severity and fire-surface extent are arguabely climatically driven (Pausas 2004; Keeley et al., 2008), many lines of evidence show that fire regime changes are not directly linked to climatic change where on a longer time outlook, fire hazard has generally increased due to increases in population size, grazing practices, and increases in human ignition (Moreira et al., 2010; Salis et al., 2014).

All these issues are addressed in this research from various aspects with the aim of demonstrating the potential impact of forest fire burn severity on mass movement occurrence in Lebanon. Damour watershed represents a good case study since:

1. Its area extends from zero to almost 2000 m in elevation; having a combination of steep slopes, erodible solids in addition to rapid land use change and human interference.
2. It offers an abaundant and complex set of MM.
3. It is categorized as a catastrophic forest fire are by the Ministry of Environment where fire events extend over areas of more than 400 ha.
4. The impact of forest fire on MM occurrence has not been studied yet in Lebanon
5. The production of a MM susceptibility map with the introduction of forest fire as an inducing factor are nonexistent in order to develop appropriate management plans.
6. Forest fire inducing factors have only been assumed whereas this research provides an initiative towards semi-quantitative assessment to whether fires are climate or anthropogenic driven.

In this context, there exists a need for mapping MM and forest fire burn severity and track their evolution. Furthermore, assessing the impact of forest fire on MM occurrence through a MM susceptibility map will definitely be a step forward in sustainable management of natural and human resources. For this reason, the work was conducted with the extensive use of GIS and remote sensing in addition to field investigation for the validation of MM and forest fire maps.

This thesis is organized in five chapters as detailed below:

The First Chapter gives an overview of existing studies on Mass movement. It explains the adopted classifications of diverse types of MM such as slides, falls and flows. It points out various MM detection methods through either geotechnical devices or remote sensing. Moreover, hazard analysis techniques were explained discussed and compared in addition to determining preconditioning and influencing factors especially forest fire.

The second studies in depth the study area of Damour watershed. Geomorphology, geology, soil and land use characteristics were explained as well as natural hazards that are already occurring in the study area. The study area, extending from the Mediterranean coast to around 2000m of elevation covering almost 3.7% of the total area of Lebanon.

The third chapter tests the influence of diverse terrain parameters either preconditioning (Soil, rock type, land use, slope degree and slope aspect) or influencing factors (Forest Fire). The considered parameters were extracted either from GIS or remote sensing. **Forest Fire was thoroughly investigated through extensive field** work and a bivariate GIS based statistical methodology for mass movement susceptibility zonation InfoVal was used to assess the individual weight factor of every parameter on mass movement occurrence. Mass movement susceptibility map (MMSM) was produced and a validation set was overlain. An accuracy of 70% was established. **In order to further highlight the impact of forest fire on mass movement occurrence, NBR was removed from the MMSM equation**. It resulted in a shift in the distribution of mass movements making the MMSM's usability for hazard and risk mapping compromised.

The fourth chapter explores the possibility that forest fire in our study area is influenced by climatic variations represented through RDISTst as a drought index or land use changes represented by NDVI as a vegetation detection remote sensing index. A forest fire burn severity (NBR) map was established. It was individually compared to NDVI maps of the same years as well as RDISTst values of the same years as well. It shows that forest fire burn severity is a consequence of interaction between the two variables and not a result of a sole factor.

The fifth chapter presents a summarizing conclusion of the results obtained throughout the thesis and setbacks of the work in addition to recommendations concerning forest fire and mass movement **adaptive management**.

CHAPTER 1 A review of Mass Movement Classification, Detection and Susceptibility Analysis

This chapter reviews the development and advancement of MM studies emphasizing on general discriminating and modeling techniques. It provides a holistic understanding of the nature of different types of MMs, parameters affecting their occurrence and put forward the wide range of MM detection, modeling and zoning techniques. The chapter concludes that despite of the operational and theoretical limitations due to the extent of data uncertainty as a result of wide range of qualitative and statistically based modeling applications and techniques; MM hazard evaluation still constitutes a suitable, cost-effective process that would eventually serve as prediction and warning systems for communities at risk.

1.1 Introduction to Mass Movement

MM can occur as sudden, short-lived events, as a slow moving slide mass, or as unnoticeably slow moving soil creep. They pose serious direct and/or indirect hazards on short or long term.MM occur in areas where other natural disasters take place such as earthquakes where the impact of the volume of mass wasting exceeds that of the earthquake magnitude. For example, the 2008 Wenchuan earthquake in China resulted in 88000 casualties where one third were killed due to MM, debris flows and rock avalanches triggered by this earthquake (Gorum et al., 2011).

The secondary effects of MM can also be very destructive. In fact, once MM occur in narrow valley floors, they create temporary dams that quickly impound water, resulting later in catastrophic flooding. The most important indirect long-term effect of MM in mountainous terrain is represented through landscape evolution. MM inflicts economic losses and causes numerous fatalities and injuries. For instance, the mean annual cost of MM in Turkey was calculated to be around 80 million USD in 2007 (Yalcin, 2008). For Italy, Austria, Switzerland and France, the damage cost is estimated between 1 and 5 billion USD for each of these countries (Kjekstad and Highland, 2009) On the other hand, an estimated 2.6 billion USD is registered by China as direct and indirect economic loss from MM (Bai et al., 2011). In Lebanon, MM results in deaths and causes damage to construction and the environment estimated at 10-15 million USD annually (Abdallah, 2012). This chapter reviews the development and advancement

of MM studies emphasizing on general discriminating & modeling techniques. It provides a holistic understanding of the nature of different types of MMs, parameters affecting their occurrence and put forward the wide range of MM detection, modeling and zoning techniques. The chapter concludes that despite of the operational and theoretical limitations due to the extent of data uncertainty as a result of wide range of qualitative and statistically based modeling applications and techniques; MM hazard evaluation still constitutes a suitable, cost-effective process that would eventually serve as prediction and warning systems for communities at risk.

1.2 Mass Movement Classification

MM represents the lateral and downslope movement of earth materials such as rock, soil, and/or artificial fill (Varnes, 1984). The terms "mass movement", "slope movement", and "slope failure" when used in a generic sense, are generally equivalent in meaning. Several classifications of mass movements exist universally (Coates, 1977; Varnes, 1984; Kehew, 1995; Cruden and Varnes, 1996). These classifications are valuable in indicating the range of mechanisms and forms of motion. But it must be appreciated that mass movements in reality involve a combination of processes. Four principal types of movement are identified and described – creep, slide, fall and flow, that are widely recognized in the Mediterranean environments (Nemeok et al., 1972). Each of these can be subdivided into more specific forms of movements. The classification is based on several criteria: 1) *type of failure, 2) type of material being displaced, 3) moisture content, 4) type of strain and nature of movement and 5) rate of movement* **(Table 1.1).** The below table shows a schematic MM classification adopting the classification of Varnes (1984), Cruden and Varnes (1996) and Hungr et al. (2001).

Table1.1 Classification of most common mass movements in the Mediterranean

Type of movement			Materials in motion	Moisture content	Nature of movement	Rate of movement
Slide	Translational	Rock slide	Unfractured rock mass	Low	Shallow slide approximately parallel to ground surface of coherent rock mass along single fracture	Very slow to extremely rapid
		Rock block slide	Fractured rock		Shallow slide approximately parallel to ground surface of fractured rock	Moderate
		Debris/earth slide	Rock debris or soil	Low to moderate	Shallow slide of deformed masses of soil	Very slow to rapid
		Debris/earth block slide			Shallow slide of largely undeformed masses of soil	Slow
	Rotational	Rock slump	Rock	Low	Rotational movement along concave failure plane	Extremely slow to moderate
		Debris/earth slump	Rock debris or soil	Moderate		Slow
Fall	Rock fall		Detached rock joint blocks	Low	Fall of individual blocks from vertical faces	Extremely rapid
	Debris/earth fall		Detached cohesive units of soil		Toppling of cohesive units of soil from near-vertical faces such as river banks	Very rapid
Flow	Rock flow		Rock (especially readily deformable types such as shales and clays)	Low	Slow plastic deformation of rock, or soil	Very slow to extremely slow
	Debris flow		Mixture of fine and coarse debris (20-80% of particles coarser than sand-size)	High	Flow usually focused into pre-existing drainage lines	Very rapid
	Earth flow	Slow	> 80% sand-size	Low	Confined elongated flow	Slow
		Rapid	Soil containing sensitive clays	Very high	Rapid collapse and lateral spreading of soil following disturbance, often by an initial slide	Very rapid

Due to the complexity of the Mediterranean terrains, the different levels of awareness of the impact of MM on the territory and somehow limited resources available for inventory and maintenance, detailed MM records occurring in the Mediterranean region still required (Guzzetti, 2000; vanWesten, 2006; Triglia et al., 2010; Guzzetti et al., 2012). Nevertheless, in some specific locations, the information is available on historical and recent MM with consequences collected from available bibliography and archives. As an example, a large database has been constructed in Italy showing 31,000 MM events at 21,400 sites (equivalent to a density of 1 MM per 15 km^2) (Guzzetti, 2000). This information was obtained from about 100,000 newspaper articles and 2,000 scientific and technical reports. In addition, the exact distribution of each type of MM (slide, fall and flow) is often restricted to particular studied zones in a given country **(Table 1.2).** The MM density varies between 0.29 and 0.54 per km^2 according to the studied region. It is highest in the case of slides reaching 0.29 per km^2 in Southeast Spain.

Table 1.2 Type and quantity of MM occurring in selected regions of the Mediterranean area over the last two decades

Studied region	Area (km^2)	Corresponding number of MM		
		Slides	Falls	Flows
Umbria region-Italy (Cardinali et al., 2001)	8456	2243	1608	381
Rio Aguas-Southeast Spain (Griffiths et al., 2002)	550	160	90	50
North Lebanon (Abdallah et al., 2005)	670	100	85	13
North West Turkey (Duman et al., 2005)	2768	10,007	-	-
North-Western Sicily (Conoscenti et al., 2008)	194	28	-	219
Mount Lebanon (Abdallah, 2010)	100	-	63	-
Northern Spain, (García-Ruiz et al., 2013)	10,500 m^3			Debris flow
Southern Italy (Santangelo et al., 2013)	-	29	47	455

1.2.1 Falls

Falls occur when masses of rock or other material detach from a steep slope or cliff and descend by free fall, rolling or bouncing. In the Mediterranean environments, falls are less frequent than slides and are restricted mostly to cliff-rock outcrops with vertical to very steeply dipping and dense joints **(Figure 1.1a to 1.1c).** Velocities are very high and they generally occur quite suddenly. Large rock falls originating from a considerable height above the ground spread their debris over an extensive area unless the dispersal of material is confined by topography (Carere et al., 2001; Fard, 2001). The highest rock fall hazard exists when joints and bedding planes are inclined at a steep angle, as in the highly folded stratigraphy common in major mountain chains like the Alps. Since a rock rarely loses equilibrium without a inducing mechanism, earthquakes and freeze-thaw are the major factors interfering with rock stability (Watts, 2001). Debris falls are similar except they include a mixture of soil, vegetation and rocks.

1.2.2 Slides

Slides are mainly defined as slope movements of coherent masses along one or more well-defined shear surfaces (Nemeok et al., 1972).The great majority of slides in the Mediterranean environments are small and shallow with lengths of a few tens of meters and depths of 2-3 m. Slides in bedrock are less common, but may attain enormous dimensions and involve the movement of millions of cubic meters of material. Some slides took place during ancient times and are still continuing their activity until today. An example is the Fadalto MM located in Italy, which goes back to the late glacial time, and includes a large scarp with debris accumulation that occupies a belt of about 280 m (Eisbacher and Clague, 1984; Pelligrini and Surian, 1996).

Slides can be subdivided into transitional slides, which have predominantly planar shear surfaces, and rotational slides in which the shear plane is concave-up **(Table 1.1, Figure 1.1d to 1.1i).** Translational failure is common in cliff forming units, particularly where there is interbedded competent and incompetent rock. It is increased by the presence of marls, and invariably marly or argillaceous limestone. Rotational failure commonly occurs in relatively unconsolidated poorly cemented sandstones, weathered basalts and the surficial cover. The rotational movement can result in the upper part of the slumped mass being back-tilted towards the failure surface. Moreover, the movement may start as translational along a joint parallel to the cliff face and either continues deeper, thus becoming prone to rotational mode, or may induce rock/debris fall. This type of slope failure creates a great deal of property damage. A good example is the MM disaster which affected the city of Ancona, central Italy, in 1982 (Alexander, 1991).

1.2.3 Flows

Debris flows (viscous flows) tend to be less deep-seated and rather less common slope failures than MM (**Figure 1.1j to 1.1l)**. The high water content means that the material moves faster and farther from the original source. Mud Flows on the other hand, are highly fluid, high velocity mixture of sediment and water that has a consistency ranging between soup-like and wet concrete. They could travel at a speed rate that reach 1 km/hr making them extremely dangerous. These usually result from heavy rains in areas where there is an abundance of unconsolidated sediment (Watts, 2001). A good example is the huge earth flow in Aquoura area (Lebanon), where the constructed artificial lakes act as an inducing parameter in activating this flow **(Figure1.1j).**

Moreover, biotic destruction by MMs is also common; widespread stripping of forest cover by mass movements (Schuster and Highland, 2007). In order to be able to create safety measures and lay hazard management foundations, we need to understand the processes that initiate land sliding and then prepare for consequent susceptibility mapping (Yalcin, 2008).

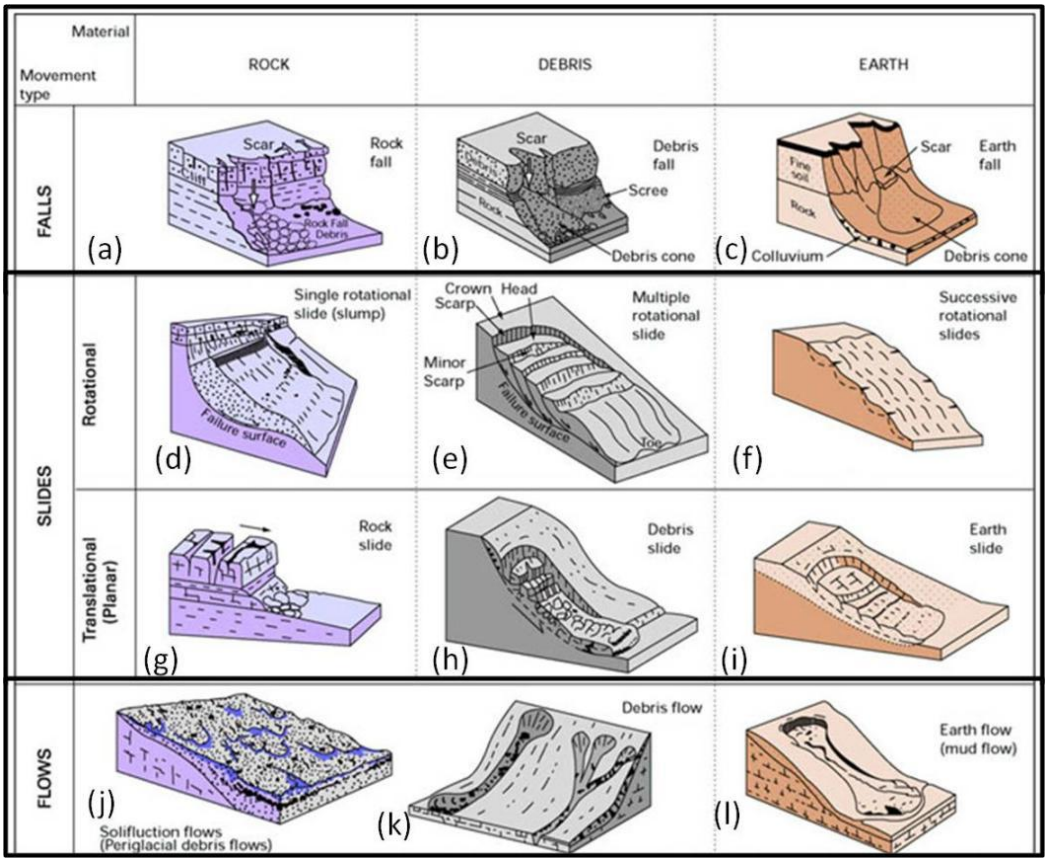

Figure 2.1 Movement and material type as classified by Cruden & Varnes (1996)

1.3 Factors Influencing the Occurrence of Mass Movement

MM do not occur randomly (Turcotte et al., 2002). Slope failures are the outcome of the interaction of physical procedures and mechanical laws controlling the stability or failure of a slope. The study of MM involves an understanding of these factors that affect their occurrence. These factors can be categorized into; (a) preconditioning (topography, geology, hydrogeology, soil, and land use) and (b) inducing factors (neotectonics, rainfall, flooding, forest fire, manmade excavation and climatic variation) (Cendrero and Dramis, 1996; Dahal et al., 2008).

1.3.1 Preconditioning Factors

Preconditioning factors are the inherent land surface characteristics and morphology and consequently determine the innate liability of a slope to failure or mass wasting. The intrinsic variables determine the pre-dispositioning of a site to MM and include bedrock geology, hydrology, soil, topography (slope aspect, slope gradient) and land use pattern. (Cendredo and Dremis, 1996 ; Sanchez et al., 1999; Dahal et al., 2009).

1.3.1.1 Topography

Topography and relief are synonymous terms used to denote the configuration of the land surface (Carte and Ciolkosz,1991). Being the element that portrays the elevation and shape of the land, topography is a decisive surface characteristic in slope failure modeling (Crozier, 1986; Datta et al., 2010). Slope characteristics used to describe relief include the aspect, gradient, length, and curvature of the slope. Gentle slopes are expected to have a low frequency of MMs because of lower shear stresses exerted on surficial materials associated with low gradients. At local scales, slope gradient affects the concentration of moisture and the level of pore pressure, and is often useful to resolve detailed patterns of instability, while at larger scales; it controls the hydraulic continuity (Abdallah, 2007). Slope orientation can influence mass wasting initiation, the distribution and density of MM by controlling the concentration of soil moisture (Wieczorek et al., 1997). Moisture retention and vegetation is reflected by slope aspect, which in turn may affect soil strength and vulnerability to slope failure (Florinsky, 2012). Moreover, if rainfall has a manifested directional constituent by influence of a existing wind, the amount of rainfall falling on a slope may vary depending on its aspect (Dai et al., 2002). Slope curvature affects flow divergence and convergence (Lewis et al., 1994) hence affects the amount of sediment loss. For instance, concave greatly reduced the total sediment loss in comparison with a uniform or convex slope.

1.3.1.2 Lithology

Lithology is one of the most important parameters in MM studies because different lithological units have different liability degrees (Yesilnacar and Topal, 2005, Yalcin and Bulut, 2007; Garcia-Rodriguez et al., 2008; Nefeslioglu et al., 2008). The physical properties of slope-forming materials such as fractures, fissures and rock strength that are involved in the mass wasting are related to the geology (Dai and Lee, 2002). The rock type, structure and texture influence MM processes. MMs are quite important where clayey rocks (clay-stones, marls, shales, muds, flysch) or morainic materials outcrop. The presence of these rock types in the Mediterranean region favors various types of mass movements, including landsliding. The clayey, shaly, or marly horizons are potential shear planes as they retain water. Once saturated, they behave like a liquid resulting in occurrence of rapidly moving mudflows. The soluble carbonate rocks also pose problems; they may include expanding clays which interact with and weaken the carbonate cement, hence weakening the rock itself (Chebbani et al., 1999, Abdallah, 2007).On the other hand, highly fractured rocks may possess both significant permeability and fracture porosity. Due to the fact that joints comprise of the weakest zones of rock masses, the anisotropy created by the joints is of significance. More specifically, in jointed rock slopes, the joints produce the natural mechanisms of planar, wedge and toppling failure (Pal et al., 2011).

1.3.1.3 Soil

The structural stability of soils is a physical characteristic that influences their behavior during processes of degradation. Soil degradation mainly involves destruction of soil structure (Baumgartl and Horn, 1991). Soil properties which influence rainfall acceptance include particle size distribution, structural stability, organic matter content, soil chemistry and clay mineralogy and water transmission characteristics (Lal, 2001).Generally, soils with faster infiltration rates, higher levels of organic matter and improved soil structure have a greater resistance to erosion.

Moreover, when soil management gives way to the accumulation of plant residues, they tend to increase the aggregate stability of the soil unlike other tillage and cropping practices which lower soil organic matter levels, cause poor soil structure, and result to an increase in soil erodibility (Rachmanet al., 2003). Crust formation in the unstable soils of arid regions usually results from the combined effect of raindrop impact energy and the dispersion of clay particles. These factors reduce the hydraulic conductivity of the soil surface and hence infiltration rate into the soil (Carmi and Berliner, 2008). A subsequent augmentation in the amount of runoff water can contribute to greater rill erosion troubles. The soils found in the Mediterranean climate are highly variable, but do have in common properties that make them susceptible to water erosion. These

characteristics lead to surface sealing during rainfall. However, in some cases, this coating might shape to decrease the amount of soil loss from sheet or rain splash erosion in the absence of any protective vegetation.

1.3.1.4 Land use

Among the factors inducing the potential intensity of mass wasting, land use is considered one of a high important factors (Ruff and Czurda, 2008; Chen and Huang, 2013). Deforestation, overgrazing and intensive agriculture as a result of anthropogenic pressure are often one of the main preconditioning factors of MM (Karsli et al., 2009). Land use change cause large alterations in the hydrological and morphological function of slopes, affecting infiltration characteristics, and runoff production, and even the shear strength of the soil. Vegetation (especially woody type) limits the movement of the debris present along slopes in two folds, i.e. hydrological (capacity of infiltration into the soils, soil moisture, groundwater level, etc.), and mechanical (root length). Where the vegetation cover is sparse, the slow movement inside the debris will not be ceased. Hence, dry environments under natural conditions are biologically marginal, and they can be expected to be highly susceptible to mass movement (Thornes, 1995; Garcia-Ruiz et al., 2010). A common method for decreasing water runoff and soil erosion is via stable and suitable vegetative cover (Dunjo et al., 2003; Chaplot and Bissonnais, 2003).

1.3.2 Inducing Factors

MMs can be prompted by a multiplicity of external Inducing or dynamic factors, such as intense rainfall, earthquake shaking, forest fires, flooding in addition to the expanded development in unstable hillslope areas under the pressures of escalating population and urbanization (Dai and Lee, 2002).

1.3.2.1 Neotectonics

MMs occur frequently in areas where minor and major morphotectonic events (uplift, subsidence, faulting, jointing and earthquakes) occur (recent or past), the latter being important throughout the Mediterranean basin (Pelligrini and Surian, 1996; Del Gaudio and Wasowski, 2004; Bottari and Sepe, 2013). Earthquakes have a decisive and clear power on slope stability; natural and man-made slopes which become equally unstable during an earthquake (Keefer, 1994). The instability of slopes due to an earthquake causes more destruction than the actual earthquake itself (Sato et al., 2007; Kamp et al., 2008; Owen et al., 2008). Ground shaking and

acceleration due to seismic waves energizes the weakened forces on the soil and rock masses even though ground displacements due to seismic waves may be sufficiently large to rupture bonds between soil particles. An earthquake does not only add adverse forces to a slope but may also enduringly diminish the shear strength in a slope (Hack et al., 2007). Earth section (mostly composed of soil and alluvium) became vulnerable to future failure through loss of cohesion and numerous cracks that were induced by the strong ground motion. According to Dunning et al. (2007) "the seismic shaking leaves an imprint (fractures, tension cracks and brittle deformation of rocks) on the slope stability of the area that may have long lasting effects on the future rates and spatial distribution of MMs". The widespread fracturing implicates that, in the future, slope failures can be effortlessly initiated by severe rainfall or low intensity earthquakes (Saba et al., 2010). Examples showing the strong relations between seismic events and mass movements were described in the historic literature. The major earthquake that hit Lebanon in 551 A.D. depicts the huge slides occurring at Chekka, and in fact was responsible for constructing its current coastal configuration (Khawlie, 1992). In 1927, a destructive earthquake affected the west bank of Jordan River inducing major MMs stopping the river flow for 21 days (Ambraseys and Barazangi, 1989). The 2002 Avaj, Iran earthquake of magnitude 6.5 triggered many MMs over an area of about 3600 km^2 (Mahdavifar et al., 2006).

1.3.2.2 Intensity Rainfall

The Mediterranean environment is characterized by seasonally contrasted climate, with low annual rainfall and irregular but frequent rain events with extreme intensities, scarce vegetation cover and poor soil characteristics (López-Vicente et al., 2008). The vulnerability of the Mediterranean region to MM hazard is mostly influenced by the frequent coincidence of dry summer periods with violent rainstorms (Petan et al., 2010). Precipitation acquires an erosive characteristic represented by an aggressive mechanism that targets soil deterioration and reduction of shear strength between its particles. (Martınez-Casasnovas et al., 2002) It is generally recognized that rainfall-induced MM are caused by increased pore pressures and seepage forces during periods of intense rainfall (Anderson and Sitar, 1995) which decreases the effective stress in the soil and thus reduces the soil shear strength, eventually resulting in slope failure (Brenner et al. 1985). The impact of raindrops on the soil surface can break down soil aggregates and disperse the aggregate material. Lighter aggregate materials such as very fine sand, silt, clay and organic matter can be easily removed by the raindrop splash and runoff water; greater raindrop energy or runoff amounts might be required to move the larger sand and gravel particles. The shallow failures of slopes in these soils are usually caused by infiltration due to prolonged rainfall (Kim et al., 2004). Furthermore, raindrop energy causes a splash coating that alters the infiltration process

and increases runoff, inhibiting a proportion of rain from percolating into the soil. But not every rainfall incident leads to runoff and erosion. The notion of a threshold value and duration below which erosion does not occur, a threshold of minimum intensity, is acquired through the combination of an erosivity index, a threshold of duration of high intensity and a duration of the rainfall which produces soil saturation and the degeneration of the soil constitution. Soil movement by rainfall (due to raindrop splash) is usually at peak and most perceptible during short-duration, high-intensity thunderstorms (Assouline and Ben-Hur, 2006). Rainfall intensity records are difficult to ascertain and even if we had a recorder, it would have short term data that could be insufficient to establish a trend or a threshold for a large study area, but it has been found by Roose (1979) that starting from long series of daily rainfall observation, it is possible to find satisfactory monthly and yearly averages of rainfall erosivity index.

1.3.2.3 Forest fires

Forest fires are a usual element in the Mediterranean basin. Forest fires have become more frequent and more severe in the last years. From 1996 to 2005, the annual average number of fires in Southern Europe exceeded 61,000, which is 34% more than recorded during 1986–1995 (Vilen and Fernandes, 2011). Furthermore and according to the European Commission, 0.5 million hectares are burned every year in Portugal, Spain, Greece, Italy and France (EC, 2010). As a result of more frequent and more severe fires, Mediterranean ecosystems can experience loss of biodiversity, MM and desertification. This increase in wildfire occurrence is associated with anthropogenic climate change. Partial or complete combustion of vegetation and litter by fire has important implications for post-fire hydrological response (Shakesby, 2011).

Depending on its severity, wildfire temporarily reduces or stops transpiration, interception and surface storage capacity for rain (Loaiciga et al., 2001). Perhaps the most discussed effect of forest fire is enhanced water repellency, termed the hydrophobic characteristic of soil particles (DeBano, 2000; Arcenegui et al., 2008; Rodríguez-Alleres et al., 2012; Beatty and Smith 2013). Water repellency diminishes the attraction of soils to water, causing the soil to oppose wetting for periods ranging from a few seconds to hours, days, weeks, or months (Doerr et al., 2000). Enhanced water repellency has considerable geomorphologic and hydrological consequences, including reduced soil infiltration ability, increased overland flow, and enhanced soil erosion. In general, water repellency in fire-affected Mediterranean type climatic regions, such as our study area, has been reported in pine forests (Arcenegui et al., 2008). On the other hand, the most commonly reported weathering effect of fire is spalling (Zimmerman et al., 1994), in which flakes of a substance are broken off a larger solid body, leading to surface failure. Vertical fracturing affecting an entire rock boulder has been reported, as have irregular linear and curvilinear

fractures (Ballais and Bosc, 1994). Fire-blackened boulder surfaces are strong evidence that rock failure occurs at a delayed stage of the fire, likely throughout cooling or days or months after a fire. In mountainous locations that are likely to be affected by freeze-thaw weathering, it is expected that weathering due to fire could be 10-100 times more effective than frost action (Shakesby and Doerr 2006, Stine, 2013).

1.3.2.4 Manmade excavation, road construction, unplanned urbanism

Unplanned housing development built on steep slopes frequently lacks any form of adequate slope drainage and hence makes steeper slopes particularly vulnerable to MMs (Anderson et al., 2007). On the other hand, urban expansion reclassified many quarries into residential areas hence increasing the risk of any potential rock failure (Kuzu and Ergin, 2005). Moreover, road construction removes the forest vegetation, disturbs forest floor, and damages soil structure, which dramatically increases the cut and fill slopes soil loss (Parsakhoo et al., 2009). Moreover, during a blasting excavation, the induced vibration propagates in a rock mass and result in damage to the surrounding rock inducing weakness and vulnerability to failure (Haibo et al., 2011). Road cuts can also intercept subsurface water by severing natural pipeflow, or by creating artificial areas of water resurgence by disrupting flow nets (Eisenbies et al., 2007).

1.3.2.5 Climatic Variations

The Mediterranean climate is characterized by episodic winter rainfall, and dry summers, with a distinctive regime of soil or rock moisture. Intense rains exhibit an erratic temporal and spatial distribution, and can be much localized, particularly in the driest parts of the Mediterranean (Alonso-Sarria and Lopez-Bermudez, 1994; Wainwright, 1996). In mountainous areas, where temperatures are usually below zero in winter, Freeze-thaw and thermal stress lead to an induced weathering and susceptibility to fracturing of rocks. The frequent fluctuation in temperature in the winter season which causes freezing and melting processes of water particles in short periods of time greatly enhances the destabilization of soil as well as rock formations. AccoRDIstng to Zaruba and Mencl (1984) "water freezing in rock fissures increases in volume and thus tends to widen them; rocks penetrated by fissures thus show decreased cohesion". Rock fall is particularly triggered by the thermal expansion of ice in cracks or the freezing of an exposed face followed by rapid warming creating hydrostatic pressures behind the frozen rock face) (Jakob and Lambert, 2009).

Temperature

According to the IPCC 4th assessment report presented in 2007, the Mediterranean region will be witnessing an increase of an average of 1.5 °C to 2 °C by 2050 and it is very likely (>90%) that cold days, cold nights and frosts have become less frequent over most land areas, while hot days and hot nights have become more frequent. Foremost, it is likely (>66%) that heat waves have become more frequent over most land areas (IPCC, 2007). Hotter, drier summers in the semi-arid regions (Plantonet al., 2005) and increase in the duration and severity of low-flow periods and a decrease in groundwater recharge (Booij, 2005) will drastically affect several previously listed factors primarily forest fire occurrences. The Mediterranean Basin fire regime has shifted during the twentieth century, and this shift was associated with the relative importance of the two drivers (human-driven fuel changes and climatic changes). Specifically, current area burnt is mainly driven by climatic conditions related to drought (Pausas and Fernández-Muñoz, 2012). An analysis of trends in forest fire occurrences in the Mediterranean shows the average annual number of forest fires throughout the Mediterranean basin is twice as many as during the 1970s. In the countries where data have been available since 1950s, a large increase in the number of forest fires can be observed from the beginning of the 1970s: Spain (from 1 900 to 8 000), Italy (from 3 400 to 10 500), Greece (from 700 to 1 100), Morocco (from 150 to 200), Turkey (from 600 to 1 400) (FAO, 1998). Furthermore, the notion that rock surface temperature changes may cause rock falls is not altogether new. It has been identified by geomorphologists as being responsible for slope instabilities (Gunzburgera et al., 2005).

Precipitation

Since the capacity of air to hold moisture is a function of temperature (Fowler and Hennessy, 1995), higher surface temperatures will definitely signify greater water-holding capacity of the atmosphere as well as increased evaporation. Both effects together should increase atmospheric moisture. Hence, climate change is expected to lead to a greater frequency and magnitude of heavy precipitation. Some observations and modeled simulations agree with this hypothesis (Groisman et al., 2005; Kharin and Zwiers, 2005). Given this possibility, together with the fact that precipitation is the most common inducing agent for mass movements, exceeding earthquakes and slope undercutting (Crozier, 1986), it is not surprising that increased mass movement activity is commonly listed as an expected impact climate change. Impacts from more intense precipitation events include increased flooding, mass movements, avalanches, and mudslides. With an irregular distribution of the rainfall throughout the year and an increasing trend of extreme events (Ramos and Martínez- Casasnovas, 2006; Alvioli et al., 2014), in which most water runs off due to the high rainfall intensity. The increase of high-intensity annual

precipitation extremes, separated by long dry periods, may cause higher runoff rates when intensity is higher than the steady-state infiltration rates. (Nearing, 2001; Pruski and Nearing, 2002; Nearing et al., 2004; Martínez-Casasnovas and Ramos, 2009) This will affect the hydrological environments governing slope instability through, for example, changes in antecedent pore pressures and alteration of trigger event magnitudes. Climate change is expected to affect soil erosion based on a variety of factors, including precipitation amounts and intensities, temperature impacts on soil moisture and plant growth (Zhang et al., 2010). Relationships between rainfall patterns and slope instability are reported in the literature for a range of slope failure mechanisms (e.g. shallow and deep-seated first-time slides and reactivated movements) and climates (Dixon and Brook, 2007). This could increase the frequency of occurrence of high pore pressures, and thus the activity of rainfall-triggered mass movements (Buma and Dehn, 1998). Quantitative predictions of changes in precipitation regimes as related to climate changes are highly uncertain, given the limited capability to simulate the fundamental processes which control the precipitation formation, particularly high for small-scale atmospheric processes (Diodato et al., 2011). Moreover, different types of mass movement will respond either to meteorological changes in the long term (monthly or yearly rainfall) or short term (daily or weekly rainfall) (Asch, 1996). Knowledge is required on how predicted climate change could modify the frequency and magnitude of slope instability events so that impact on the built environment can be assessed and remediation strategies developed. Annex 1 presents a combination of preconditioning and inducing parameters affecting MM Occurrence including techniques used to extract these data layers.

1.4 Land Instability Detection and Zonation Methods and Techniques

Detecting the spatial distribution and amount of deformation is critical for understanding the physical causes and eventually warning of possible occurrence. Several innovative instruments and techniques are now available to monitor the activity of slopes (Bozzano et al., 2011). These instrumentations and techniques can be mainly classified as geotechnical and remote sensing techniques **(Table 1.3)** . MM inventory maps are prepared for multiple reasons including: (1) detecting the extent of MM in a certain watershed (Duman et al., 2005; Trigila et al., 2010), (2) being an essential step in MM hazards and hazard mapping (Bălteanu et al. 2010), and more importantly (3) to analyze the development of the landscapes that are regularly attained by MM events. MM maps can be prepared using different techniques (Guzzetti et al., 2006) . Selection of a specific technique depends on several criteria: the use of the inventory, the coverage of the region studied, the base maps scale, the characteristics of the available imagery, the experience of the investigators, and the resources available to complete the work (Guzzetti et al., 2000; Van

Westen et al., 2008). Hence, MM inventory data are gathered at dissimilar scales, using a diversity of methods. MM inventory includes the location, classification, volume of MM in an area. Inventories need data that is continuous and extends over the entire MM distribution. MM inventory maps are prepared for different objectives such as: localization and classification of MM in an area, determining the frequency-area statistics of slope failures, representing the abundance of MM, and most importantly, supplying relevant information to construct MM hazards or hazards (Galli et al., 2008). Simply, MM inventories can be divided into two main types: archived and geomorphological. Achieved can be retrieved from literature and other archive sources and geomorphological can be classified as event-based, seasonal or multi-temporal (Galli et al., 2008; Guzetti et al., 2012).

1.4.1 Geotechnical Methods

Geomorphologic MM mapping is hindered by the complexity of detecting MM in the field, particularly old ones. The complexity has various causes, including: (1) the size of the MM, often too outsized to be entirely located, (2) the standpoint of the filed examiner is sometimes insufficient to see all parts of MM with the same accuracy, and (3) the fact that old MM are habitually partly or entirely covered by trees, or have been partially distorted by other MM processes and anthropogenic activities such as agricultural and forest practices (Santangelo et al. 2013). The most used geotechnical methods are Total Station Theodolite (TST), Electronic Distance Measurement (EDM), Slope Inclinometer, Wire Extensometer, and Global Positioning Systems. On the case of geotechnical and geodetic methods, all of the proposed techniques are applicable for obtaining general and specific information on the type and (visual) characteristics of MM: (1) to exploit for improved visual interpretation of the aerial photographs or satellite images and (2) to check (validate) inventory maps prepared using other techniques, chiefly the interpretation of aerial photographs (Guzzetti et al., 2000; Cardinali et al., 2001). On the other hand, it is always recommended to accompany results obtained by remote sensing with geotechnical techniques in order to calibrate obtained results and evaluate the performance of new (remote sensing) technology.

1.4.2 Remote Sensing in MM interpretation and analysis

The use of ground based monitoring techniques proves to be complex and resource exhaustive particularly where investigation has to cover a large area for an extended period of time. For this reason, old, recent and new methods and technologies are being exploited to help detect and map MM. They can be generally divided into (i) interpretation of the aerial photographs (ii) interpretation and analysis of satellite images including panchromatic, multispectral and Synthetic Aperture Radar (SAR) (iii) analysis of surface morphology mainly from very high resolution DEMs obtained from LiDAR. We now examine the characteristics, advantages, limitations of different techniques based on results published in the literature and on our experience.

1.4.2.1 Aerial photography

Aerial photographs have been extensively applied in MM investigations, detection and characterization. It also provides a stereoscopic view of the area and makes it possible to take horizontal or vertical measurements. This is a feature that is missing in some remote sensing satellite images (Thomas et al., 2004; Shroder, 2013). Even though considered as a classic method for MM detection, visual interpretation of aerial imagery continues to be widely adopted because: (1) a trained geomorphologist can readily recognize and map MM on the aerial photographs, assisted by the stereoscopic vision; (2) interpretation of stereoscopic aerial photography is an intuitive process that does not require complicated technical skills. The tools needed to interpret aerial photographs are simple (e.g., a stereoscope) and inexpensive (Nichol et al., 2006), (3) and the size and scale of the aerial photographs allow for the coverage of large territories with a reasonable number of photographs. Availability of multiple sets of aerial photographs for the same area allows investigating the temporal and the geographical evolution of slope failures(Guzzetti et al., 2005; Fiorucci et al., 2011) and the essential information landscape evolution and for erosion (Larsen et al., 2010). Nevertheless, recognition of MM through the visual analysis of stereoscopic aerial photography is an empirical and uncertain technique that requires experience, training, a systematic methodology, and well-defined interpretation criteria (Antonini et al., 2002). Because aerial photographs are not readily available in a timely manner for MM events, other remote sensing approaches such as optical satellite imagery, Radar satellite imagery and Light Detection and Ranging (LiDAR) has become an alternative data source.

1.4.2.2 Optical Satellite Imagery

In the mid 1970's, the exploitation of satellite imagery in distinguishing and mapping MM became accessible using optical images provided by satellite sensors. Researchers used mainly LANDSAT images for the detection of MM (McDonald and Grubbs, 1975). The augmented availability of high resolution (HR) and very-high resolution (VHR) sensors increased considerably the use of satellite data in MM detection . Visual interpretation of optical satellite images can identify and map various MM types such as: (i) debris slides and flows, (ii) rock falls and (iii) shallow and entrenched slides. In order to detect an individual or group of MM where the visual evidence of slope failure is sufficiently clear, HR and VHR optical images can be used (Marcelino et al., 2009). Abdallah et al. (2007) compared the use of Landsat TM, IRS and SPOT4, in rugged terrains (case study Lebanon) where they concluded that slides were best detected with the use of SPOT4 stereo anaglyphs as well as rock and debris falls with an accuracy of 67% and 63% respectively. But the latter was also well detected with the use of Landsat TM and IRS images with an equal accuracy of 62%. Cheng et al. (2004) offer an approach for delineating MM using band ratios of multi-temporal satellite images such as SPOT to detect changes on land use pre and post-MM occurrence. Weirich and Blesius (2007) and Fiorucci et al. (2011) compared satellite images (Spot 5 and Ikonos,) and aerial photo to identify MM. They concluded that VHR can provide same and/or complementary MM information than the aerial photography. Moreover, the repeat cycle of satellite imagery makes way to the for the production of event, seasonal, and multi-temporal inventory maps (Guzzetti et al., 2012).The introduction of Google Earth, which provides VHR optical satellite images (even multi-temporal in many cases), and the capability to look at the images in 3D, has provided new opportunities to make use of satellite images for the detection of MM (Sato and Harp, 2009). Pleiades1 (and soon Pleiades-2) not only provide a 1 day revisit time which is ideal for land surface monitoring but also provide a 1m DEM. Alternatively, VHR satellite images can be combined with DEMs to obtain 3D-views of the terrain, which can be visually interpreted to detect and map MM (Nichol et al. 2006; 2009). **Annex 2** presents a list of optical satellites with their respective resolution, available spectral bands, stereo capabilities, revisiting times, achieved dates and articles dealing with MM and ancillary data using the corresponding imagery. Moreover, Sentinel 2 satellite is scheduled to be launched in April 2015 having 13 spectral bands (4 bands at 10 m, 6 bands at 20 m and 3 bands at 60 m spatial resolution (the latter is dedicated to atmospheric corrections and cloud screening) with a swath width of 290 km and a revisit of 2-3 days. With this increased swath width along with the short revisit time allows rapid changes to be monitored, such as land-change and geophysical variables detection maps.

Automatic and Semi Automatic Methods

Visual interpretation is not the only employed method for MM detection and delineation. Borghuis et al. (2007) demonstrate how "unsupervised classification" can distinguish 63% of the MM detected manually. Further known automatic techniques would be similar to the change detection which was studied by Nichol and Wong (2005) where they showed how to separate MM and spectrally similar elements (i.e. bare rocks). Moreover, authors have utilized multispectral data received from optical satellite sensors , such as NDVI (Normalized Difference Vegetation Index), for automatic or semi-automatic MM detection (Cheng et al., 2004; Borghuis et al., 2007; Veraverbeke et al., 2010). After MM events, the most evident features are (1) the loss of vegetation, and (2) exposure of rock and soil. This change in land use leads to an increase in local brightness of the image, and can very well be represented by NDVI, which is sensitive to low levels of vegetation change. For this reason, previous researchers have used NDVI as an effective discriminator for separating MMs from vegetated areas (Barlow et al., 2006).

The beginning of classification from aerial images dates back around 70 years (Anderson et al., 1976). It is an essential source of information for change detection applications. Techniques for the semi-automatic detection of MM features include the analysis of high-resolution DEMs (Tarolli et al., 2010) and change detection techniques (Mondini et al., 2010). These techniques are distinguished in two main ways as pixel-based (Lu et al., 2004; Jianyaa et al., 2008; and Object Oriented Image Analysis (OBIA) (Benz et al., 2004, Blaschke, 2010; Chen et al., 2012; Platt, 2014; Kassouk et al., *in Press*). The former classification method is partitioned into supervised and unsupervised classifications. The former classification method is partitioned into supervised and unsupervised classifications. Additionally, supervised classification has different sub-classification methods which are named as parellelpiped, maximum likelihood, minimum distances and Fisher classifier method. Unfortunately, for MM detection, these classifications are pixel-based; hence they marginally consider the geomorphological context of the extracted features, hence oversimplifying the complex aspects of MM (Martha 2010; Mondini et al. 2011). In order to surmount the issue with pixel-based classification, Object-Based Image Analysis (OBIA) has been introduced as an effective tool for analyzing satellite images (Martha et al. 2010) and high resolution elevation data (Van Asselen and Seijmonsbergen 2006; Antonarakis et al. 2008). OBIA often uses a multi-resolution segmentation algorithm that clusters individual grid cells into image objects. It observes, apart from spectral properties, characteristics like shape, texture or adjacency criteria (Fröhlich et al., 2013) Image objects ideally be of almost the same size as, or slightly smaller than, the feature to be classified. Choosing an appropriate scale parameter value is therefore a crucial step. Yet segmentation parameter values and classification rules call for a manual trial-and-error optimization (Van Asselen and Seijmonsbergen, 2006; Kim et al., 2008). In

this way, OBIA allows full control by the expert, but the degree of objectivity and automation is limited compared to pixel-based approaches.

1.4.2.3 RADAR Satellite Imagery

SAR (Synthetic Aperture Radar) images are used chiefly to detect and monitor deformation of the topographic surface produced by slow moving MM (Berardino et al. 2002; Hooper et al., 2004; Cascini et al., 2009; Cascini et al., 2010; Chang et al., 2012; Akbarimehr et al., 2013). Airborne and satellite SAR data are both used to detect map MM. Czuchlewski et al. (2003) exploited L-band airborne SAR to detect changes formed by Tsaoling MM that was triggered by a 7.6 earthquake. Singhroy and Molch (2004) demonstrated that SAR techniques can support researchers in detecting and monitoring MM using ERS 1/2 and Radarsat-1 images. Farina et al. (2006) assembled a time series of MM from SAR interferometry to assess the situation of movement around 3550 MM in Arno River basin, Italy. Strozzi et al. (2005) found that during the studies in the Alta Val Badia region, Italy, MM are good examples for presenting the improved performance of L-band in comparison to C-band for vegetated areas, in particular concerning open forest (the penetration depth of radar wave increases with radar wavelength). Alternatively, the X-band allows more precise detection of slower ground movements with respect to C-band because of the smaller wavelength. Additionally, available VHR X-band satellite radar sensors have more possibilities for MM hazards assessments on a detailed scale such a hill slope. This is illustrated by Bovenga et al. (2006) through the results obtained by processing different SAR datasets acquired by Cosmo-SkyMed (X-band) and ASAR (C-band) on two MM-prone areas. Geomorphologists exploit images taken SARsensors primarily to measure surface deformations, and to construct time series of surface deformations, at single points. In this context, Differential Synthetic Aperture Radar Interferometry (DInSAR), utilizes the phase difference (interferograms) between pairs of SAR acquisitions for the same area at different times allowing to calculate displacement maps with centimetre to millimetre accuracy (Colesanti and Wasowski, 2006; Delgado et al., 2011; Hererra et al., 2013 ; Calò et al., 2014). Until recently, the main limitation to the application of InSAR was the relatively long revisiting time (24 or 35 days) even though X band satellite SAR constellations like Cosmo Skymed and TerraSAR-X have also a short revisiting time, from 4 to 11 days. However, their coverage is limited to well definite areas. The new Sentinel-1 mission, based on a constellation of two satellites, is expected to reduce such limitations guaranteeing a revisit cycle of 6 days on a global scale and in particular over Europe and Canada and providing a high level of service reliability with near-real-time delivery of data within 24 h, important for risk management applications (Rucci et al. 2012). For this reason, mapping and monitoring capabilities of the DInSAR techniques present a remarkable

advancement in MM investigation at different scales (Cascini et al., 2009; Bovenga et al., 2012; Bonano et al., 2013) due to the improvements in temporal and spatial resolution where the increase in measurement points improving the capabilities of DInSAR in MM mapping. Examples also exist from the use of SAR data for the detection of single, large, rapid MM (Singhroy and Molch 2004; Lauknes et al. 2010; Zhao et al., 2012 ; Raucoules et al.,2013 ; Del Ventisette et al., 2014). Zhao et al. (2012) introduce a method for automatic detection of slowly moving MMs using InSAR products including InSAR coherence maps, SAR intensity images, deformation maps and digital elevation models (DEM). For the case of localized slow MM, GB-SAR (Ground-Based SAR) is another pioneering system for the remote estimation of ground displacements which showed high accuracy in MM detection when compared with conventional monitoring systems such as GPS and extensometers as shown by Noferini et al. (2007). GB-InSAR works with the similar principle as space borne InSAR but instead of acquiring the images from several hundred kilometres away, the images are acquired by a radar moving on a rail within a couple of kilometres of the area in time interval of approximately 10 minutes, surmounting some of the constraints of satellite data acquisition (Antonello et al. 2004). The GB-InSAR can function with steep slopes where satellite images carry out ineffectively.

The improved capabilities of the new SAR sensors are of particular interest for site-specific investigations of MM (Garcia-Davalillo et al., 2014) and promise to turn DInSAR derivative products such as deformations and velocity maps into complementary assets to traditional monitoring techniques (Giordan et al., 2013). Eventhough SAR images are not particularly relevant for the production of MM inventory maps, it can be used to help in determining the state of activity of MM and identifies movement of the topographic surface in case of an undetected MM event (Cigna et al., 2011)

Annex 3 presents a list of radar satellites with their respective resolution, available spectral bands, stereo capabilities, revisiting times, achieved dates and articles dealing with MM and ancillary data using the corresponding imagery.

1.4.2.4 LiDAR

When a MM occurs, "it changes the surface topography leaving a distinct signature" (Pike 1988). Hence it is only normal that researchers have tried to utilize digital illustrations of the topographic surface to distinguish MM. LiDAR (Light Detection And Ranging) is a widely used RS technique used to acquire these digital representations for areas extending from a few to thousands of kilometer. Very-high resolution DEMs obtained from LiDAR have been used to detect, map, and monitor MM (Schulz 2007; Corsini et al. 2009; Lan et al. 2010; Derron and

Jaboyedoff, 2010; Razak et al., 2011). AccoRDIstng to Baldo et al. (2009), LiDAR surveys can assess quantitative MM volumetric estimates as well as multi-temporal analyses.

Alternatively, many researchers have compared MM maps obtained through the visual analysis of LiDAR-derived DEMs and stereoscopic aerial photographs (Schulz 2007; Booth et al. 2009; Razak et al. 2011). In a wooded terrain, LiDAR can penetrate the canopy, providing quantitative descriptions of the topographic surface of unmatched detail (Guzzetti et al. 2012). This ability proves particularly important to detect and map MM in forested areas, with a competitive advantage over other methods based on the visual interpretation and analysis of optical aerial or satellite images that do not penetrate the canopy. On the other hand, major disadvantages of LiDAR include (1) its higher cost of acquisition as compared to other sources (2) are not readily available for all parts of the world (3) challenged by very steep terrain and cliffs due to lack of clear shots (4) Processing and analyzing LiDAR data sets require specialized skills and software.

Table 1.3 Overview of techniques for the collection of MM information H= Highly Relevance; M=Medium Relevance; L= Low Relevance)

Technique	Data Source	Importance to Scale of Study area		
		Medium 1:25,000 to 1:200,000	Large (>1:25,000)	Detailed
Geotechnical and Geodetic Methods	Extensometer	_	L	H
	EDM	_	L	H
	GPS	_	L	H
	Theodolite	_	L	H
	Ground-based InSAR	_	L	H
	Terrestrial LiDAR	_	L	H
Image Interpretation	Stereo aerial photographs	H	H	H
	High Resolution Satellite images	H	H	H
	LiDAR shaded relief maps	M	H	H
	Radar images	M	M	M
Image Classification	Medium Resolution multi spectral Image and VHR	H	H	M
	Using combinations of optical and radar data	M	M	M
	InSAR	M	M	M
	LiDAR	L	M	H
	Photogrammetry	M	H	H
	Field mapping	H	H	H

1.5 Guidelines for Mass Movement Zoning and Mapping

Mass movement susceptibility and hazard zoning, and to a slighter degree, mass movement risk zoning, have undergone extensive development (Poiraud, 2014; Wu et al., 2014; Göransson et al., 2014). Most of these zoning studies are qualitative in nature, although more recently there have been examples of quantifying the hazard by assigning frequency to the potential mass movements and quantifying the risks for existing development (Fell et al., 2008). Unfortunately, there is rarely a standardization in terminology and the results of mass movement zoning are often not precisely defined, and susceptibility, hazard and risk are often exchanged in mass movement zoning maps.

Below are definitions for terms used in mass movement zoning and risk management as described by Fell et al. (2008), Hervás and Bobrowsky (2009) and Van Den Eeckhaut and Hervás (2012).

Susceptibility: A quantitative or qualitative assessment of the classification, volume (or area), and spatial distribution of mass movement which which exist or may potentially take place in an area. Although it is expected that mass movement will occur more frequently in the more susceptible areas, in the susceptibility analysis, time frame is clearly not taken into consideration.

Hazard: A situation with the probability to produce an detrimental consequence. The description of mass movement hazard should include the same input as susceptibility analysis with the addition of the velocity of the potential mass movement and any resultant detached material, and the probability of their occurrence within a given period of time.

Vulnerability : The degree of loss to a given element or set of elements within the area affected by mass movement (Fell et al.2008). It is expressed on a scale of 0 (no loss) to 1 (total loss). For people, it will be the probability that a particular life (the element at risk) will be lost, given the person(s) is (are) affected by mass movement, for property, the loss will be the value of the damage relative to the value of the property.

Risk: A measure of the severity and probability of an adverse outcome on health and the environment. Risk is often estimated by the product of probability of a phenomenon of a given magnitude times the consequences. For life loss, the annual probability that the people at risk will lose their life taking into account of the landslide hazard, and the temporal–spatial probability and vulnerability of the person. For property loss, the annual probability of a given level of loss taking into account the elements at risk, their temporal and spatial probability and vulnerability.

Landslide susceptibility zoning usually involves developing an inventory of landslideswhich have occurred in the past togetherwith an assessment of the areas with a potential to experience landsliding in the future, butwith no assessment of the frequency (annual probability) of the occurrence of landslides. Landslide hazard zoning takes the outcomes of landslide susceptibility mapping and assigns an estimated frequency (i.e. annual probability) to the potential landslides. It should also consider all landsliding which can affect the study area Landslide risk zoning takes the outcomes of hazard mapping, and assesses the potential damage to persons (annual probability of loss of life), to property (annual value of property loss), and environmental features (annual value of loss) for the elements at risk. We will be focusing on susceptibility mapping the hazard factor is not in the scope of our study.

1.6 Mass Movement Susceptibility Assessment Methods and Mapping

To address natural hazards issues, scientists and engineers have developed physical parameters, equations and environmental process models that can be used as assessment tools for administration, development and legislative purposes. In developing such approaches, experts analyze any environmental system to build a conceptual model of processes, and their interactions, to allow for assessment of how a system will react under natural and anthropogenic changes. Among the measures that have been taken to reduce losses from MM is the production of susceptibility maps. In general, methods of MM susceptibility assessment may be either qualitative or quantitative (Aleotti and Chowdhury, 1999).

Qualitative MM susceptibility assessment has been made in different countries of the world, depending on expert opinions (Atkinson and Massari 1998; Irigaray et al. 1996; Amaral and Furtado, 2004; Abdallah et al., 2007). Heuristic qualitative approach, also defined as expert evaluation approaches (Aleotti and Chowdhury, 1999), is particularly appropriate for small scale regional surveys. The scale of such surveys is in the order of 1:100,000 to 1:250,000. Knowledge on the causes of MM is essential in the decision making and therefore the method relies heavily on the professional experience of the expert. The most common qualitative approach would be the overlay or combination of index maps or parameter maps with weights. In this case, the expert selects and maps the factors that affect slope stability and, based on personal experience. Weighted values are assigned to each factor according to its expected contribution in generating failure (Soeters and Van Westen, 1996) Such models lack deterministic capability, because they neither simulate nor explain the mechanisms involved in Mass Movements. They are not able to take into consideration, for the purpose of prediction, the role played by the activating factors. In order decrease subjectivity in the weight assessment process in MM assessment, early attempts defined susceptibility classes through the factor overlaying of geological and topographic attributes to MM inventories.

Quantitative techniques are based on numerical expressions of the relationship between controlling factors and MM activity and ability to recognize areas that are susceptible to future MM. They are divided into two main categories: statistical (or probabilistic) and deterministic. Statistical methods analyze the historical link between MM-controlling factors and the distribution of MM. On the other hand, deterministic are based on slope stability studies, expressed in terms of the safety factor (Refice and Capolongo, 2002). Review of recent publications exposes a large number of papers and conferences dealing with statistical MM deployed in different regions of the world especially in Italy (Rapolla et al., 2010; Sterlacchini et al., 2011), Turkey (Nefeslioglu et al., 2008; Akgun, 2012), and Iran (Ilanloo, 2011; Pourghasemi

et al., 2012). The most frequently used MM assessment techniques are statistical such as Information Value Method (InfoVal), Logistic Regression (LR), Analytical Hierarchy Process (AHP), Frequency ratio (FR), Artificial Neural Network (ANN), Fuzzy Logic, and Decision Tree since they are considered to be semi-quantitative. They are not as subjective as heuristic methods but are not as concrete and time consuming as deterministic methods. Reliability of susceptibility maps depends mostly on the amount and quality of data, the working scale and the selection of the appropriate methodology of analysis and modeling. Accordingly, all the suggested statistical techniques have advantages and disadvantages as shown in **Annex 4.**

Information Value method assumes that MM will happen under influence of the same combination of factors whereas field observations indicate that some slides are caused by a specific set of factors (e.g. proximity to a river in conjunction with other factors like land use and slope gradient. This susceptibility analysis requires continuous updating of the input factors: a change in the land use might, for example, significantly increase the MM susceptibility of a specific area (Che et al., 2012). InfoVal tends to oversimplify factors while neglecting the geotechnical characteristics of the soil which vary enormously in space.

Results of ***Weights-of-evidence (WOE)*** are strongly dependent on the number of events introduced in the model (e.g., on the estimation of probabilities) and on the quality of the MM inventory map. Therefore, probabilities are very low if the area is distinguished by exceptional events, and the results have to be interpreted carefully (Lee et al. 2002; Cevik and Topal 2003; Xu et al. 2012).

Alternatively, ***Logistic multiple regression*** considers several physical parameters that may affect probability (Dai et al., 2001). Logistic regression permits one to type a multivariate regression relationship between a dependent variable and several independent variables. The advantage of logistic multiple regression modeling over other multivariate statistical techniques including multiple regression analysis is that the dependent variable can have only two values—an event is either occurring or not occurring, and that predicted values can be interpreted as probability since they are constrained to fall in the interval between 0 and 1. As compared to a heuristic estimation, low, medium and high are translated into digits. A susceptibility index with a range from 0 (low) to 1 (high) will be obtained (Ruff and Czurda, 2008). But some factors may have weak relationship with MM occurrences. The combination of such factors with the others may generate data which is difficult to interpret.

Correspondingly, ***Discriminant Analysis*** simply converts a multivariate problem into a univariate contingency-table analysis. This latter is the simplest prediction method in which a cross-tabulation is made between two outcome states (MM and non-MM) versus the discrete

categories of a predictor variable (Dong et al., 2009) . Unfortunately, no way exists to express Discriminant scores as probabilities of occurrence of MM, except by categorizing the scores and computing proportions of misclassifications (He et al., 2012).

Analytical Hierarchy Process (AHP) is a multi-objective, multi-criteria decision-making approach that enables the user to arrive at a scale of preferences drawn from a set of alternatives. During the last decade, distribution-free methods such as neural network (Chauhan et al. 2010; Pradhan et al., 2010), neuro-fuzzy-analysis which is a combination of AHP and Fuzzy logic described below (Vahidnia et al., 2010; Bui et al., 2012), and decision tree models (Abdallah 2010; Yeon et al., 2010) have been also implemented for MM prediction and mapping.

The ***Artificial Neural Network*** (ANN) method allow the target classes to be defined in relation to their distribution in each source data set, facilitating the integration of data emerging from remote sensing, GIS, etc. Among the disadvantages is ANN's "black box" approach where the adjusted weights are used to determine the outputs of each unknown data sample whenever the network is tested with acceptable accuracy. The discussion of the quality of the results is often rather limited, which may be due to the difficulties to apply methods for exploring the behaviour of the networks (Yesilnacar and Topal, 2005; Kanungo et al., 2008; ; Conforti et al., 2014).

The idea of ***Fuzzy Logic*** is to consider the spatial objects on a map as members of a set. It has been widely used in many different fields including, for instance, soils and land evaluation (Lee, 2007; Kanungo et al., 2008). Fuzzy logic relationships are applied in order to avoid subjectivity in parameter selection when using a large number of MM factors inherent to the way experts approach their problems. Fuzzy Logic also allows one to take into account the relationship among these factors, which seems to be crucial in assessing the potential of failure of soil slope (Saboya et al., 2006; Ilanloo, 2011).

Decision-trees can identify the most decisive variables, which are those that are used for creating the splits near the top of the tree. This technique helps to explain data and to make predictions using the data (Witten and Frank, 2005). A decision tree can also handle data measured on different scales, without any assumptions concerning the frequency distributions of the data, based on its non-linear relationship. The main purpose of using the decision tree is to attain a more concise and perspicuous representation of the relationship between an objective variable and explanatory variables (Saito et al., 2009).

When compared to numerically oriented techniques such as LR and ANNs, a decision-tree model has a number of advantages. Decision-trees are easy to build and interpret, and can automatically handle interactions between both continuous (ordinal, interval) and categorical (nominal) variables. Artificial Neural Networks (ANNs) are often compared to decision-trees models

because both methods can model data that have nonlinear relationships between variables, and both can handle interactions between variables. However, ANNs do not present an easily understandable model allowing researchers to get the full explanation of the underlying nature of the data being analysed. They handle only binary categorical input data, and not those with multiple classes. It is difficult also to incorporate a neural network model into a computer system without using a dedicated interpreter for the model. In contrast, once a decision-tree model has been built, it can be converted to statements that are implemented easily in most computer languages without requiring a separate interpreter. Moreover, decision-trees can identify a target (dependent) variable. In addition, decision-trees can indicate the relative weight of each predictor variable in explaining the training data, while InfoVal and WoE analysis demonstrate only the implication of a couple of predictor variables against the target variable. Therefore, if the goal of an analysis is to predict the value of some variable, then decision-tree modelling is a recommended approach. But predicting the future remains a hard task, even with decision-trees. A comparison study was conducted by Yalcin et al. (2011) between FR, AHP, InfoVal (Wf in particular) and LR for MM susceptibility mapping. The article concluded that InfoVal, a bivariate statistical method, captured the highest accuracy of active MM areas. This could be attributed to the fact that it presents much more distinct and homogeneous values for wide study areas such as this application. But a pioneer study done by Choi et al. (2012) suggested the combination of individual FR, LR and ANN susceptibility maps. Each map was the introduced as a new impact factor. The combined map did show improved accuracy compared to individual maps. We can safely say that until this moment, a total agreement about the ideal method for producing a MM susceptibility map has not been reached yet.

Even though heuristic and statistical methods are widely used in large-scale MM hazard and risk analysis, these methods cannot expressly take into account the influences of geo-mechanics (cohesion, friction angle), geological structures (rock massif discontinuities) and pore water pressure. These factors are considered by ***Deterministic*** investigation and interpretation methods include the use of survey markers, extensometers, inclinometers (Okimura and Kawatani, 1986; Romeo, 2000; Refice and Capolongo, 2002; Carro et al., 2003; Shou and Wang, 2003; Moon and Blackstock, 2004). Unfortunately, deterministic methods comprise of a high degree of oversimplification when the data are incomplete especially since data requirements for deterministic models can be prohibitive, and frequently it is impossible to acquire the input data necessary to use the model effectively (Gomez and Kavzoglu, 2005). Another significant limitation of these approaches is the need of material data (mechanical properties, water saturation, etc.) that are difficult to obtain over large areas . Deterministic approaches can be used for the small and relatively homogenous areas and require detailed and are based on physical models and geotechnical parameters and are capable of identifying the triggering threshold as

shown in the work of Montgomery and Dietrich (1994). When trying to use the deterministic methods to predict slope stability over a large area, one ofc the main issues is the not the model itself but the spatial variability of the input parameters as well (Jia et al., 2012) Annex provides a holistic comparison between the most widely used for mass movement susceptibility assessment methods.

Despite all the improvement in susceptibility zoning and mapping, it must be recognized that mass movement zoning results only in geomorphological spatial predictions based on the available data. There are a number of limitations including limitations in the mass movement inventory upon which the susceptibility zoning maps are based. The process of building a MM inventory and a corresponding susceptibility map will be dealt with in the following chapter.

CHAPTER 2 Detailed Description of the Study Area

This chapter presents the geographic context as well as diverse geo-environmental aspects (geology, soil, hydrology, climate etc.), socio-economic characteristics and hazards of the study area within Lebanon. It exposes the MM occurrence, concrete examples of MM prevailing in the area, their negative impacts and the applied mitigation measures. It also highlights the MM studies being conducted in the country.

2.1 Geographic Location

Lebanon is a typical Mediterranean country with a total area of 10,425 km^2 characterized by irregular and highly intense rainfall and natural vegetation with interspersed, well-contrasted landscape units in terms of lithology, morphology, pedology, hydrology, and climatic diversity. Lebanon includes many sites that have experienced major mass movements (Abdallah et al., 2005) and experiences for instance approximately 50-70 tons/ha/yr of soil erosion (Bou Kheir et al. 2008). Damour watershed (**Figure 2.1**) is in the southern part of Lebanon between latitudes 33°48'42.65"and 33°36'18.42"N and longitudes 35°45'55.88" and 35°32'57.70"E. It is bounded by the Mediterranean Sea to the west, Baadba Caza to the North, West Bekaa Caza to the East and Saida Caza to the South. The total area sums up to 317 km^2 (3% of Lebanon's total area). It extends 24 km from north to south and spans 32 km from east to west at its widest point.

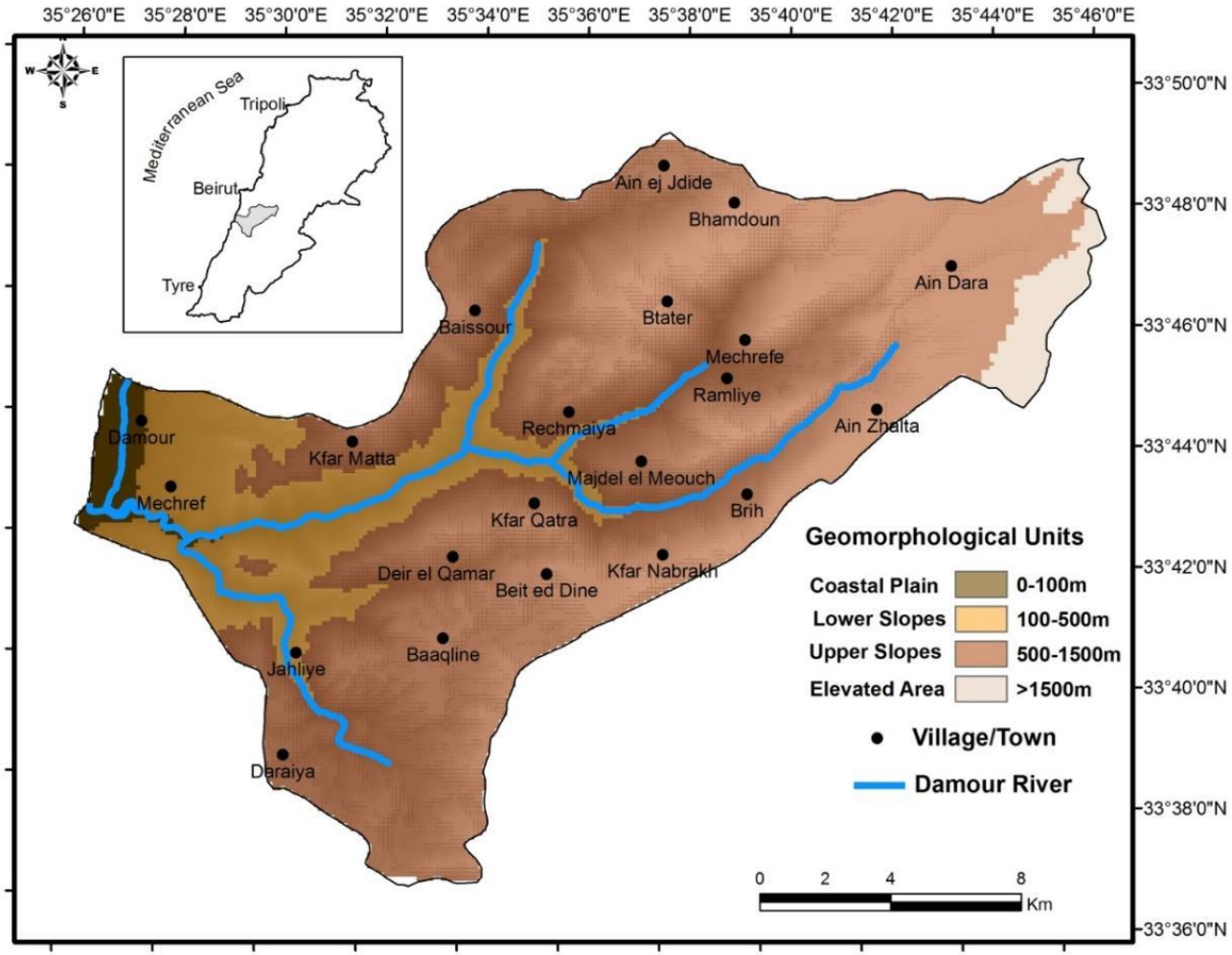

Figure 2.1 Study Area and its geomorphologic unit

2.2 Geomorphology

The geopmorphological units of the Damour river are distinguished from west to east depending on different altitudes and topo mass distribution as follows:

- The coastal plain, occupying around 3%, is narrow, less than 5 km in width and less than 100 m in altitude, and covered by dense clusters of urban congregations. It is dominated by carbonate rocks of the Middle Cretaceous and overlain by alluvial and beach Quaternary deposits.
- The uplifted faulted and folded Mount Lebanon, parallel to the shoreline, running the entire length of the area with a SSW-NNE trend with elevations ranging between 100 m and more than 3000 m. It dips steeply seaward, with an east-west gradient of 75-100 m/km. It can be further divided into two major parts:

- The lower slopes (17%) cover almost all the rock units existing in the study area. They lie parallel to the coastline with an elevation between 100-500 m. The width averages about 10 km.
- The upper sloping plateaus (77.6%) range from 500 to 1500 m in elevation. They are dominantly of the Jurassic, Lower Cretaceous and Cenomanian age. Valleys are deeply incised with scattered villages. The elevated crests exceed 1500 m altitude and are made up of the Cenomanian limestone and dolomitic limestone occupying 2.4%.In this zone, villages are sparse and human action is limited to quarrying leading to massive landscape degradation and occasionally to slope instability.

2.3 Geology

According to the 1:50,000-scale geological maps of Lebanon (Dubertret, 1945), the study area has a predominance of calcareous shale as well as marly limestone and dolomitic limestone. They are highly jointed and fractured carbonates and friable units.

The Jurassic rocks occupy 20 km^2 comprising around 6.3% of the study area and are subdivided into Middle and Upper Jurassic as seen in **Figure 2.2**.

Middle Jurassic

Callovian (J4): massive, thick bedded, fractured and karstified dolomites and dolomitic limestones with marl intervals.

Portlandian (J7): oolitic limestone with marly limestone intercalations. This unit is an unconformity and is thus absent in many localities indicating a non-depositional or at the level of differential erosional period during the late Jurassic uplift.

Cretaceous

At the end of the Jurassic, further tectonism continued to occur in the region. There was a widespread eruption of basalt lava and ashes from a number of vents. The tectonic phase and volcanism were temporary and the area underwent block faulting with emergence and erosion that lasted for ten million years or so, resulting in the deposition of the sandy Lower Cretaceous.

During that Early Cretaceous, Lebanon was covered by a series of swamps, rivers and deltas which gave a widespread sequence of sands and shales. During the latter part of the Early Cretaceous, sea level began to rise and marine incursions became increasingly dominant. The Late Cretaceous witnessed a high sea level transgression which contributed to thick sequences of limestones. The Cretaceous rocks comprise the major rock body in the area, occupying 283 km^2, i.e. 89.2%.

Lower Cretaceous

Neocomian-Barremian (C1) is composed of fractured, quartzitic and calcareous continental sandstone, with intercalations of siltstones and clays, with locally interbedded lignite, to near-shore shales and sandy limestone. The porosity of the sandstones is reduced due to the presence of the impermeable clay beds.

Lower Aptian (C2a) is a moderately thick-bedded, clastic limestone, interbedded with marly argillaceous sandy limestones and shales.

Upper Aptian (C2b) (muraille blanche) is a massive, thick bedded, jointed, stylolitic, partially karstified limestone and dolomitic limestone. The volcanism that began in the Upper Jurassic persisted throughout the Lower Cretaceous (bC2b)

Albian (C3) is made of thin-bedded, marly limestone and shales, upgrading into moderately thick-bedded limestone, interbedded with marl. Its distribution is patchy in Mount Lebanon.

Late Cretaceous

Cenomanian (C4) is the most dominant formation in the study area. It is formed of chert-bearing, massive to thinly bedded, highly fractured and jointed outcrops. It is a well karstified limestone and dolomitic limestone.

Senonian (C6) made up of marl and marly limestone, altering from massive to jointed, fractured to soft, and friable in some localities.

Quaternary

Pleistocene (qd): dunes and alluvial deposits, covering 2.38% of the region, from which scree (eboulis) are dominant (1.28%) and well distributed in the upper slopes and elevated crests of the area. They are followed by siltstones (1.1% of the area) indicating a big water retention, inducing MM.

Holocene (qat): Alluvial terraces, occupying 2.12% of the area. They are constituted by fluvial terraces (1.8%), beach terraces (0.01%) and tuffs (0.01%) in the lower slopes, while alluvial terraces are prevailing in the coastal plain. Fluvial and alluvial terraces are nearly equally distributed in the area, with a higher distribution dominance than beach terraces and tuffs.

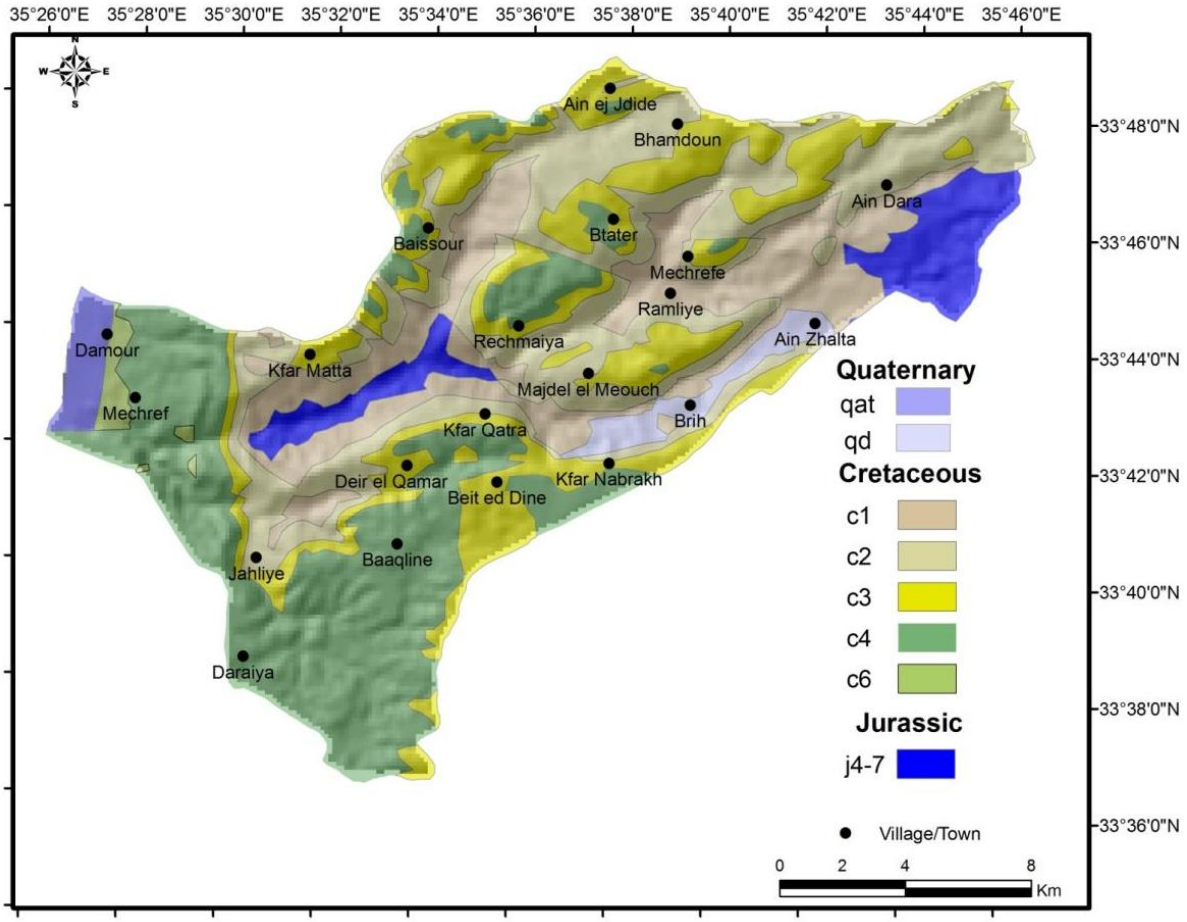

Figure 2.2 Simplified Geologic Map of the study area

2.4 Soils

The soils of Lebanon have been well studied by many researchers: Gèze (1956) and Darwish and Zurayk (1987). The dominant types of soils in the study area are shown by the soil map of Lebanon established by Gèze (1956) at a scale of 1:200,000 (Figure 2.7). The characteristics of the different soils covering the study area are detailed in **Table 2.3**.

Twelve different soil units were identified of which eight are pure soil types and four are soil associations (**Figure 2.3**). Among these soil associations, three represent association of two "soil types" and one is formed with association of three "soil types" (Gèze, 1956). These soils are typically Mediterranean in character. The most widely represented soils are Alluvium assocciated with rossa (red mountainous soils) occupying an area of 146.9 km^2.These soils reach a thickness ranging between 110 and 165 cm and have a well-developed profile. Generally, they are decarbonated, rich in iron oxides (e.g., hematite and goethite), with a neutral to a slightly acidic pH value (6.7-7.2) and high clay content (30 to 50%). These soils are of a strong surface structure, with medium gravel size (5-35%) and organic matter (2-2.5) contents, compacted in the subsoil, thus having a low to moderate infiltration rate (2.0-6.0 cm.h1). Over saturation of these soils with water leads to loss of entire soil strength and hence soil movement (Darwish, 1988; Darwish and Zurayk, 1997).

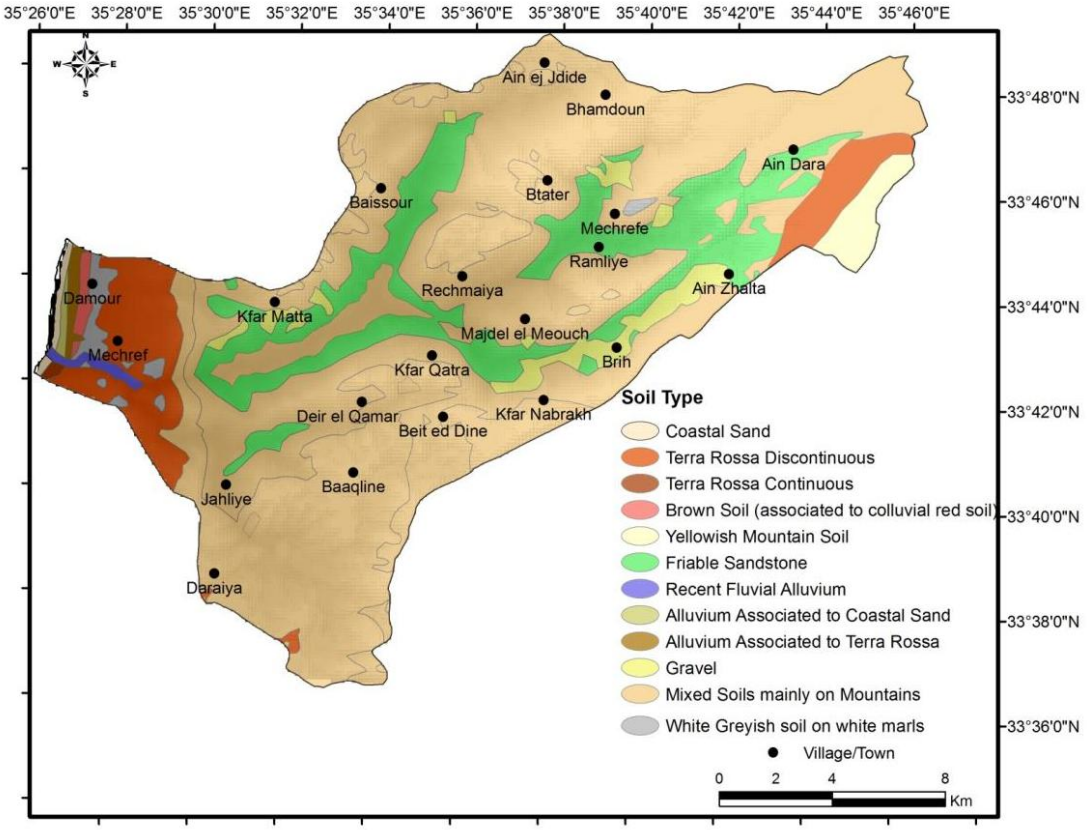

Figure 2.3 Soil Map of the study area

2.5 Land use

A recent land use map at a scale of 1:20,000 was adopted from a project done by the Lebanese National Council for Scientific Research and the Lebanese Ministry of Agriculture (LNCSR-LMoA, 2010) based on CORINE (Coordination des informations sur l'environnement) Land use methodology (level 4).This map was established using a visual interpretation of pan-sharpened Landsat TM (30 m) acquired in October 2010. Mainly six categories (or classes) were plotted: (1) Forests and natural areas, (2) agricultural lands, (3) bare lands, (4) wetlands (5) artificial areas **(Figure 2.4).** Each class in turn can be further subdivided into a number of sub-classes. The land use or vegetation cover plays a significant role in slope stability. Many studies accentuated the importance of vegetation cover or land use characteristics on slope stability (Van Beek and Van Asch, 2004; Karsli et al., 2009; Corminas et al., 2014) and used them to evaluate the conditioning factors of the Mass Movement.

1) Damour's natural vegetation occupies about 36% of the watershed area with 25% wooded lands and 11% shrublands. Pinus brutia and Cedrus libani and broadleaves trees, such as Quercus calliprinos and Quercus infectoria. The Pinus brutia are the most widespread trees (59%). They appear on the Jurassic (J6) and Cenomanian (C4) rocks and on the red, yellowish, sandy and mixed soils.

2) Agricultural land however occupies 29% including mainly olive trees and greenhouses. These lands can be either cultivated by one type of crop, such as olive trees, or by a combination of field crops or fruit trees. Bad irrigation practices and excess input of fertilizer application are common in the study area inducing the spread of secondary soil salinization which results in the destabilization of soil aggregates. This reduces soil water holding capacity, enhances runoff and increases sliding.

3) Bare lands are ascribed to the unexploited and unemployed terrains that are dominated by rocks, soils and beaches. These lands constitute 22.81% of the study area.

4) Water bodies include water surfaces such as lakes and rivers. They are very local patches occupying only 0. 38% of the study area.

5) Artificial Areas grouped into discontinuous and continuous urban areas, activity zones (industrial areas), artificial green zones, roads/highways, material extraction (quarries), embankments, etc. They occupy 11.32% of the study area with 9.36% for the discontinuous urban. The area comprises 127 villages that are part of the cazas (within larger governates divisions, i.e. the Mohafazats) of Aley (56 villages) and Chouf (71 villages) belonging to

Mohafazat (or governorate) of Mount Lebanon. The density of urban settlements is concentrated on the coastal stretch. Population increased from 221.000 inhabitants in 1997 to more than 310.000 in 2008 which is almost a 30% increase in 11 years. This rapid urban chaotic growth is one of the principal causes of natural resources depletion that leads to induce natural hazards such as desertification, mass movements, flash floods, etc. Moreover, The associated urban sprawl, road construction and excavation works are possibly reducing the local shear strength of these shale and limestone environments, making them more susceptible to mass movements. The problem will be aggravated since no attempt has been made to stabilize mountain slides and abandoned rock quarries in the perspectives of rehabilitation and restoration.

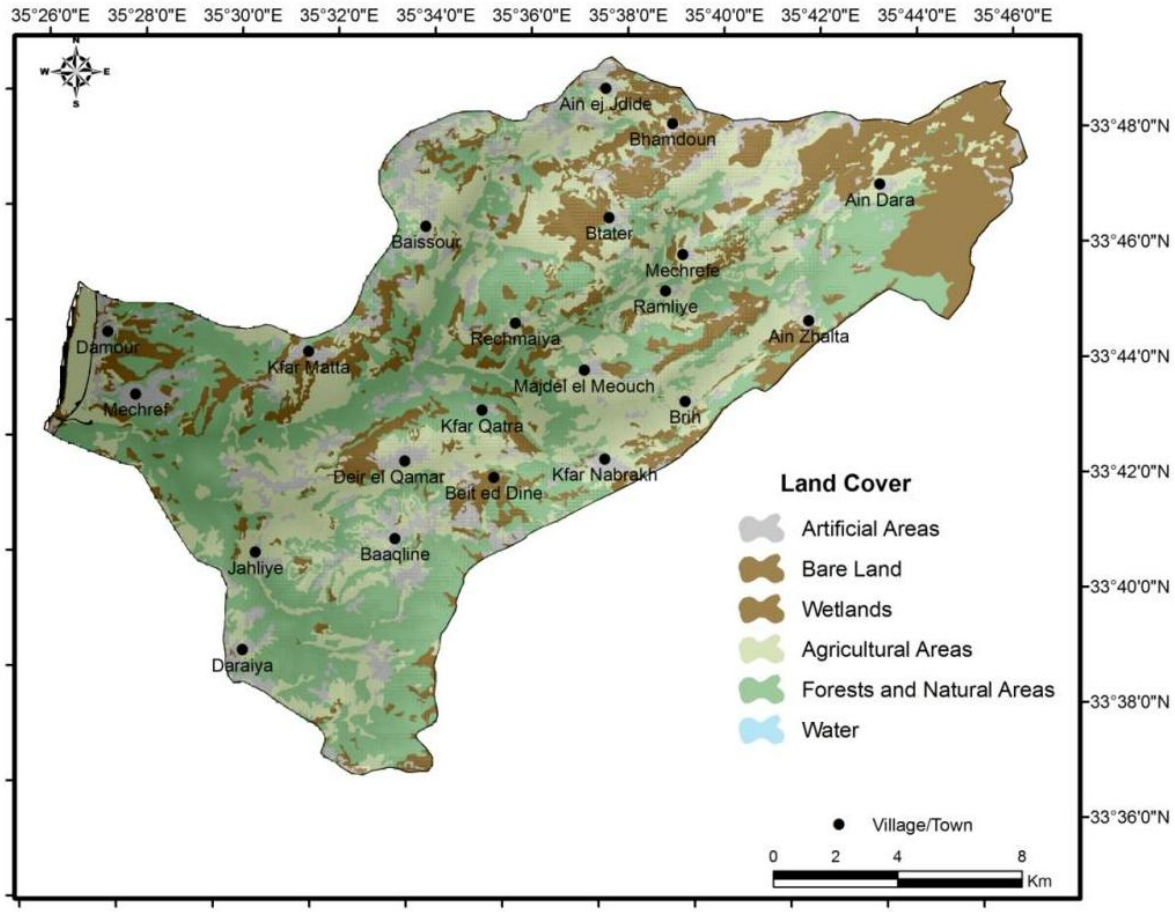

Figure 2.4 Land use map of the study area based on CORINE classification of Level 1 description

2.6 Climate

Annual rainfall ranges from 700 mm to over 1400 mm. Most of the rainfall (75% to 80%) takes place between November and March (the winter season) hence very negligible amounts of precipitation occurs during the hot and dry months of June, July and August and average daytime temperatures exceeding 33°C. This reduces the moisture content of forest litter to below 5%.Furthermore, the summer and eastern dry autumn winds distinguished by high speed and

strong dehydrating potential intensify the situation (Mitri, 2010). According to the available pluviometric map at 1:200,000 scale (Plassard, 1971), the annual precipitation rate ranges between 700 mm on the coastal plain and more than 1400 mm over the crests, and decreases again to 700 mm in the elevated plateaus of Mount Lebanon facing the Bekaa valley **(Figure 2.5)**. The huge mountain mass is an effective barrier to all moist-laden winds or cold fronts coming from the Mediterranean sea. Thus, there is an increase in the amount of rain from west to east (coast to inland), i.e. an altitude-related phenomenon. Significant portions (33%) of the area are under rainfall quantities ranging between 1100 and 1300 mm/year.

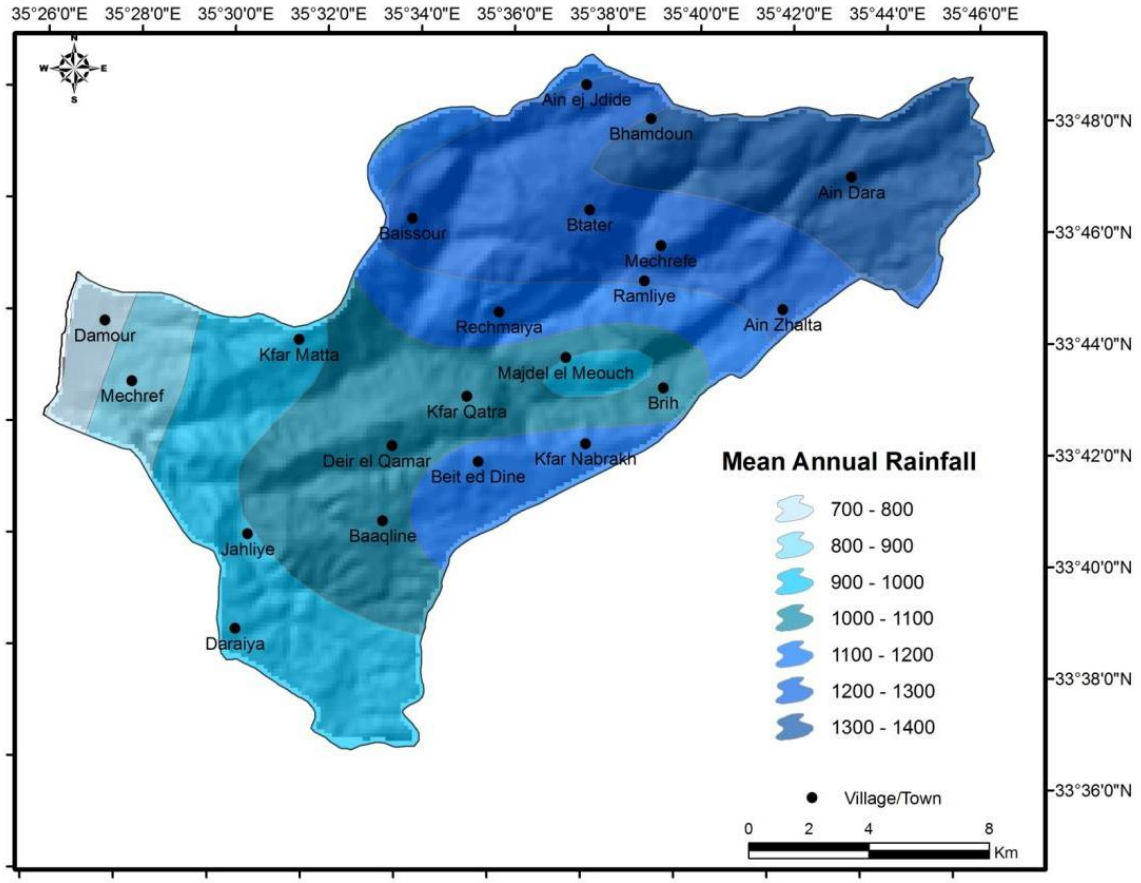

Figure 2.5 Rainfall map of the study area

Most of the rainfall and snow takes place during the period extending from November to March (period responsible for 75-80% of precipitations with a climax in January which at some instances yields about 160-180 mm/month).

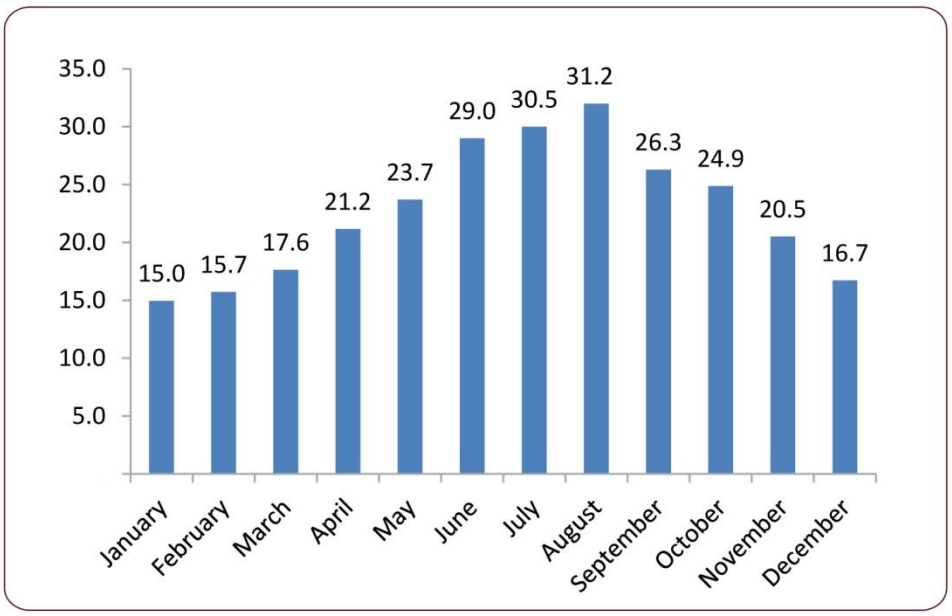

Figure 2.6 Average Monthly Temperature of Damour Watershed for the years 1984-2012

Dryness takes over again from April to October. During this period of increasing average temperatures aittaining almost 32°C **(Figure 2.6)** and precipitation decreasing to almost zero mm **(Figure 2.7)**, evaporatranspiration is calculated in an attempt to assess water loss from open water bodies and plants.

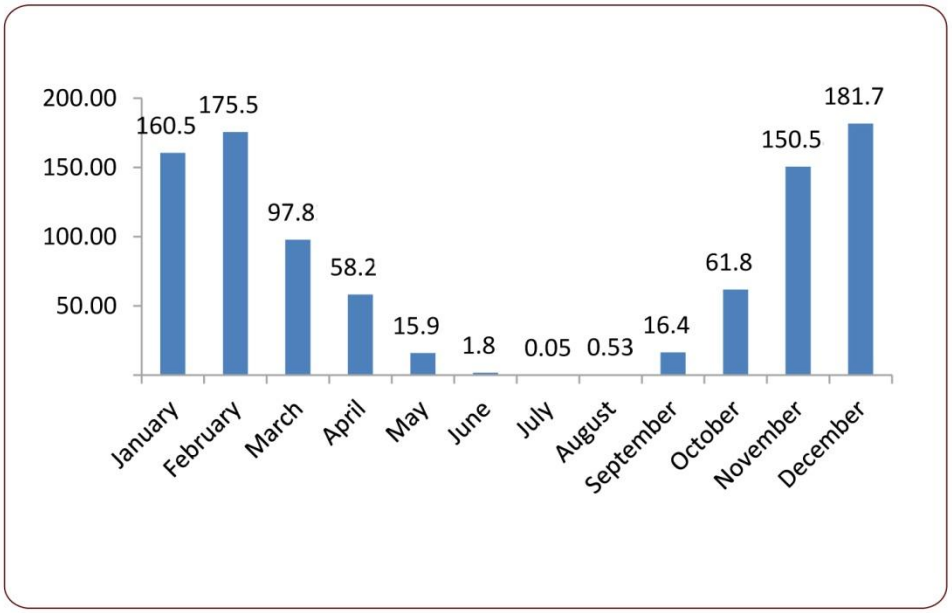

Figure 2.7 Average Monthly Precipitation of Damour Watershed for the years 1984-2012

Dryness takes over again from April to October. During this period of increasing average temperatures aittaining almost 32°C **(Figure 2.6)** and precipitation decreasing to almost zero mm.

The potential evapotranspiration (PET) is an integrated climate parameter depends on climatic factors (Easterling et al., 2007; Corti et al., 2009). Evapotranspiration, as an important component of the hydrologic cycle, affects the availability of water (Burn and Hesch, 2007). It is water lost to the atmosphere through two processes which are evaporation (water lost from open water bodies such as lakes, snow, wetlands as well as bare soil) and transpiration (water lost from living plants). Evapotranspiration depends mainly on solar temperature, relative humidity wind and solar radiation hence it changes with latitude, time of day and season of year (Hanson, 1991).

This chapter demonstrates the susceptibility of the area to MM is due to a combination of weak geology, steep slopes, intensity rainfall events, active tectonic movements, being categorized as a catastrophic forest fire zone by the Ministry of Environment and rapid land use change. In truth, the chaotic urban expansion Damour watershed has aggravated the MM impacts since a large portion of the population occupies areas with high MM hazard. Therefore, due to the lack available MM susceptibility studies and maps of the study area, especially due to Forest fire events, it is crucial to develop MM susceptibility analysis enclosing the preconditioning factors and Forest Fire as the inducing factor for or sustainable management plans. For this reason, the following chapter will focus on the utilization of different satellite imageries and various processing techniques that help in MM delineation. Similarly, GIS can assist the incorporation of multiple layers explore MM cause effect relationships and susceptibility zonation.

CHAPTER 3 Analysis of the potential effect of Forest fire on Mass Movement in the study area

3.1 Introduction

The severity of Mass Movement issues worsen in the midst of increased urban development and change in land use in addition to weak geological structures, steep and rugged land surfaces and extreme climatic conditions resulting in a high degree of fragility (Vijith et al., 2009). In the study area, mass movement occurrence has increased by almost 60% between 1956- 2008. Similarly, forest fire has emerged as another hazard and has destroyed over 25% of forests in less than 40 years. For this reason, forest fire burn severity was introduced as a potential mass movement inducing factor.

The identification of Mass Movement-prone regions is essential for carrying out quicker and safer mitigation programs, as well as future strategic planning of the area. It is known that a Mass Movement susceptibility map relies on a rather complex knowledge of slope movements and their controlling factors. GIS-aided Mass Movement susceptibility mapping involves various techniques that can be considered as either qualitative or quantitative. Qualitative methods rely on expert opinions, and are frequently used for regional assessments (Aleotti and Chowdhury, 1999; Van Westen et al., 2003). In order to remove subjectivity in the analysis, many statistical methods have been utilized for Quantitative techniques rely on observed relationships between controlling factors and Mass Movement (Guzzetti et al., 1999). Following the standardization of the effect factors into layers using geographic information systems (GIS), the weight factor (W_f) of each layer for inducing mass movement was evaluated using the modified InfoVal method, and an mass movement susceptibility map was generated and classifyied into different susceptibility zones. Preceded only by soil, the NBR obtained the highest W_f, making forest fire burn severity the second-highest impacting factor on mass movement occurrence in the study areas. This chapter demonstrates the potential effect of forest fire on mass movement occurrence in Damour compared to the most influential preconditioning factors, such as soil type, geology, rainfall, and slope gradient as summarized in the below workflow diagram.

3.2 Mass Movement Inventory Map Production

Mass movement inventory maps are prepared for various purposes including (i) studying the evolution of landscapes dominated by mass-wasting processes (Malamud et al., 2004; Guzzetti et al., 2008; Parker et al., 2011) (ii) as a preliminary step towards MM susceptibility assessment (Bălteanu et al., 2010; Pradhan and Lee, 2010; Pourghasemi et al., 2012). A MM inventory map portrays the location, numbers and other data of occurrence and the types of mass movements. MM maps are classified by their scale and the type of mapping (Guzzetti et al., 2000; Galli et al., 2008). Small-scale (<1:200,000) are compiled mostly from data obtained by searching journals, technical, and scientific reports, or by interviewing MM experts (Glade, 1998; Salvati et al., 2009). Medium-scale MM inventories (1:25,000 to 1:200,000) (Duman et al., 2005) are prepared through the systematic interpretation of aerial photographs at print scales ranging from 1:60,000 to 1:10,000 (Guzzetti et al., 2012). Large-scale inventories (>1:25,000) are prepared, usually for limited areas, using both the interpretation of aerial photographs, very high resolution satellite images and digital terrain models, in addition to extensive field investigations (Ardizzone et al., 2007; Ghosh et al., 2012) which were conducted and described in the following sections. A detailed and accurate MM inventory is an essential part of MM susceptibility analysis. An ideal inventory would cover the entire area and include all of the MM that are possible to detect down to sizes of 1–5 m in length. MM must also be located accurately and mapped as polygons illustrating their shapes. Such mapped MM distributions can then be used to perform MM susceptibility analysis in addition to other quantitative analyses. In recent years, advances in technology have resulted in the accessibility of satellite imagery with sufficiently high resolution to identify MM.

3.2.1 Visual Interpretation of Mass Movement and Forest Fire Mapping

Visual interpretation, a remote-sensing (RS) technique, was used to detect the distribution of mass movements over the study area. Such techniques offer promising possibilities for identifying and securing information on mass movement and Forest Fire detection in several difficult-to-access, rugged mountainous landscapes that are present throughout this area. An inventory was compiled to establish an understanding of the mass movement status in our study areas.

Visual interpretation of stereoscopic aerial photographs remains widely adopted since it is considered by geomorphologist as an intuitive process that does not require complicated technological skills (Ardizzone et al., 2013); The size (commonly 21 cm×21 cm) and scale of the

aerial photographs allow for the coverage of large territories with a reasonable number of photographs in our case 17 photographs; and the availability of multiple sets for the same area allows investigating the temporal and the geographical evolution of slope failures (Fiorucci et al., 2011). Using ERDAS Leica Photogrammetry Suite version 9.0, aerial photos of the year 1956 were orthorectified. The scale of photography was 1:10000, scanning resolution 600 dpi, camera flight height was 3125m and focal length was 125.000 mm. Therefore, photo pixel resolution which is obtained by dividing Photography scale by Scanning resolution (10000/600) is 16.6 inches which is equivalent to 42 cm. However, aerial photographs of 2008 had a photo pixel resolution of 30cm **(See Figure 3.1)**.

On the other hand, visual interpretation of passive sensor imagery, in this case multispectral Ikonos 2005 with spatial resolution of 80cm depends not only on spectral signatures but also on other properties such as reflectance of the earth's surface and neighborhood context (Chorowicz and Deroin, 2003). Ikonos images were draped on a 10m resolution DEM in order to create a 3D visualization and improved morphological information to a planimetric image interpretation (Nichol et al., 2006). Various types of mass movements (landslides, rock and debris falls) were delineated in the study area. For landslides as seen in **Figure 3.2a** displaced rocks like sandstones, limestone, or marls, are moving upon clay, soil moisture of MM will be low, and vegetation cover will be poor. Hence, light toned areas appearing in the VIS-NIR range can then give an idea about fresh landslides (Abdallah et al., 2007). As for rock and debris fall as seen in **Figure 3.2b, 3.2c, 3.2d**, they tend to have the same spectral signature. The neighboring context however facilitates the distinction.

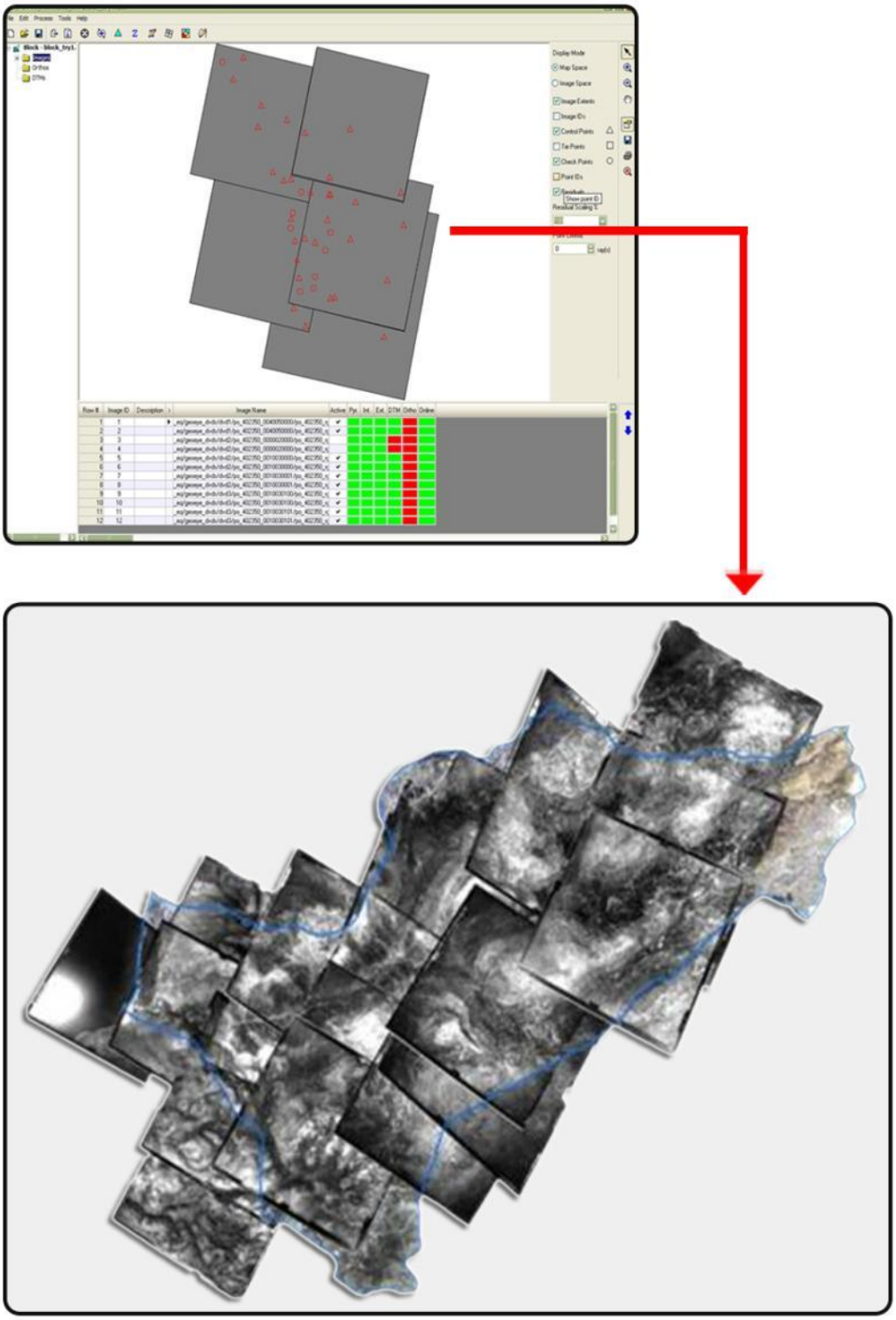

Figure 3.1 Orthorectification of Aerial Photos using ERDAS LPS

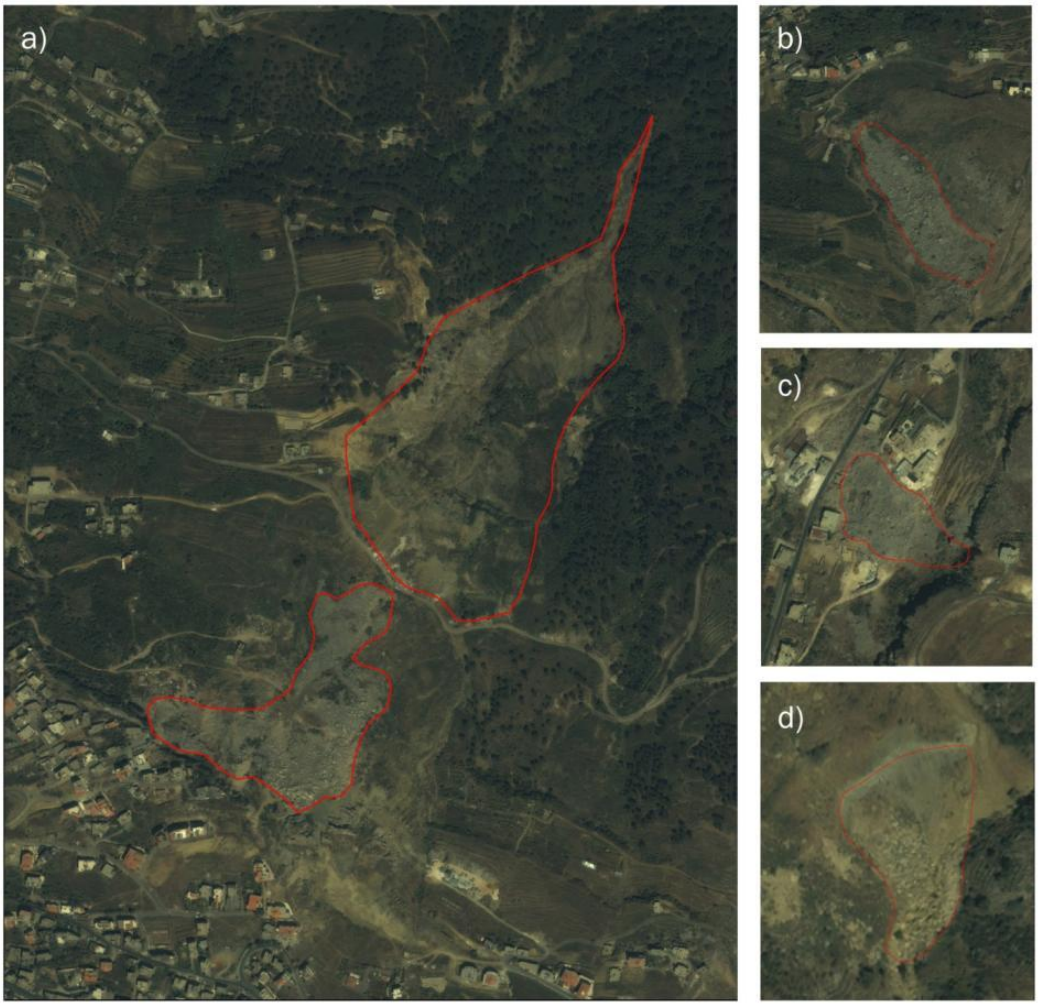

Figure 3.2 Mass Movement delineation using IKONOS satellite images 2005

Google earth timeline was also used for mass movement and forest fire detection and delineation in order to fill in the gap in aerial and satellite images. Furthermore, the 3D terrain **(Figure 3.3)** facilitates the geomorphic analysis and verification of previously delineated mass movements and forest fires.

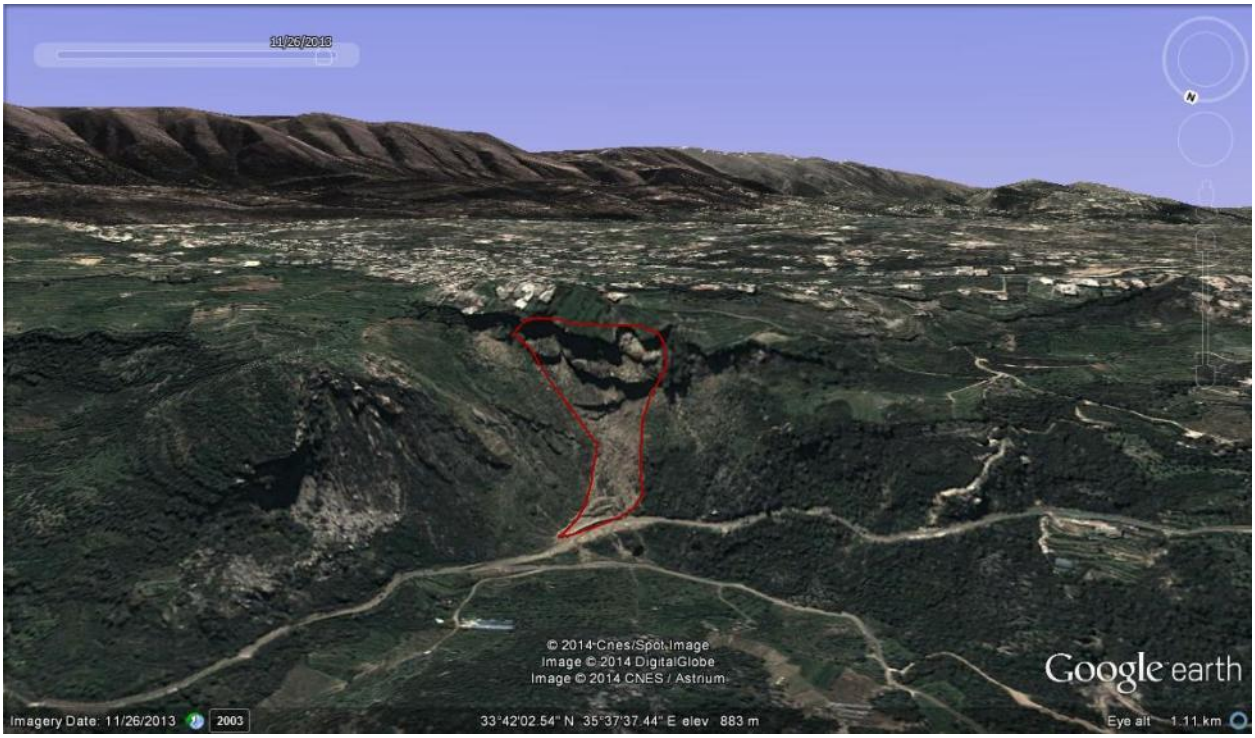

Figure 3.3 Google Earth 3D terrain for enhanced visual interpretation of Mass Movement

Table 3.1 explains in details the number of MM detected through visual interpretation of each photo type in addition to the percentage of the increase in detected MM over the years.

Table 3.1 Number and percentage of Mass Movement delineated between 1956 and 2012

Source/Year	Number of MM	% increase
Aerial photography 1956	389	
Ikonos satellite imagery 2005	574	47%
Aerial photography 2008+ Field investigation 2012	694	21%

On the other hand, fire affected areas can be distinguished due to the strong contrast with the unburned areas. Fire scars appear dark due to the deposition of black char, which suppresses the reflectance in the visible (R), and near infrared (NIR) wavelength bands. Maps of fire affected areas was generated by delineating observed burn scars (Liew et al., 1998). These maps provide information on the spatial extent and distribution of the fire affected areas, and the total area burned.

Even though aforest fire inventory map was compiled using the same images as MM inventory, and although delineated FF indicate the locations of recurrent forest fires consequently provide

locations with higher land instability factor, FF maps will not be introduced into the MM susceptibility model. They will be used as a guide for field investigation for infiltration measurement and map validation. However, and since, burned areas generally show a higher reflectance in the 1.6 μm band (SWIR) compared with the surrounding unaffected forest, a RS burn severity index, the Normalized Burn Ratio (NBR) discussed below will be inserted as the inducing factor affecting MM occurrence since as discussed earlier, fire event by itself is not an indicative of possible changes in hydrological and geomorphological characteristics of an area (Campo et al., 2006). FF burn severity should be assessed.

3.3 Burn Severity Estimation Using Remotely Sensed Data

Forest Fire burn severity extraction was achieved using the most common satellite imagery derived burn severity indices are the Normalized Burn Ratio (NBR) (Epting et al., 2005; Soverel et al., 2010; De Santis et al., 2010; Schroeder et al., 2011). After a fire, a sequence of spectrum changes occurs due to the fire consuming the vegetation, destroying the chlorophyll, leaving the soil bare and changing its moisture content (Escuin et al., 2008). NBR is based on the difference between the Near Infrared (NIR) and Middle (MIR) or Short Wave Infrared (SWIR) as seen in **Equation 1** where:

$$NBR = (NIR - MIR)/(NIR + MIR) \quad (1)$$

The NIR band is predominantly reliant on the leaf morphology index and discontinuities within the leaf and sensitive to changes in vegetation cover, so a decrease in cover due to combustion causes a decrease in NIR reflectance. The SWIR and MIR wavelengths are sensitive to changes in water content in soils and vegetation associated with a fire increases MIR reflectance is sensitive (Avery and Berlin, 1992; Key and Benson, 2006). Therefore, the effect of a forest fire is to decrease NIR and increase MIR/SWIR so more negative NBR values tend to be associated with greater burn severity (Epting et al., 2005).Multispectral RS devices such as Landsat Thematic Mapped (TM) and Enhanced Thematic Mapped Plus (ETM+) can identify modifications in the near-infrared (NIR 0.76–0.96μm) and short-wave infrared (SWIR 2.08–2.34μm) bands 4 and 7 respectively. Practical data ranges from approximately –500 to +1,300 when scaled by 10^3 (FIREMON, 2004). Burn severity is generally classified into low, moderate and high (Bento-Gonçalves et al., 2012). Since there is not a common rule to group the NBR ranges into these fire severity classes, the class divisions are prone to subjectivity (Roy et al., 2006; Menga and Meentemeyer, 2011). We formed three main severity classes as follows: low (-500 to +99), moderate (+100 to 659), and high (+656 to 1,300). Values less than approximately -550 or greater

than approximately +1,350 may occur but are typically not considered burned. In this case Equation 1 becomes **Equation 2**:

$$NBR = (NIR - SWIR) / (NIR + SWIR) = 1000(B4 - B7)/ (B4 + B7) \quad (2)$$

LANDSAT imagery was used since it offers moderate spatial resolution (30 m), is freely accessible, and has the longest archive of highly calibrated, multispectral data for change detection applications.

Even though dry summers, typically from June to September, offer great opportunity for cloud free images, forest fires tend to occur in this period making it difficult to assess burn severity. October is on average between the end of the fire season (post-fire) and the first precipitation. All of the analyzed Landsat satellite images are October images and of similar acquisition time between 7:30 and 8:10 am (**Table 3.2**) since they should match phenologically in order to avoid any misinterpretation for the post-fire comparison (Lhermitte et al., 2008) especially to changes due to solar illumination changes.

Table 3.2 Aerial and satellite images that were used in the process of mass movement (MM) and forest fire (FF) detection and delineation for GIS database compilation

Image	**Resolution**	**Purpose**
Aerial Image 1956	40 cm	MM and FF delineation
Ikonos 2005	80 cm	MM and FF delineation
Aerial Images 2008 date complète	30 cm	MM and FF delineation
Google Earth Timeline		MM and FF delineation
Landsat 5 (TM) 24/10/1984	30 m	NBR and NDVI extraction for Damour Watershed
Landsat 5 (TM) 30/10/1986	30 m	NBR and NDVI extraction for Damour Watershed
Landsat 5(TM) 1/10/1987	30m	NBR and NDVI extraction for Damour Watershed
Landsat 4 (TM) 6/10/1992	30m	NBR and NDVI extraction for Damour Watershed
Landsat 5(TM) 15/10/1998	30m	NBR and NDVI extraction for Damour Watershed
Landsat 7(ETM+) 18/10/2002	30m	NBR and NDVI extraction for Damour Watershed
Landsat 5(TM) 5/10/2006	30m	NBR and NDVI extraction for Damour Watershed
Landsat 7(ETM+) 15/10/2008	30m	NBR and NDVI extraction for Damour Watershed

Image	Resolution	Purpose
Landsat 7(ETM+) 5/10/2009	30m	NBR and NDVI extraction for Damour Watershed
Landsat 7(ETM+) 9/10/2010	30m	NBR and NDVI extraction for Damour Watershed
Landsat 7(TM) 11/10/2011	30m	NBR and NDVI extraction for Damour Watershed
Landsat 7(ETM) 13/10/2012	30m	NBR and NDVI extraction for Damour Watershed

Eventhough widely used, NBR has been criticized by many users like Roy et al. (2006) and Verbyla et al. (2008) as being sensitive to the effect of the topography of the area at hand especially in high latitudes where a low sun angle may enhance the topographic effect. But the application of a ratio-based remote-sensing index has been recommended to reduce topographic effect on spectral response (Short 1982; Key and Benson 2005). Based on this rationale, most studies using NBR have assumed the effect of topography on spectral response to be minor and can usually be ignored (Matsushita et al. 2007)

But in May 2003, the scan-line corrector (SLC) of Landsat ETM+ failed permanently. Without an operating SLC, the Enhanced Thematic Mapper Plus (ETM+) line of sight traces a zig-zag pattern along the satellite ground track making images unexploitable. For these reason, the attained images where treated using a gap filling techniques as it shows in the following paragraph.

3.3.1 Gap-Filling LANDSAT 7 SLC-off Single Scenes

As explained by the US Geological Survey (2013), The SLC-off effects are most pronounced along the edge of the scene and gradually diminish toward the center of the scene. The middle contains very little duplication or data loss, and this region of each image is very similar in quality to previous ("SLC-on") Landsat 7 image data. An estimated 22% of any given scene is lost because of the SLC failure. The maximum width of the data gaps along the edge of the image would be equivalent to one full scan line, or approximately 390 to 450 meters. The precise location of the missing scan lines will vary from scene to scene.

Maintaining the continuity of the ETM+ images' SLC is crucial, and thus, methods have been developed to fill the data gaps to ensure the continuity of this longest satellite observation (Zhu et al., 2012). Gap filling was established through focal analysis which is designed to modify neighboring pixels using Erdas 9.1. But since any geostatistical interpolation method holds to some extend a degree of uncertainty, pixel mean distribution and standard deviation were

compared on every band level between pre-gap filling and post-gap filling (**Figure 3.4**) to verify that the process did not cause any image distortion. The distribution and standard deviation exhibited almost identical values on all band levels **(Figure 3.5)**. Furthermore, and in order to allows the full Landsat data set to be used in a quantitative sense, radiometric calibration of all Landsat images was performed.

3.3.2 Radiometric Calibration of LANDSAT images

Data continuity requires consistency in the interpretation of image data acquired by different sensors. Radiometric and atmospheric calibration is one of the most important steps before conducting a change detection analysis. Calculation of radiance is the fundamental step in putting data from multiple sensors and platforms onto a common radiometric scale (Chander and Markham, 2003). Band4 and Band7 raw data where transformed to Radiance (Li) which refers to any radiation leaving the Earth (**Equation 3**) and Reflectance (Ri) which refers to the ratio of upwelling to downwelling radiation (**Equation 4**) for calibration. Satellite sensors also record the intensity of reflected electromagnetic radiation for each pixel that is captured in a given scene from the Earth's surface as a digital number (DN) for each spectral band that the satellite acquires. A spectral signature with meaningful units can be compared from one image to another. This would be required where the area of study is larger than a single scene or if monitoring change at a single site where several scenes taken over a period of years are being compared.

$$Li = DNi * Gb + Bb \quad (3)$$

$$Ri = (Li * \pi * d2) / (Esib * cos(zs)) \quad (4)$$

Where : DNi = per-pixel raw brightness value; Gb and Bb = per-band gain and bias from scene header; d= daily earth-sun eccentricity from lookup table ; Esib = per-band exoatmospheric solar irradiance from published L5 and L7 tables; zs = per-scene solar zenith angle (90-solar elevation angle reported in scene header). Once Landsatimages are calibrated, NBR maps can be analyzed.

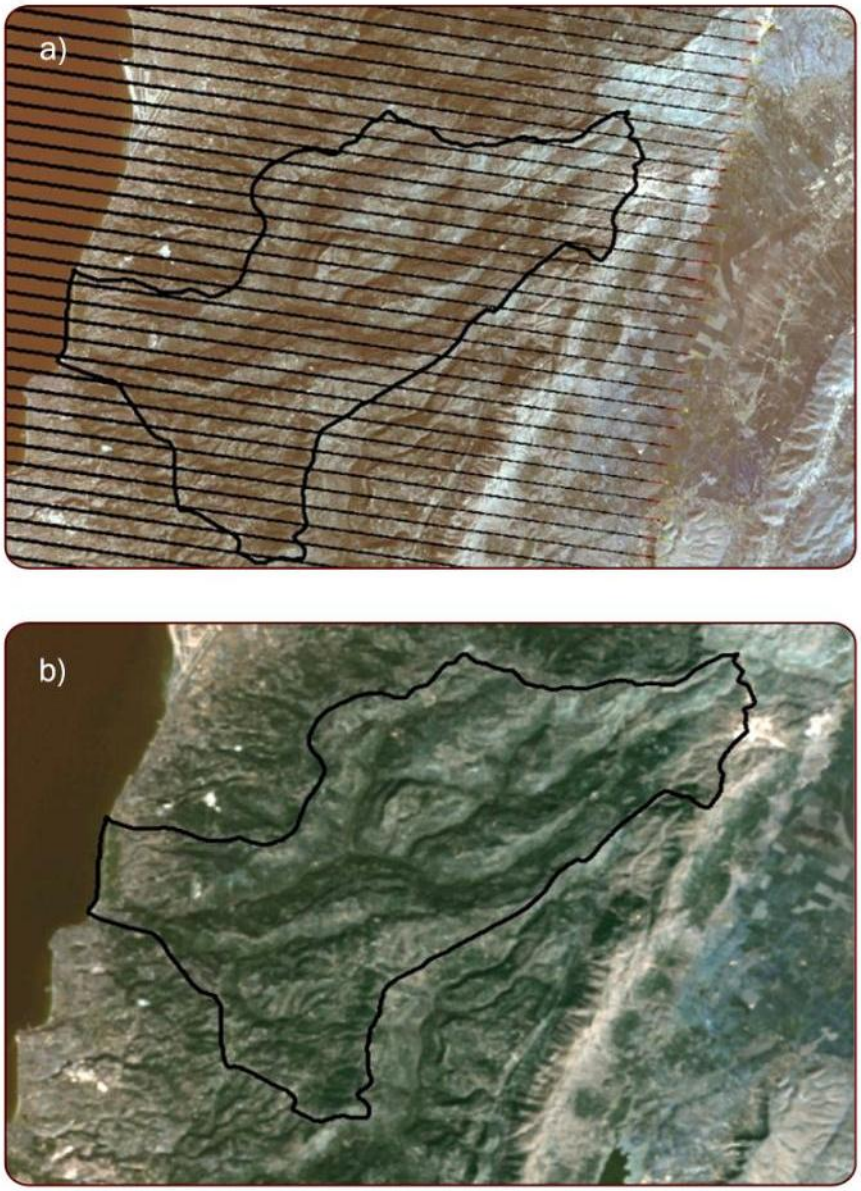

Figure 3.4 Damour Watershed pre gap filling (a) and post gap filling (b) Landsat 7 image (9/10/2010)

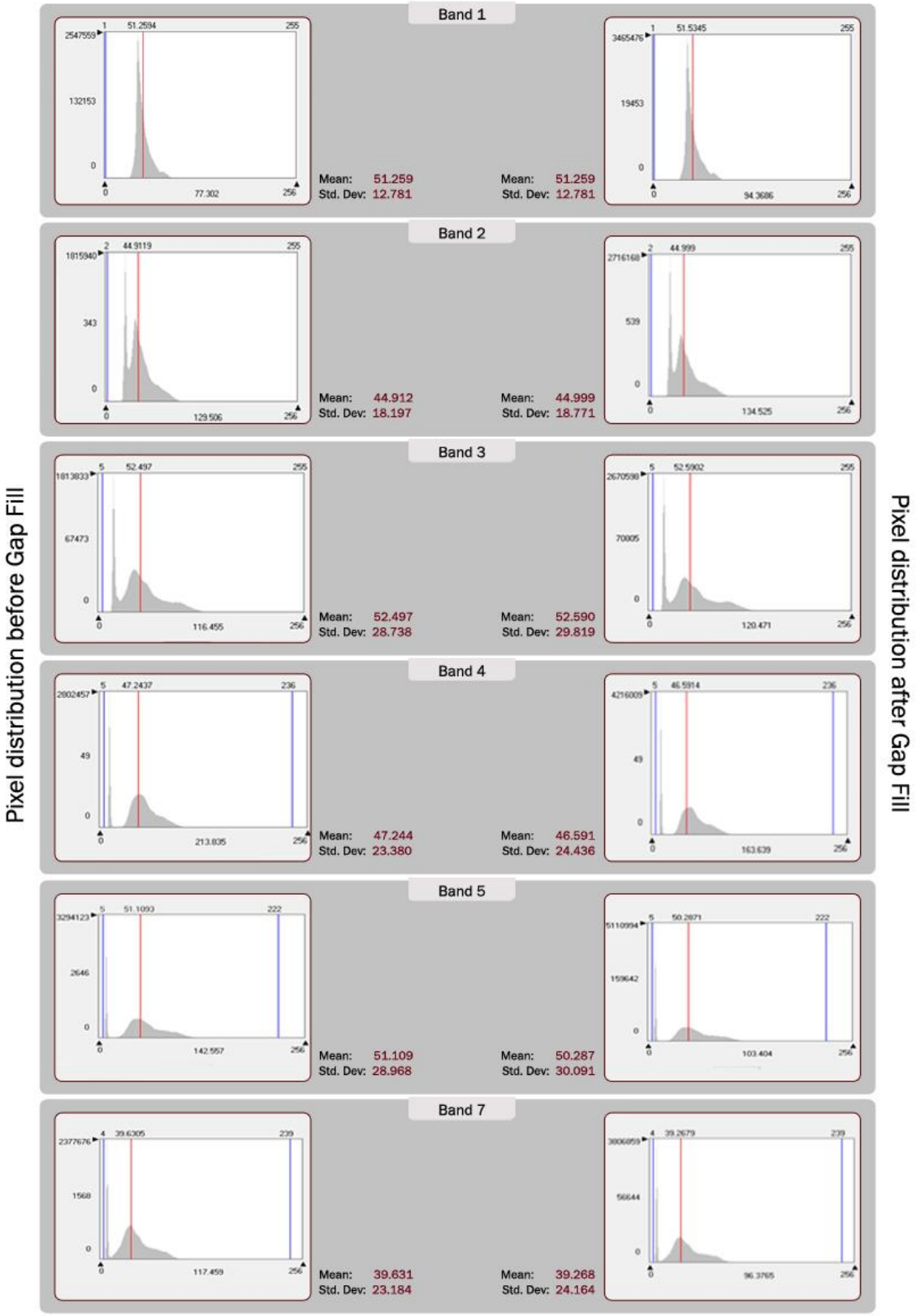

Figure 3.5 Comparison of pixel mean distribution and standard deviation of pre and post gap filling

3.3.3 Change detection of Normalized Burn Ratio Maps

Normalized burn ratio maps have been computed using **Equation 2.** As described earlier, NBR values were divided into three burn severity classes: High, moderate and low burn severity. As seen below in **Figure 3.6,** forest fires have the tendency to reoccur in the same place. Burn severity will eventually accumulate gradually into higher severity areas hence increasing soil water repellency and susceptibility to mass movement.

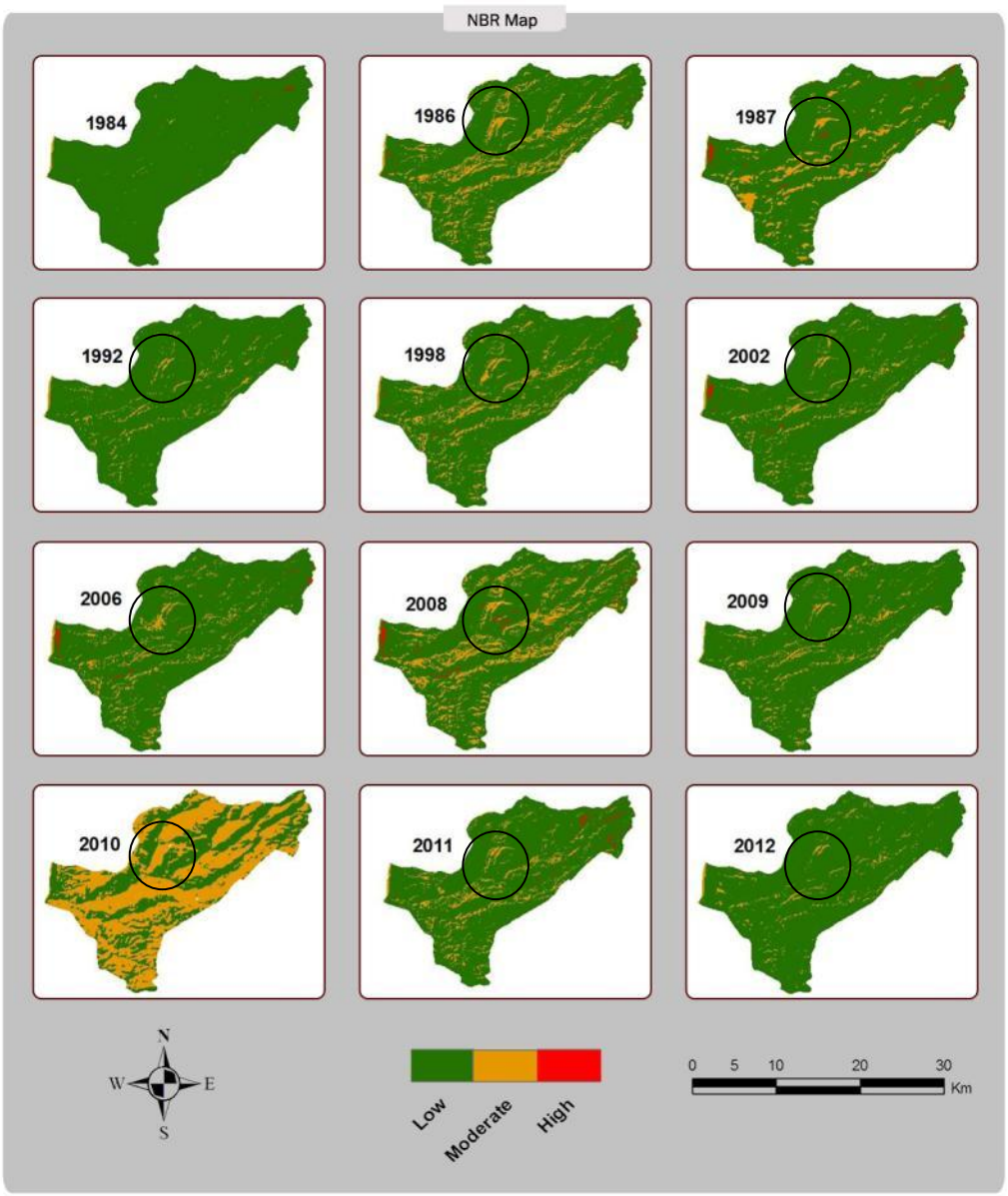

Figure 3.6 Normalized burn ratio (NBR) variation maps in Damour watershed showing the progression of burn severity from 1986-2012

3.3.4 Cumulative NBR map

Since many of the forest fire events were recurrent, the attained sites could have accumulated burn severity and water repellency hence lower water infiltration characteristics than sites attained once by fire events. For this reason and in an attempt to evaluate the current burn severity situation in the study area, NBR_c was introduced. NBR_c was extracted from the summation of all NBR maps and will be used later on as a base for the forest fire burn severity impacting factor in Mass Movement Susceptibility Map (MMSM). It represents the approximate burn severity status of the study area till date. It was calculated using ArcGIS 9.3 Raster Calculator with the following **Equation:**

$$NBRc = (NBR84 + NBR86 + NBR87 + NBR92 + NBR98 + NBR02 + NBR06 + NBR08 + NBR09 + NBR10 + NBR11 + NBR12)/12 \quad (5)$$

It might be argued that using NBRc values could give coarse results but several of the forest fires detected earlier through remote sensing and field investigation were recurrent events. Although water repellency duration of the soil after a fire varies from minutes to months (Doerr et al., 2004; Certini, 2005; Malkinson and Wittenberg, 2011), NBR values of the study areas did sustain the hypothesis of long term water repellency especially in recurrent fire event locations.

According to these recurrent fire locations; the forest fire inventory map and MM inventory map, an extensive binary forest fire and MM field investigation was performed.

3.4 Mass Movement Field Investigation

The fundamental data layer, representing previous Mass Movement, is a requirement to execute statistical analysis on the relation between the distribution of Mass Movement and impacting parameters. A total of 694 mass movements of various dimensions have been identified representing 7.1% of the watershed area (**Figure 3.7**).

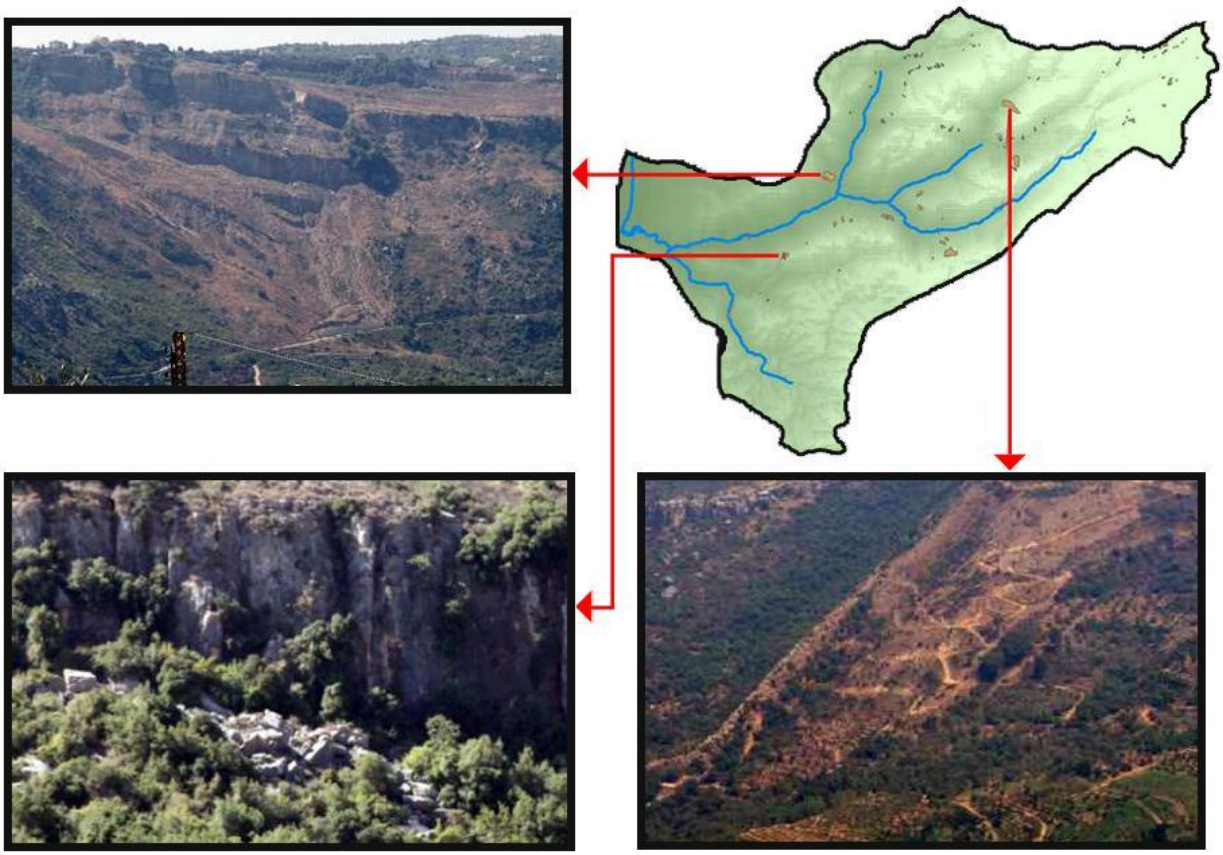

Figure 3.7 Mass Movement inventory field investigation

Field investigation was then performed (**Figure 3.8**) to (1) validate the interpretation of the satellite images, (2) verify features that can be attributed to mass movements but are not easily identifiable on the satellite images, and (3)support the relations between the mass movements and affecting factors. A field format was established for each mass movement location considering information related to the geology, soil, water, land use/use and slope, corresponding causes of mass movement, and human activities protecting against this phenomenon (**Annex 5** for field survey format).



Figure 3.8 Mass Movement delineation using Google Earth (on the right) vs. field investigation (on the left)

3.5 Forest Fire Burn Severity Field Investigation

Field investigation for remote sensing data (**Figure 3.9**) concerning forest fire were collected utilizing an adaptation of the composite burn index (CBI) field protocol that considers the visible and averaged burn severity condition found in a plot (Key and Benson, 2005). The CBI assessment is a subjective assessment of the entire averaged burn severity across multiple layers at a plot and is heavily weighted to measuring fire effects on vegetation (Soverel et al., 2010). Furthermore, an important index that reveals soil water repellency status in a burned area is soil infiltration rate; the less the infiltration rate, the greater the susceptibility to instability. For this reason, a manual Mini Disk Infiltrometer (MDI) was acquired.

3.5.1 The Mini-Disk Infiltrometer (MDI)

The Mini-Disk Infiltrometer (MDI) is a device that is used for soil infiltration rate and hydraulic conductivity both accurately and affordably. "The top chamber (or bubble chamber) controls the suction. The lower chamber contains a volume of water that infiltrates into the soil at a rate determined by the suction selected in the bubble chamber. The bottom of the infiltrometer has a porous sintered stainless steel disk which will not allow water to leak in open air. The small diameter of the disk allows for undisturbed measurements on relatively level soil surfaces. Once you place the infiltrometer on a soil, water begins to leave the lower chamber and infiltrate into the soil at a rate determined by the hydraulic properties of the soil. As the water level drops, you record the volume at specific time intervals". (Deacon Devices, 2012). It was adjusted for field tests of post-fire infiltration and soil water repellency. Although the water drop penetration time

(WDPT) test has been the common field test for soil water repellency, the MDI test is less subjective and requires less time (Lewis et al., 2006). It measures the volume of water (mL) that passes from the infiltrometer into the soil in 1 min.

The MDI test provides a relative infiltration rate that can be used to classify soil water repellency and compare the infiltration capacities of tested sites (Parsons et al., 2010). The test was repeated three times and the mean MDI value was used as the indicative repellency rating for each sample location. MDI value determines the degree of soil water repellency (strong, weak, or none) at each depth sampled at each location **Table 3.3**)

Table 3.3 Mini-Disk infiltrometer (MDI) test values interpretation as suggested by the field guide for mapping post-fire soil burn severity which was developed by Parsons et al 2010 for the United States Department of Agriculture (USDA)-Forest Service reference

MDI test	**WDPT test**
Strong (0 to < 3 mL min–1)	WDPT values > 40 sec
Weak (3 to < 8 mL min–1)	WDPT values of 11-40 sec
None (> 8 mL min–1)	WDPT values of 0-10 sec

The field investigation was held between June and August 2012 through the dry months. 30 measurements were recorded in the Damour watershed. Because water repellency is difficult to define and the implications for potential watershed response can be ambiguous, we suggest using water repellency classes of strong, weak and none (Parsons et al., 2010). Strong water repellency is indicative of significantly reduced infiltration and increased potential for watershed response. Areas with strong water repellent soils are typically targeted for post-fire erosion and runoff mitigation. MDI testing sites were selected according to previously collected data from the Ministry of Agriculture, the Ministry of the Environment, and the Association of Forests, Development, and Conservation (AFDC) on forest fire events that affected the watersheds in previous years to establish sites of recurrent forest fires.



Figure 3.9 Forest fire field investigation using the Mini Disk Infiltrometer (MDI)

Once remotely sensed data collected, calibrated and compiled to be introduced into the mass movement susceptibility model under the form of MM inventory and burn severity maps, GIS data collection will provide the environmental parameters that are preconditioning to MM occurrence as well.

3.6 Selection and Acquisition of Thematic Database Using GIS

While preparing a Mass Movement susceptibility map for a site, it is of crucial significance to distinguish the conditions that caused instability of the slope and the processes that generated the movement (Ercanoglu et al., 2004). Factors influencing mass movements can be represented by parameters, and each one can be extracted either from remote sensing or digitized ancillary maps through ArcGIS 9.3. It provides an interactive framework for processing, analysing and reporting on complex spatial data that represent the preconditioning and trigger factors mentioned above. Rock type, soil type, land use, slope gradient, slope degree, and mean annual precipitation based on available data were investigated statistically for their relationship to the occurrence of mass movements within the study area. Data was digitized from 1:50,000 scale maps and topology was built to assure data precision and accuracy. Land use maps of 2010 were classified according to CORINE classification. Rock type, soil type, land use, slope gradient, slope degree, and mean annual precipitation based on available data were investigated statistically for their relationship to the occurrence of mass movements within the study area. A Digital Elevation Model (DEM) characterizing the terrain is a key to produce a variety of topographic parameters, which influence the Mass Movement activity in an area such as slope angle, slope aspect, have been prepared. DEM was extracted from 10 m contour lines. Aspect is referred to as the direction of maximum slope of the terrain surface. It is divided into Flat, S, SW, SE, E, N, NE, W and NW. **Table 3.4** shows the environmental variables used for the preparation of mass movement susceptibility zonation map.

The quantitative correlation between Mass Movement and factors affecting their occurrence are established by the data driven-Information Value (InfoVal).

Table 3.4 Environmental attributes used for the preparation of mass movement susceptibility zonation

Data	Factor Class
a) Geology	Sandstone
	Clastic Limestone
	Calcereous Shale
	Jointed and Karstified Marly Limestone
	Dolomitic Limestone
b) Soil	Marly Limestone
	Alluvial Terrasses
	Coastal Sand
	Consolidated dunes (Ramleh)
	Stones and bare rocks
	Sand and calcareous layer
	Red soil (Terra Rossa) (discontinous)* on compacted calcium carbonate
	Yellowish mountain soil
	Yellowish mountain soil (with humus)
	Torrential fan deposit
	Alluvium associated to red soil (Terra Rossa)
	Alluvium associated to light-chesnut soil
	Alluvium associated to dark-chesnut soil
	Alluvium associated to black or greyey soil
c) Land use	Artificial Area
	Agricultural Area
	Wooded Land
	GrassLand
	Bare Land
	Water bodies
d) Slope Gradient	0.00-2.22
	2.22-7.16
	7.16-11.49
	11.49-15.34
	15.34-19.26
	19.26-23.61
	23.61-28.77
	28.77-35.79
	35.79-90
e) Slope Aspect	Flat
	E
	N
	NE
	NW
	S
	SE
	SW
	W
f) Average Annual Precipitation	700-900
	900-1100
	1100-1200
	1300- >1400

3.7 Statistical Correlation Using Information Value Method (InfoVal)

Mass movement susceptibility can be assessed through deterministic, heuristic, or statistical approaches (Dai and Lee, 2002; Duman et al., 2005; Ruff and Czurda, 2008). In this study, we implemented a data-driven bivariate mass movement susceptibility model to build a susceptibility zonation map. The InfoVal method was developed by Yin and Yan (1988), Zerere (2002), and Saha et al. (2005) with a modification proposed by Cevik and Topal (2003) and Oztekin and Topal (2005). It is defined as the logarithm of the ratio between the densities of mass movements in a class over the density of mass movements for the entire study area. Univariate and multivariate statistical approaches have been used in many areas of the world to indirectly map mass movement susceptibility (Greco et al., 2007; Nefeslioglu et al., 2008; Nandi and Shakoor 2010; Vahidnia et al., 2010; Lucà et al., 2011). A significant problem with such approaches is that the contribution of each preconditioning and inducing variable to the model cannot be evaluated. The information value method (InfoVal) was implemented in this study to estimate the effect of each mass movement occurrence parameter.

The InfoVal method is a bivariate statistical approach that objectively assists in the assessment of mass movements. The Information Value Method (InfoVal) is an indirect statistical approach that has the advantage of assessing mass movement susceptibility in an objective way. The method allows the quantified prediction of susceptibility by means of a score, even on terrain units that are not yet affected by mass movement occurrence. Each instability factor is crossed with the mass movement distribution, and weighting values based on mass movement densities are calculated for each parameter class, as it happens with all bivariate statistical methods. The method implies prior definition of terrain units and the selection of a set of instability factors. This procedure permits the quantified calculation of susceptibility by a certain weight, even for areas in which mass movements do not occur. The preconditioning and inducing factors are crossed separately with the mass movement distribution, and a weighting value (W_i) based on the density of mass movements is calculated for each parameter class. This weighting value evaluates the influence of each factor class on mass movement susceptibility:

$$Wi = \ln \frac{Densclas}{Densmap} = \ln \frac{Npix(Si)/Npix(Ni)}{\sum_{i=1}^{n} Npix(Si) / \sum_{i=1}^{n} Npix(Ni)} \quad (6)$$

where ***(W_i)*** is the weight given to the ith class of a particular thematic layer (i.e., limestone or dolomitic limestone in the thematic layer lithology); ***Densclass*** is the mass movement density within the thematic class; ***DensMap*** is the mass movement density within the entire thematic

layer; ***Npix(Si)*** is the number of mass movement pixels in a certain thematic class,; ***Npix(Ni)*** is the total number of pixels in a certain thematic class; and ***n*** is the number of classes in a thematic map (Saha et al., 2005). The weight map of considered causal factors can be overlayed and integrated in GIS environment and InfoVal (Total weight Wi) of each pixel in the study area can be determined. The relative susceptibility of a terrain unit to the occurrence of a particular type of slope movement is given by the total weight W_i. The larger the value, greater the risk while smaller the value, lesser the risk to mass movement occurrence. Negative values of W_i mean that the presence of the variable is not relevant in mass movement development, while positive values of W_i indicate a relevant relationship between the presence of the variable and mass movement distribution. The weight map of preconditioning and inducing factors can be superimposed and integrated in GIS. The conventional InfoVal method considers that each parameter/thematic map has an equal effect on mass movements, which may not actually be the case (Oztekin and Topal, 2005). A weighting factor **(W_f)** for each parameter map has been produced. First, the W_i value of the different parameters for each pixel was determined by the abovementioned method; then, all of the pixel values belonging to each layer were totaled. The results were stretched by using the maximum and minimum of all layers (Cevik and Topal, 2003), with larger values denoting higher susceptibility to mass movements. The weighting factor, which ranged from one to 100 for each layer, was determined by the following formula:

$$Wf = \frac{(TWivalue) - (MinTWivalue)}{(MaxTWivalue) - (MinTWivalue)} x100 \quad (7)$$

where W_f is the weighting factor calculated for each layer; TW_{ivalue} is the total weighting index value of cells within the mass movement bodies for each layer; $MinTW_{ivalue}$ is the minimum total weighting index value within selected layers; and $MaxTW_{ivalue}$ is the maximum total weighting index value within the selected layers (Kundu et al., 2011). The existing mass movement distribution data layer was compared with the various thematic data layers separately to evaluate the contribution of each factor toward mass movement susceptibility. The number of mass movement pixels falling on each class of the thematic data layers was recorded, and the weights were calculated using **Equation 6**. These weights were stretched using the formula (Cevik and Topal, 2003) shown in **Equation 7.** The weighting factor, which ranges from one to 100, was assigned based on the degree of influence of the factor in initiating mass movement activity in the study area. The weight factor (W_f) was then multiplied by the weight of the individual classes (W_i).

3.8 Mass Movement Susceptibility Assessment and Validation of Result

The comparative analysis between the mass movements detected from the satellite images and field verification was conducted. An overall accuracy of 72% (i.e., 498 mass movements out of 694) was observed. The majority of mass movements occur in the upper sloping plateaus of Mount Lebanon (elevation between 500-1500m). The mass movements were intersected using GIS with the eight parameters mentioned above, and the statistical correlations were computed. The GIS overlay function for intersecting purposes is algorithmically simple, rapid, and easily computed. It highlights the degree of spatial coincidence between the occurrence of mass movements and specific parameters.

3.8.1 Establishing relationship between impacting factors and Mass Movement

Although each parameter is considered to affect mass movement frequency and occurrence independently of all of the physical terrain parameters taken together, histograms were plotted to detect the bivariate relations between mass movement frequency and the different categories of each parameter (**Figure 3.10**). These correlations and field observations support the results obtained by the correlation matrix of the natural parameter weighting.

3.8.1.1 Rock Type

The mass movement frequency according to lithological categories is presented in Figure 3.10. Mass movements are more abundant in the marly limestone and dolomitic limestone areas. Marly limestone displays a high frequency because it is dominated by impermeable, friable, and chalky marls that dissociate and slide easily. It exhibits characteristics such as bedding planes and jointing, which act as weak discontinuity planes. Furthermore they comprise of sandstone that is prone to the destabilizing action of water because of its poor cementation and open texture. Dolomitic limestone area also has a high frequency of movement because of the fractured cliff-forming units that lead to the presence of rock falls, and the failure of materials from the upper and weaker successions (detachment area) leading to frequent debris falls.

3.8.1.2 Soil

Among the 16 types of soils dominating Damour watershed, three exhibit a high mass movement frequency: Luvisols, Calcaric Regosols (becomes equivalent to red soil with elevation on compacted calcium carbonate) and Fluvisols associated Luvisols. Luvisols soils are unstable

because of their high clay content, making them susceptible to compression and volume change. The other types of soil are non-uniform and heterogeneous, with many discontinuities.

3.8.1.3 Land use

The relationship between land use and mass movement frequency is illustrated in **Figure 3.10**, which demonstrates that the frequency of occurrence is highest on bare land. In fact, bare areas tend to be the most prone to mass movement activity, as observed in both watersheds, in which 68% and 38% of the mass movements occurred on bare land in Damour watershed. The stability of soil tends to increase with increasing vegetation and wooded density. Vegetation limits the movement of rock debris along slopes. In areas in which the vegetation cover is sparse or there are only shrub species, the slow movement inside the rock debris can be detected from the curving at the bases of plant stems and from soil degradation. Forests play an important role in the reduction of mass movements. The high frequency of mass movements in agricultural areas in Damour (22%), where fruit trees are more abundant, is because those trees can grow on non-maintained terraces and some of these areas receive abundant water from irrigation; furthermore, the saturated soil conditions likely result in an increased likelihood of mass movements.

3.8.1.4 Slope Aspect

The slope aspect distribution between the mapped mass movements is illustrated. It indicates that mass movements with south, west, and south west-facing aspects are the most common. Slopes exposed to the south and west are warmer than those exposed to the north and east. In addition, rainfall affects the slope aspect depending on the direction of winds during rainfall, which commonly has a W and SW trend in Lebanon.

3.8.1.5 Slope Degree

Slope failure is more frequent on steep slopes than gentle slopes. Beyond a certain threshold, the frequency of mass movements diminishes as extremely elevated slope gradients will not sustain the accumulation of soil (Che et al., 2012). This finding is valid where approximately 50% of mass movements occur on slopes less than 35° .

3.8.1.6 Mean Annual Precipitation (MAP)

The mean annual precipitation is considered a factor that may contribute to slope instability because rainfall is the principal source of groundwater recharge and the area is characterized by a rainy season that lasts at least five months each year. The spatiotemporal distribution of rain is variable within this region. The lack of long-term daily rainfall data and of well-dated mass movement events limits our ability to analyze rainfall as a preconditioning factor controlling the timing of mass movement occurrences. The mass movement distribution in the Damour watershed exhibited a decrease in mass movement frequency to >1,400 mm/year. This finding indicates the absence of a direct relationship between mean annual precipitation (meaning the average of precipitation/year) and the occurrence of mass movements. But the effect of intense rainfall events on mass movement occurrence has been demonstrated in a number of works (Dai and Lee, 2001; Lee and Chi, 2011; Peruccacci et al., 2012).

3.8.1.7 Normalized Burn Ratio

The presence of vegetation and wooded area has proven to be an important factor in decreasing the occurrence of mass movements in the low-, moderate-, and high-severity classes. In Damour, 65% of the mass movements that occurred were in low-burn-severity. This finding demonstrates that even slight changes in the vegetation regime lead to an increase in the occurrence of mass movements.

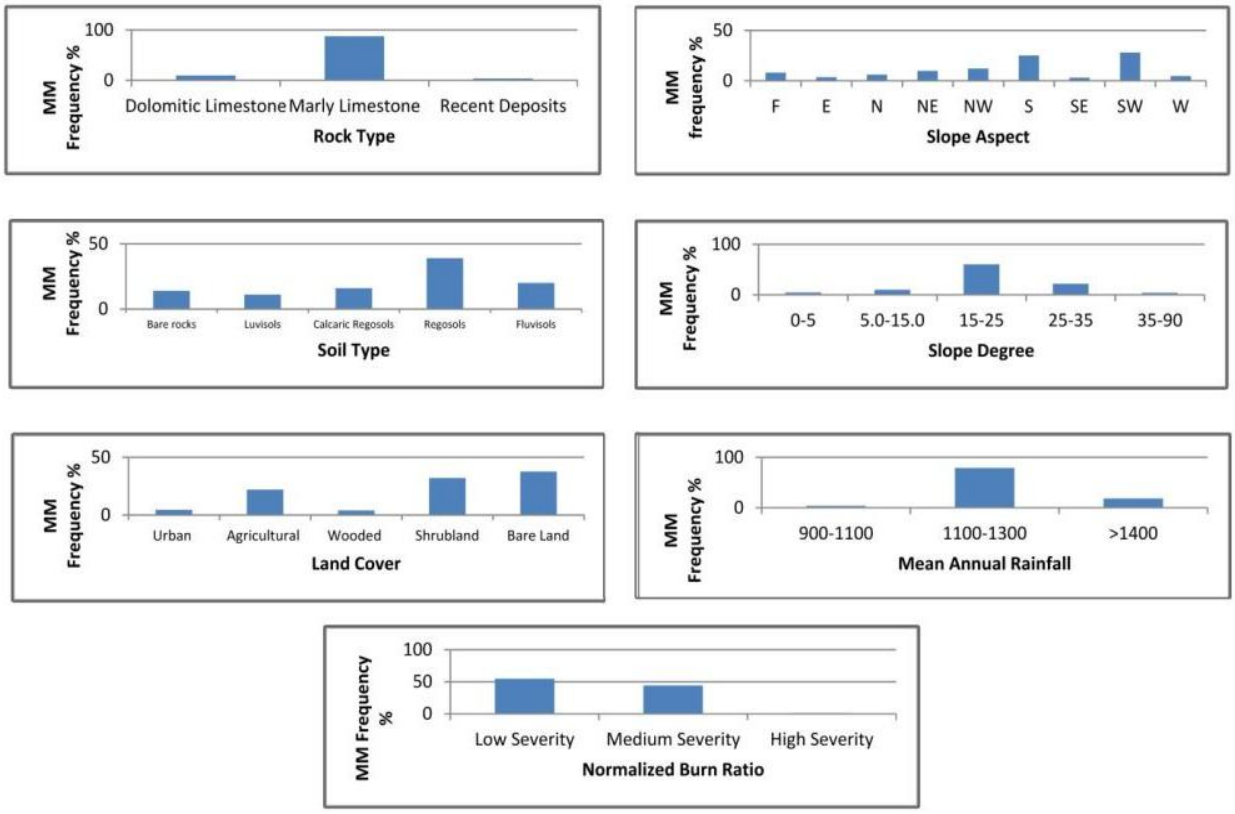

Figure 3.10 Relationship of mass movement (MM) frequency with Rock Type, Slope Degree, Mean Annual Rainfall, Normalized Burn ratio, Land Cover, Soil Type and Slope Aspect in Damour

With the purpose of further demonstrating the impact of burn severity on soil water repellency, below are the results of infiltration rate measurements of burned areas of the study area.

3.9 Soil Water Repellency Status by Means of Infiltration Rate

MDI testing sites were selected according to previously collected data from the Ministry of Agriculture, the Ministry of the Environment, and the Association of Forests, Development, and Conservation (AFDC) on forest fire events that affected the watersheds in previous years to establish sites of recurrent forest fires. The delineated forest fires were introduced in the selection of sample sites. The MDI results were overlain on a cumulative NBR map composed of the six previously obtained NBR maps (**Figure 3.11**).

Infiltration rates of the measurement plots lie in the moderate-burn-severity zones of the cumulative NBR map which represents the mean NBR values compiled from the previously used Landsat images. It might be argued that using mean NBR values could give coarse results but several of the forest fires detected earlier through remote sensing and field investigation were recurrent events. Although water repellency duration of the soil after a fire varies from minutes

to months (Doerr et al., 2004; Certini, 2005; Malkinson and Wittenberg ,2011), NBR values of the study areas did sustain the hypothesis of long term water repellency especially in recurrent fire event locations.

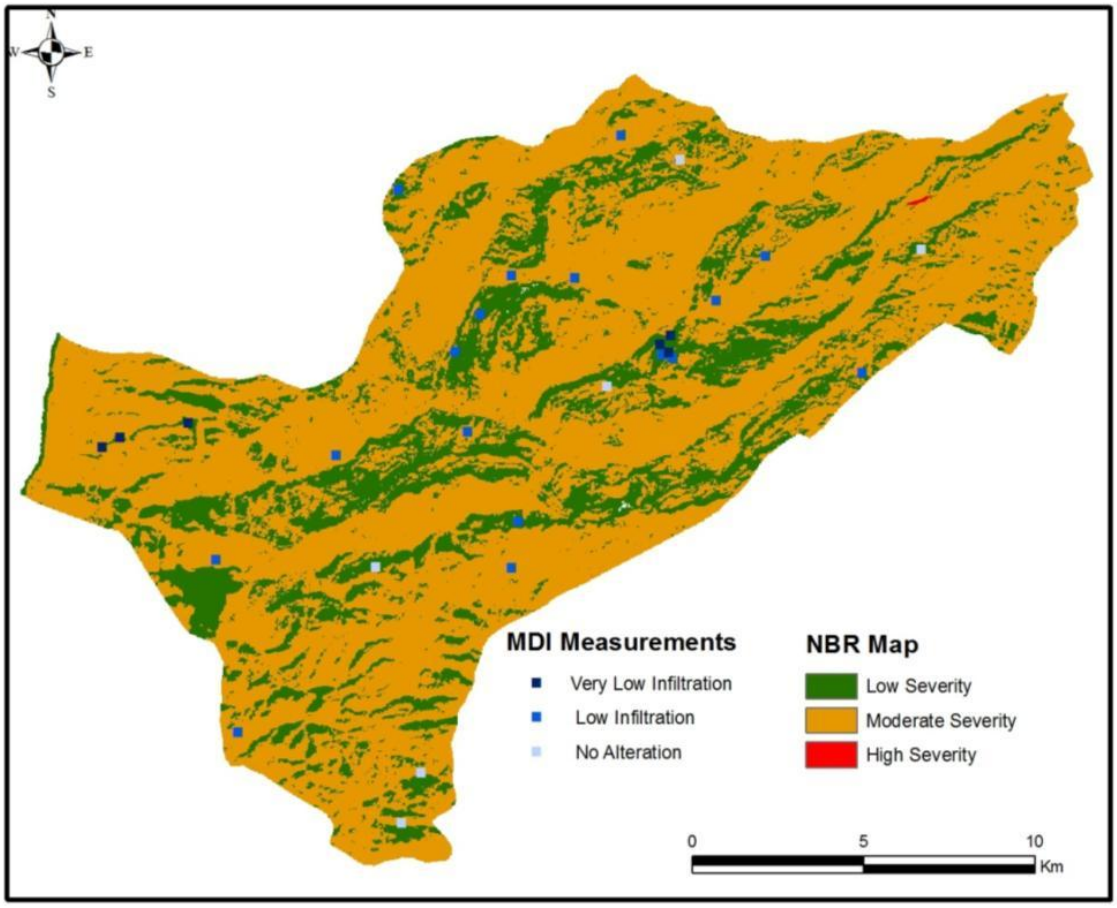

Figure 3.11 Mini disk infiltrometer (MDI) measurement points distribution over the cumulative Normalized burn ratio (NBR) map. Water repellency (WR) interpretation used accoRDIstng to Parsons et al 2010 for the United States Department of Agriculture (USDA)

Considering all preconditioning and forest fire burn severity that were transformed into thematic maps using GIS, they were introduced into the mass movement susceptibility model. A Mass Movement Susceptibility Map (MMSM) was generated and validated using an individual set of MM.

3.10 Mass Movement Susceptibility Map and Model Validation

The weights were assigned to the classes of each thematic, respectively, to produce weighted thematic maps, which have been overlaid and numerically added using the raster calculator to produce a Susceptibility Index (SI) map. Dividing these values into susceptibility classes was, however, not easy as there are no statistical rules which can guide the categorizing of continuous

data automatically. The problem of changing continuous data into two or more categories always remains unclear in mass movement susceptibility mapping. In the present study, susceptibility index values were segmented into four classes; non susceptible, less susceptible, moderately susceptible and highly susceptible. Mass movement susceptibility analysis result was tested using an individual set of Mass Movement extracted from the inventory map that was used to build the model. To evaluate the contribution of each factor towards mass movement hazard, the existing mass movement distribution data layer has been compared with various thematic data layers separately. The number of mass movement pixels falling on each class of the thematic data layers has been recorded and weights have been calculated and these weights are given in **Table 3.5**. Further these weights have been stretched using formula (Cevik and Topal, 2003) given in **Equation 7**. Finally, the weighting factor ranging from 1 to 100 has been assigned based on the degree of influence of the factor in initiating mass movement in the study area. The weight factor (Wf) was multiplied with the weight of individual classes (Wi). The resultant weighted thematic maps have been overlaid and numerically added to generate a Mass Movement Susceptibility Map (See the workflow diagram below)

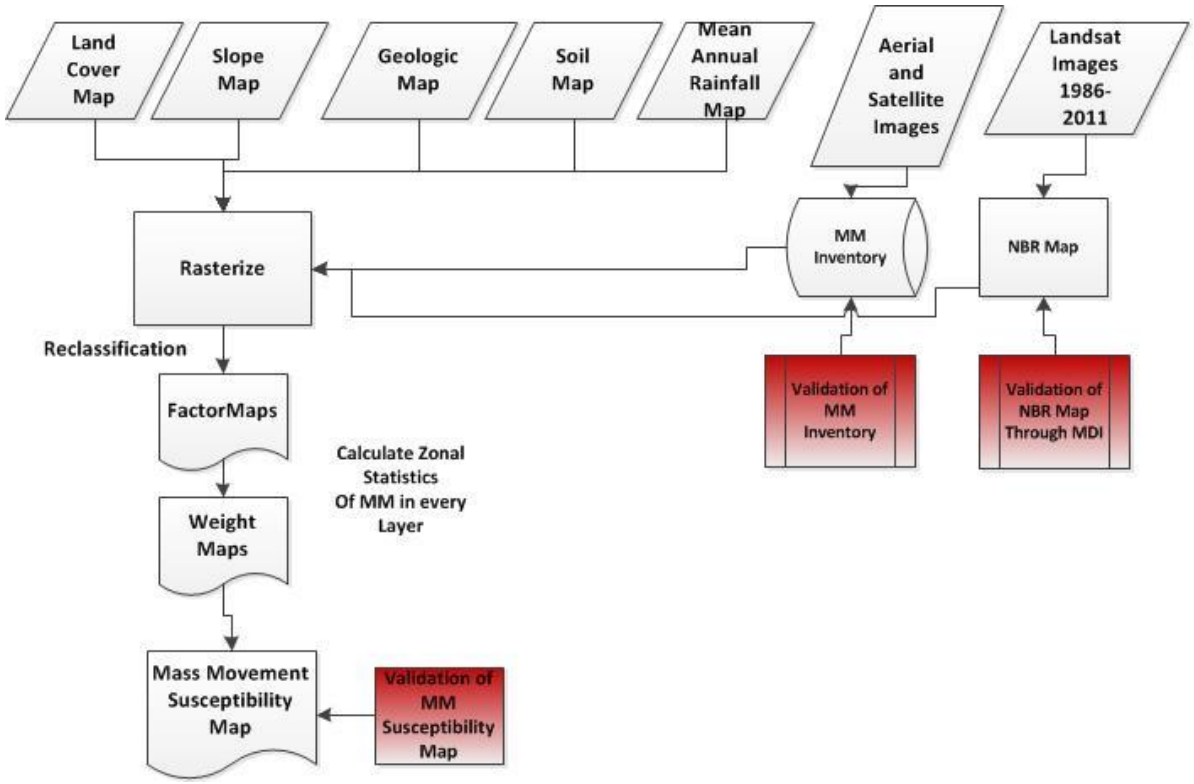

Figure 3.12 Workflow Diagram for Mass Movement Susceptibility Map generation

The analysis of the relationship between mass movement occurrence and the factors derived from InfoVal illustrates that W_f of the NBR layer has the maximum weight of 67 in Damour, which was overrated by the soil factor. The slope aspect had the minimum weight of 26 in

Damour. Rainfall and lithology also have an important effect on mass movement occurrence, with weights of 84 and 67 in Damour.

These weight factors were assigned to their corresponding factors to produce weighted thematic maps, which were overlaid and numerically added in the GIS environment to produce the MMSM using:

$$MMSM = (Wf)SI + (Wf)SA + (Wf)Li + (Wf)NBR + (Wf)S + (Wf)MAP \quad (8)$$

where *SI, SA, Li, Lc, NBR, S,* and *MAP* are the products of the derived weights and weight factor for slope inclination, slope aspect, lithology, land use, NBR, soil type, and MAP, respectively.

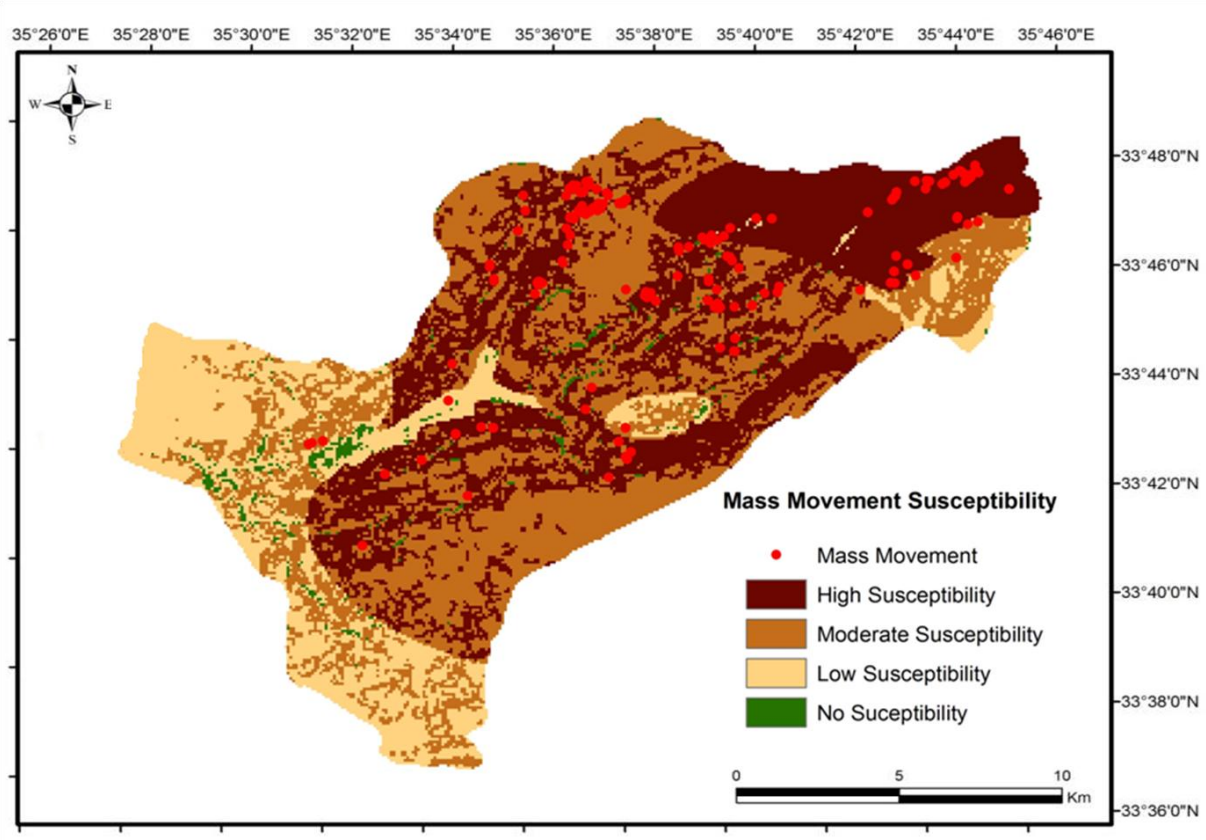

Figure 3.13 InfoVAL susceptibility model maps validated through an independent mass movement validation set extracted from MM inventory

The susceptibility map generated using all six factors considered in this study correctly classifies 69% of the training mass movement in high-susceptibility zones for Damour and displays a lower prediction performance of 1% for the no-susceptibility zones. Based on this factor combination, 38% of Damour watershed falls in the high- and moderate-susceptibility categories. Only 4% of the validated mass movements are attributed to the no-susceptibility zones. This finding is an indication that the model has a high predictive power. The distribution of the various

susceptibility ranking, training, and validation results for the watershed is provided in **Figure 3.13**. **Table 3.6a** indicates that 78% of the existing mass movements occur in the predicted high- and moderate-susceptibility zones in Damour watershed. Moreover, 21% of the mass movements in the Damour watershed occur in no- or low-susceptibility zones, which comprise 61.9% of the land area. The area in the predicted high- and moderate-susceptibility zones must be monitored, and preventive measures should be initiated to protect lives and property from future mass movements. Even though topography, soil type, lithology, and vegetation cover are characteristically more important indicators for mass movement hazard than just the event of a fire (Cannon and Reneau, 2000; Larsen et al., 2006), post- forest fire mass movement monitoring has led to the evaluation of their impact on short- and long-term land degradation. For instance, Inbar et al. (1997) reported 100–500 times more mass movement in burnt compared with those in unburnt terrain., whereas Mayor et al. (2007) reported 37,000 times higher sediment yields on burnt compared with unburnt plots. In the Damour watershed, soil had the highest effect factor of 84, followed by the NBR (67) and Lithology (67).

Table3.5 Weight of each parameter defining its contribution to mass movement occurrence in our study areas as well as the percentage of impact of each parameter on the Mass Movement Susceptibility Map (MMSM) Damour

Factor	Damour(W_f)	%Impact on MMSM
Soil	84	21
NBR	67	17
Lithology	67	17
Rainfall	62	16
Land use	58	15
Slope Degree	28	7
Slope Aspect	26	7

Table 3.6 Highlighting the impact of Normalized burn ratio (NBR) on the mass movement susceptibity map through demonstrating the shift in area distribution of the susceptibility classes when NBR was induced and deduced from the (MMSM) equation

a) With NBR	% of Total Area	% of MM
High Susceptibility	29.8	71
Moderate Susceptibility	8.3	7
Low Susceptibility	58.3	20
No Susceptibility	3.6	1
b) Without NBR	**% of Total Area**	**% of MM**
High Susceptibility	29.5	49
Moderate Susceptibility	9.0	10
Low Susceptibility	35.0	33
No Susceptibility	26.4	9

To further emphasize the influence of forest fire on MMSM dynamics, the NBR layer was extracted from the MMSM equation in both watersheds. The resulting maps are shown in Figures 38. The effect can be detected with the shift in the mass movement locations from high- and moderate-susceptibility areas to low-, and no-susceptibility areas. The most remarkable shift was in the low-susceptibility class where % of total area increased from 3.6% to 26.4% as shown in **Table 3.6b**. This transformation has a drastic impact on the MMSM exposing its usability. In Damour W_f (67), removing the NBR from the MMSM equation had a high effect on the distribution of mass movements. The percentage of mass movements decreased by 16% in high-susceptibility areas, increased by 18% in moderate-susceptibility areas, increased by 21% in low-susceptibility areas, and increased by 12% in no-susceptibility areas as compared to when the NBR was included in the equation (**Figure 3.13**).

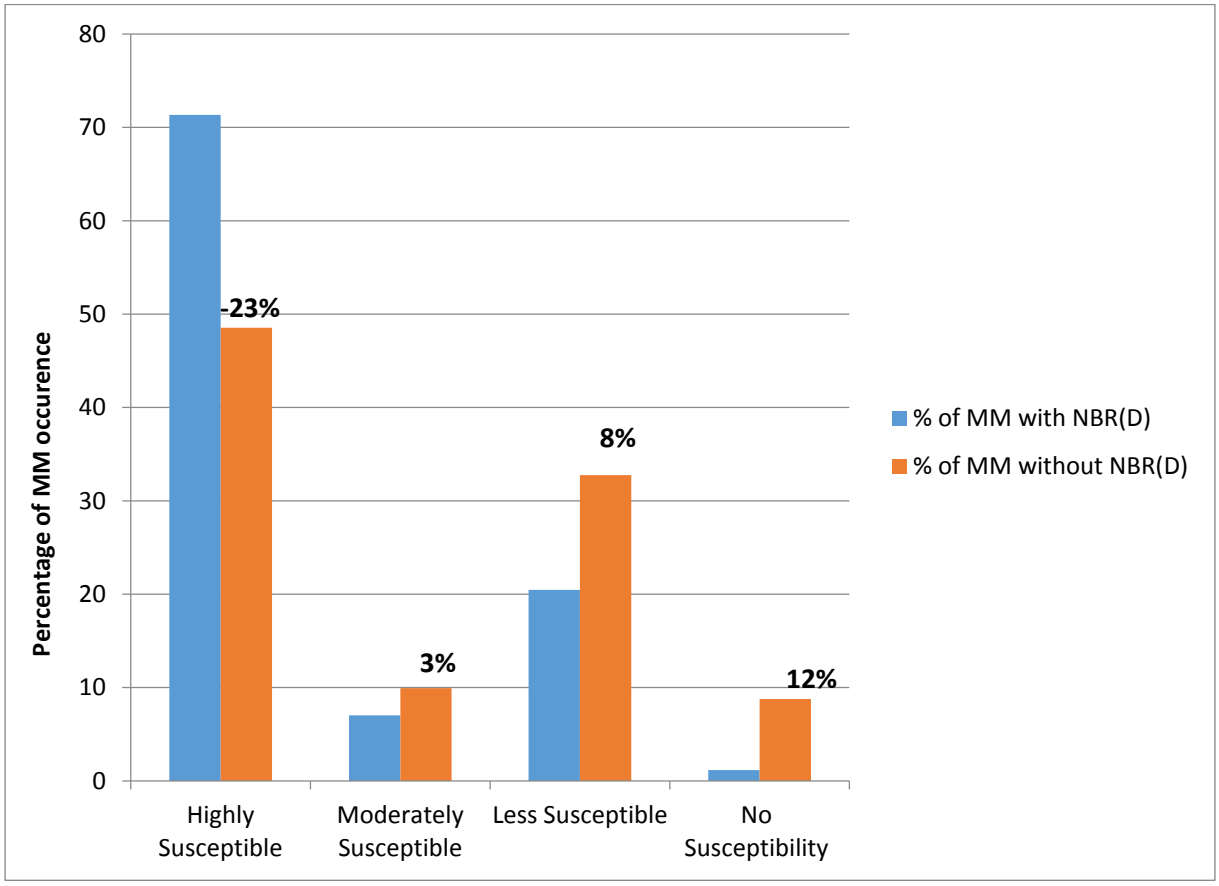

Figure 3.13 Impact of Normalized Burn Ratio (NBR) as an inducing factor on Mass Movement Susceptibility Map (MMSM) observed through Shifts in Mass Movement (MM) potential occurrence from High and Moderate to Low and No susceptibility in Damour (D) watershed

Because the Damour watershed had a lower weight factor for the NBR, it experienced a less dramatic change in the distribution of mass movements when the NBR was removed from the MMSM equation; the percentage of mass movements in high-susceptibility areas decreased by 23%, whereas in moderate-, low-, and no-susceptibility areas, it increased by 3%, 12%, and 8%, respectively. This shift in the distribution (**Figure 3.14**) of potential mass movements from high- and moderate-susceptibility areas to low- and no-susceptibility areas clearly illustrates the impact of the NBR as an inducing factor. By withdrawing NBR from the MMSM equation, the equation's accuracy decreased and thus its usability for hazard and risk mapping.

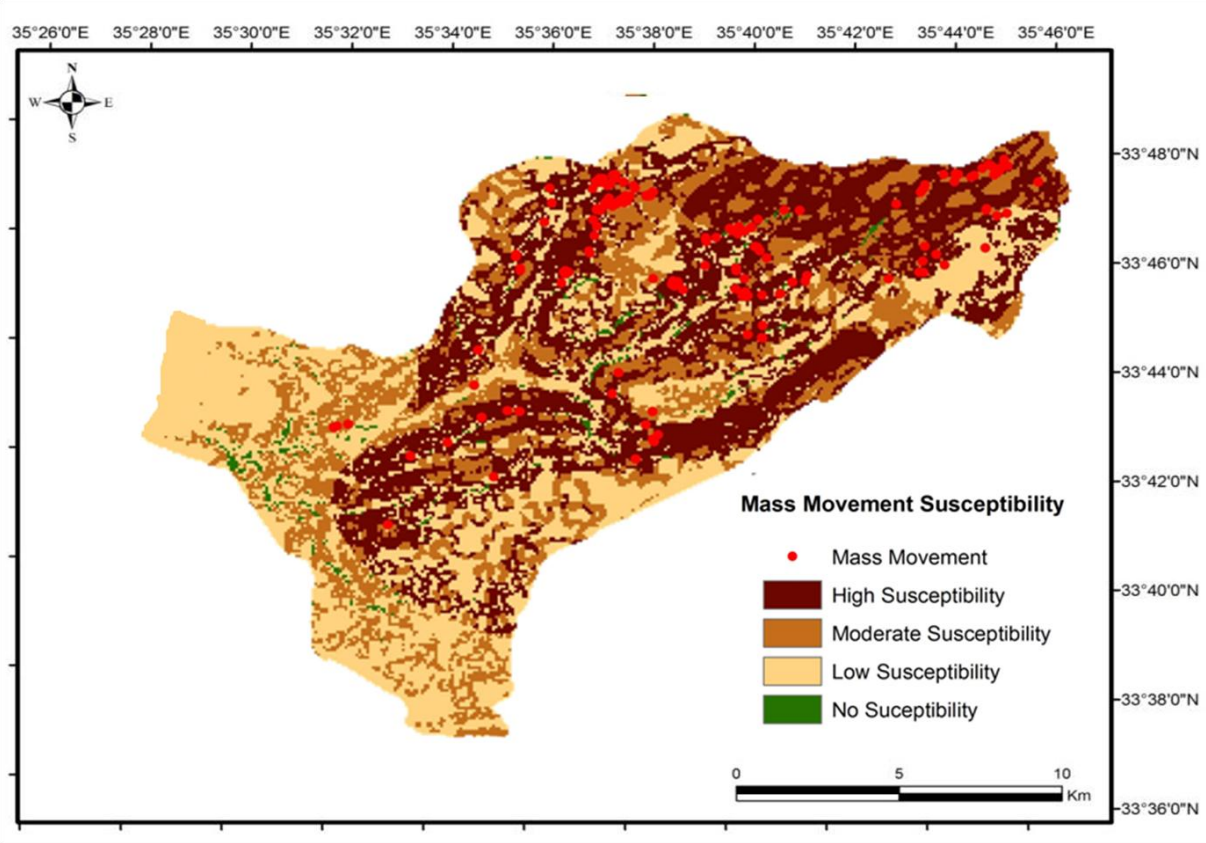

Figure 3.14 InfoVAL susceptibility model maps validated through an independent mass movement validation set extracted from MM inventory and NBR weight factor removed from MMSM equation

3.11 Major constraints in Evaluation Mass Movement Susceptibility Maps

Due to the techniques used to compile the inventory maps, MM inventories are subjective products, whose quality depends on the skill and the experience of the investigators, the complexity of the study area, and the completeness and reliability of the available information, including the aerial photographs used to identify the MM (Guzzetti et al., 2000; Malamud et al., 2004). MM inventory data; for example, may be poor in terms of the length or detail of the records, and it is unlikely that very specific MM-related predictor parameters, such as material shear strength, are mapped to the detail required for statistical analysis (Schicker and Moon, 2012). As resources often do not permit collection of complete MM inventory data on the scale for regional planning, and input data are likely to be standard parameters such as geology, soils, and rainfall mapped to a 1:50,000 or 1:250,000 scale, methods that allow prediction from relatively sparse data, would be useful. Despite the wide range of techniques used for MM susceptibility maps, only some studies have been carried out to evaluate the validity of the results obtained, through the examination of their predictive potential with respect to prospect MM. The majority of the published papers presents a statistically based hazards model and discusses the

data and the method used to prepare the model, but provide little or no information on the quality of the proposed model. Validation can be performed using a MM population independent from the one used to construct the map. The former allows for (i) evaluating the degree of match between the predicted hazards levels in a given region, and the distribution and abundance of known MM in the same region; (ii) evaluating the role of the thematic information in constructing the model; (iii) assessing the ability of the model to cope with variations in the input data; and (iv) determining the error associated with the obtained hazards estimate. The latter allows for determining the prediction skill of the model to forecast the location of new or reactivated MM (Guzetti et al., 2005). Validation involves comparison between the map, hence model, and the independent data set. Strictly speaking, validating predictions of future events is not possible unless there is a lapse of time between prediction and validation. However, it is not practical to wait until a number of possibly catastrophic events have occurred to evaluate a prediction methodology. It is essential that prior estimates of the relative predictive power of alternatives be made in order to select the most effective technique. For instance, and despite the promising results obtained here, this study is not without limitations. Regardless of its high predictive power, the model assumes that mass movements will occur under the influence of an identical combination of factors, whereas field observations indicate that a number of mass movements are caused by a specific set of factors (Che et al., 2011). The bivariate approach considers the independent relationships of individual factors with the occurrence of mass movements without accounting for the possible combination of factors that might act together in increasing slope instability. The probability values from this type of predictive modeling are not absolute and represent a relative degree of hazard. But these values can provide a measure of mass movement initiation localities.

Since results demonstrate that NBR, which represents fire severity, has a significant effect on mass movement occurrence and susceptibility prediction, it is only logical to investigate further on forest fire generating factors. The impact of climatic variations is obtaining increasing attention as well as understanding the role of land use in shaping forest fire regimes. The coming chapter will attempt to quantify a correlation between forest fire and climate on one hand and forest fire and land use on another. This can enhance chances to decrease MM occurrence through approptite mitigation measures.

CHAPTER 4
Comparative correlation of Forest Fire burn severity with climatic fluctuations and land use change

Understanding the factors driving fire regimes is crucial as a basis for predicting future changes in MM events since Forest fire has shown earlier to have a high impact on MM occurrence. In this chapter, we aimed to identify the impact of climate and human activity on fire occurrence in Damour watershed. We considered forest fire burn severity, land use and meteorological data over the period 1986–2012. Climatic factors causing prolonged droughts are observed using the Standardized Reconnaissance Drought Index (RDI_{st}). Evidence also show that forest fire has generally increased due to increases in population size, grazing practices, and increases in human ignition. The role of land-use in shaping forest fire regimes was carried out using Normalized Difference Vegetation Index (NDVI). This chapter utilizes remotely sensed data of Landsat to compare the NBR values with their corresponding yearly NDVI and RDI_{st} over the watershed of Damour River. The combined empirical analysis provided an approach to comprehend the dynamics of forest fire burn severity with respect to climatic variations and land use changes.

4.1 Introduction

In the last decades, the fire system in the Mediterranean has altered, becoming larger and more intense (Lloret et al., 2009; Moreira et al., 2011). Forest fires have been especially damaging in recent years, representing one of the most important elements that destroy Lebanon's natural resources where they reduced the forest cover to 13% in a relatively very short period of time and raised concern at the national and international levels that they could lead to total eradication of forests. Of the important determinants of forest fire occurrence are climate and weather (Johnson, 1992; Whitlock et al., 2003; Fried et al., 2004; Westerling and Bryant, 2008; Wastl et al., 2012). Accordingly, strong emphasis has been put on the prediction of forest fire severity using climatic variables especially changes in precipitation and temperature trends which were also investigated, searching for changes in variability. Several studies of climate variability over the Mediterranean are reported in El Kenawy et al. (2011) and Ruiz-Leo et al. (2011). A new study by US National Oceanic and Atmospheric Administration (NOAA) (2011) has highlighted that climate change is a major contributor to more frequent Mediterranean droughts; the last 20 years have witnessed 10 of the driest 12 winters in the lands surrounding the Mediterranean Sea.

Figure 4.1a shows Precipitation change in the Mediterranean Region according to NOAA (2011). Reds and oranges highlight lands around the Mediterranean that experienced significantly drier winters during 1971-2010 than the comparison period of 1902-2010. It also suggested that winter precipitation in the Mediterranean over the last three decades has witnessed a higher frequency of dry years where precipitations decreased by over 60mm/year from the cumulative annual average as seen in **Figure 4.1b** increasing fuel availability for possible fire events.

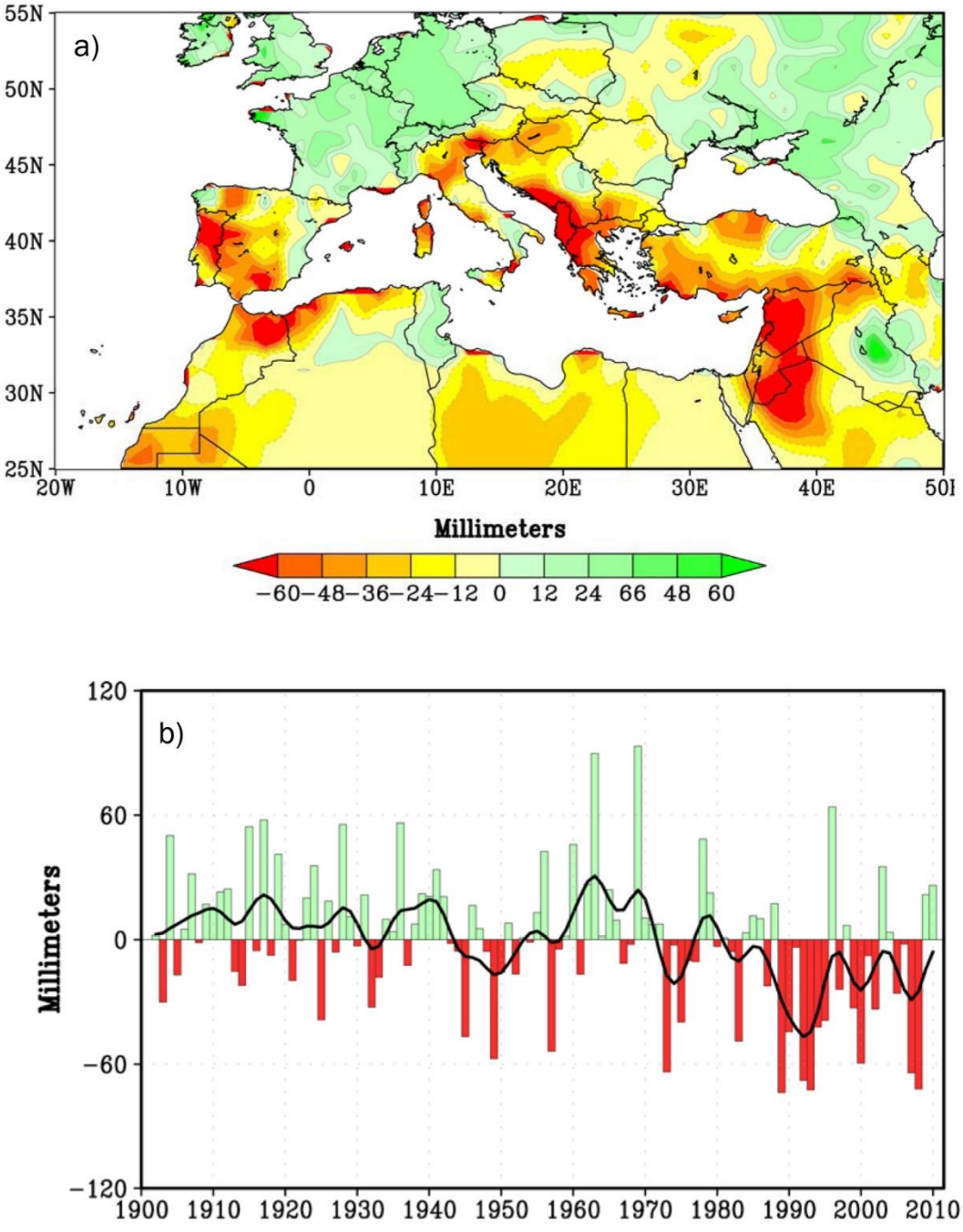

Figure 4.1 US National Oceanic and Atmospheric Administration (NOAA) study on Mediterranean changing precipitation trends: la qualité de la figure n'est pas bonne

More specifically, climate change scenarios have been developed for Lebanon where temperatures by 2040 will increase from around 1°C on the coast to 2°C in the mainland, and

by 2090 they will be 3.5°C to 5°C higher. Difference in temperature might not be the only influencing climatic factor. Rainfall projections are to decrease by 10-20% by 2040 and by 25-45% by the year 2090, compared to present (MOE, 2011). Burning depends on fuel flamability affected by the duration and degree of the dry season, thus this combination of significantly less wet and substantially warmer conditions will result in an extended hot and dry climate (Pausas, 2004; Westerling et al., 2006; Pausas and Bradstock, 2007; MOE, 2011). Furthermore, persistent weather anomalies can directly impact fire activities during a fire season. Under prolonged warm and dry conditions, fires are easier to ignite and spread and a fire season often becomes longer (Liu et al, 2014).

Since Evapotranspiration (ET) is an integrated climate parameter and an important component of the hydrologic cycle affecting water availability (Easterling et al, 2007; Corti et al, 2009), a widely used meteorological Reconnaissance Drought Index (RDI_{st}) which incorporates potential evapotranspiration (PET) and precipitation is applied to asses the impact of climate variations on forest fire burn severity (Tsakiris et al, 2007; Amor et al, 2009; Asadi Zarch et al, 2011) in preference to Palmer Drought Severity Index (PSDI) or Standardized Perecipitation Index (SPI). Eventhough forest fire severity and fire-surface extent are "arguabely" climatically driven (Pausas, 2004; Keeley et al, 2008), many evidence show that fire regime changes are not directly linked to climatic change where on a longer time outlook, fire hazard has generally increased due to increases in population size, grazing practices, and increases in human ignition (Moreira et al., 2010; Salis et al., 2014). Understanding the role of land-use in shaping wildfire regimes has become a major concern (Cumming, 2001; Nunes et al., 2005; Bajocco et al., 2010). Furthermore, Mediterranean rural areas are facing a relevant process of land abandonment, which might result in the buildup of large and continuous fuel beds and a progressive cover by spontaneous Mediterranean shrublands and forests, usually highly combustible and able to sustain high intensity fires (Badia et al, 2002 ; Castellnou and Miralles, 2010). Because of the relevance of role of human activities (e.g. ignition or fire-suppression management) and changes in land use (Barbero et al., 1990; Améztegui et al., 2010; Gimmi et al., 2010) on fire severity, frequency and extent, Normalized Difference Vegetation Index (NDVI), a remotely sensed index, is utilized. It is commonly used for land use and land use detection (Lunetta et al, 2006; Tittebrand et al., 2009; Wright et al., 2012; Ali et al., 2013).

4.2 Climatic variability Detection Utilizing Evpotranspiration and Drought Indices

Among natural disturbances, forest fire is one of the most climate-sensitive events (Mori and Johnson, 2013). Several studies have designated that increases in the frequency and the severity of temperature-driven droughts are probable, thus creating more fire-prone conditions (Gonzalez et al., 2010; Mastrandrea et al., 2011; Pechony and Shindell, 2011).

4.2.1 Potential Evapotranspiration

There are different means for calculating evapotranspiration. One such method is the Thornthwaite method (**Equation 9**). Thornthwaite (1948) method operates with meteorological variables, irrespectively to the vegetation, i.e. potential evapotranspiration (PET). It is estimated as evaporation of bare surface, only and is based on the experience that PET is competently determined by temperature. The procedure can be used for calculating PET of large regions; however, it does not explicitly reflect its dependence from air humidity and windiness (Horváth et al., 2010). The thornthwaite method is often used (Ahmadi and Fooladmand 2008; Özhan et al., 2010; Alves et al., 2013) due to its simplicity unlike the FAO Pennman-Monteith method, which can be more accurate than Thornthwaite, but requires various inputs that might not be readily available. Moreover, a recent study done by Vangelis et al. 2013 shows that there is no deviation between various PET calculation methods such as the Pennman –Monteith, Blanely-Criddle and Thornthwaite, but the overall annual PET trend obtained by the compared methods proves to be almost similar.

$$\mathrm{PET} = 16.\left(\frac{10\mathrm{T}}{\mathrm{I}}\right)^{\mathrm{a}}\left(\frac{\mathrm{N}}{12}\right)\left(\frac{\mathrm{m}}{13}\right) \tag{9}$$

Where: PET = monthly potential evapotranspiration (cm); T= monthly mean temperature (◦C); N is the mean monthly possible sunshine hours (Hr/day), m is the number of days of each month, a is empirically determined exponent $= 0.49 + \mathrm{I} - 0.0000771 * 12 + 0.000000674 * 13$ (Thornthwaite, 1948)

I= a heat index which is a constant for a given location and is the sum of 12 monthly index values i, where i is a function of the monthly normal temperatures calculated by the following **Equation 10**:

$$I = \sum_{i=1}^{12} \left(\frac{Timean}{5}\right)^{1.514} \quad (10)$$

Where *Timean* is the 12 monthly mean temperatures

4.2.2 Drought Indices

Defining and developing an index to measure drought is a difficult task due to the wide multiplicity of fields affected, the diverse geographical and distribution, and the various degrees of drought occurrences. Of the several indices developed, Palmer Severity Drought Index (PSDI) as well as the Standardized Precipitation Index (SPI) are usually the most recognized (Hayes, 2007). PSDI's main objective was to obtain indices of drought years independent of the influence of a wet spell in a long-term drought. The same concept was applied in the case of a sequence of "near-normal" set of years interrupted by a spell of drought (Palmer, 1965). Identifiable standards for establishing the beginning and end of dry and wet years were elaborated (Hayes, 2007). PDSI's major drawback is that it is complex through its calculation and the parameters it requires and is less suited for mountainous areas. SPI, On the other hand, requires a minimum of 30 years of continuous data (like all other drought indices) in order to model and quantify the amount of precipitation decrease over a period of time. This quantification helps in the assessment of drought impact on various water sources (Giddings et al., 2005). Even though it is widely used, the major disadvantage of SPI is that it depends solely on precipitation data while drought is a very complex phenomenon dependent on many parameters such as temperature, relative humidity etc.

A new reconnaissance drought identification and assessment index (RDI) was first by Tsakiris et al (2007). According to Kanellou (2012), RDI is used to estimate the hydro-meteorological drought conditions based on cumulative Precipitation (P) and Potential Evapotranspiration (PET). It can be used for agriculture since it is a meteorogical drought index used towards agricultural applications (Niemeyer, 2008). RDI is based on the ratio between aggregated quantities of precipitation and potential evapotranspiration (Tsakiris, 2007). It is expressed in three forms: the initial value ($\boldsymbol{a_0}$),normalized RDI (RDIn) and standardized RDI (RDIst). The initial value (αk) is presented in an aggregated form using a monthly time scale and may be calculated on a monthly, seasonal or annual basis. The $\boldsymbol{a_0}$ can be calculated by the following equation:

$$\boldsymbol{a_0^{(i)} = \frac{\sum_{j=1}^{12} Pij}{\sum_{j=1}^{12} PETij}} \quad (11)$$

Where Pij and PETij are the precipitation and potential evapotranspiration within the month "j" of hydrological year "i" that usually starts in October. This coincides with the period chosen for the manipulation and index extraction from Landsat images. The Standardized RDI_{st} (RDI_{st}) is computed using:

$$RDI_{st(k)}^{(i)} = \frac{y_k^{(i)} - \overline{y}_k}{\widehat{\sigma_{yk}}} \quad (12)$$

Where : $y_k = \ln(a_0^{(i)})$

$\overline{y_k}$ = arithmetic mean of y_k

$\widehat{\sigma_{yk}}$ = standard deviation of y_k

The RDI_{st} behaves similar to the SPI and so is the interpretation of results as seen in the **Table 4.1** below (Tsakiris, 2007)

Table 4.1 Standardized Reconnaissance Drought Index (RDI_{st}) values which are similar to SPI Values

RDI_{st} Values	Description
2.0 +	Extremely Wet
1.5 to 1.99	Very Wet
1.0 to 1.49	Moderately Wet
-0.99 to + 0.99	Near Normal
-1.0 to -1.49	Moderately Dry
-1.5 to -1.99	Very Dry
-2.0 and less	Extremely Dry

This index was selected because (1) It is especially developed to fit the Mediterranean and it has been used with good results in various studies (Tsakiris, 2005; Farjalla and Ziade, 2010; Asadi Zarch et al., 2011) (2) It is simple to use and requires few and readily available parameters (3) It uses parameters which allow the index to be used in studying scenarios of the impact of climate change. Moreover, RDIst has proven to be highly sensitive and resilient (Khalili et al., 2011). According to Vangelis et al. (2013), and since PET is one of the two main inputs for RDI_{ST} calculation, the authors compared the impact of several PET calculation methods including Thornthwaite and FAO Pennman Monteith on the drought severity characterization derived

from RDI_{st}. No significant influence on RDI_{ST} results was detected proving the robustness of RDI_{st} and its independence from PET calculation method.

Land use on the other hand was assessed using a remotely sensed vegetation index for change detection.

4.3 Evaluating Land Use Change Using Normalized Difference Vegetation Index

Land use changes can be related to natural dynamics or human activities (Bakr et al., 2010). Land use and human/natural modifications have largely resulted in deforestation and increase of natural disaster such as MM. Therefore, available data on land use changes can provide critical input to probable forest fire ignition basis. Monitoring land use changes using multi-temporal remotely-sensed data provides an effective evaluation of human impact on the environment and is important for establishing links between it and forest fire occurrence. Landsat Multispectral Scanner (MSS), Thematic Mapper (TM) and Enhanced Thematic Mapper Plus (ETM+) data have been broadly employed in studies towards the determination of land use because of the rich archive and spectral resolution of satellite images.

There are several methods for mapping land use changes using remotely sensed data such as: image differencing (ID) which involves change detection technique is performed by subtracting the digital number (DN) value of a pixel in one date for a given band from the DN value of the same pixel for the same band of another date, pixel by pixel (Bindschadler et al., 2010; Afify, 2011), principal component differencing (PCD) which is often regarded as an effective transform to extract information and compress dimensions and change detection is implemented based on thresholds (Deng et al., 2008) , image ratioing (IR) involves calculation of the ratio of the DN values of corresponding pixels on the two images at different dates but has been criticized due to the non-normal histogram distribution of the resultant image (Lu et al., 2005)and vegetation index differencing (VID).

Vegetation index differencing is often regarded as an effective method to enhance the difference among spectral features. Enhanced Vegetation Index (EVI), Soil Adjusted Vegetation Index (SAVI) and Integrated Forest Index (IFI) are well known and used change detection indices that have been corrected for the influence of soil brightness. But this enhancement reflected negatively on their sensitivity to vegetation change . For this reason, various researchers have discussed the use of normalized difference vegetation index (NDVI) in monitoring vegetation dynamics through land use changes due to its high sensitivity to vegetation change (Verhoef et

al., 1996; Li et al., 2005; Morawitz et al., 2006; Lunetta et al., 2006; Wright et al., 2012). Using NDVI, the reflectance from chlorophyll and distinguished varying amounts of vegetation at the pixel level were mapped. NDVI indicates the presence and absence of vegetation therefore, its comparison may provide information on qualitative and quantitative changes in land use known that vegetation is the primary indicator of land use and its change (Alphan and Derse, 2011). Furthermore, and as mentioned earlier that topographic effects in remotely-sensed indices having only band ratioing are usually ignored (Matsushita et al. 2008), NDVI has the ability to compensate for changing illumination condition sand viewing angle and retains the ability to minimize topographic effects (Simonetti et al. 2014) where the soil factor in SAVI for instance make it more vulnerable to topographic effect. The calculation of NDVI is given by:

$$\boldsymbol{NDVI = (NIR - R)/(NIR + R)} \quad (13)$$

In the case of TM satellite data, NIR is band 4 and Red is band 3. NDVI is a ratio from −1 to +1. Water bodies such as lakes and rivers have a low reflectance in both visible Red and NIR hence resulting in slightly negative values. Moreover, bare soil exhibit a NIR spectral reflectance to some extent larger than visible RED thus tend to produce rather small positive NDVI values (0.1 to 0.2). Moreover, 0.2 <NDVI<0.5, the surface is then assumed to be a mix of bare soil and Vegetation. Contrarily, areas containing a vegetation canopy will tend to positive values (NDVI> 0.5) and the surface is assumed to be vegetation only (Morawitz et al., 2006; Julien et al., 2011)

4.4Analysis of Climate and Land-use Variations

A full weight of scientific evidence is further confirming that the perceptible change in Forest fire regimes is being exacerbated by both climatic variations and land use changes (Brown et al., 2004; Schumacher et al., 2006; Pitman et al., 2007; Kilpeläinen et al., 2010; Zumbrunnen et al., 2012; Ganteaume et al., 2013). Therefore, analyzing the variations in their trends is necessary to be able to situate their potential impact of forest fire burn severity.

4.3.1 Drought as a major Forest Fire driver

Assessing inter-annual variability of precipitation and potential evaporation hence mean annual potential evapotranspiration helps in understanding drought severity and frequency in the study area. One way to analyze this relationship is by using raw meteorological data taken from one meteorological station in the study area during the period 1986 till 2012 on a yearly basis. As seen in **Figure 4.2**, precipitation between 1986 and 2000 maintained a rather stable trend compared to the acute fluctuation in the years between 2007 and 2012.

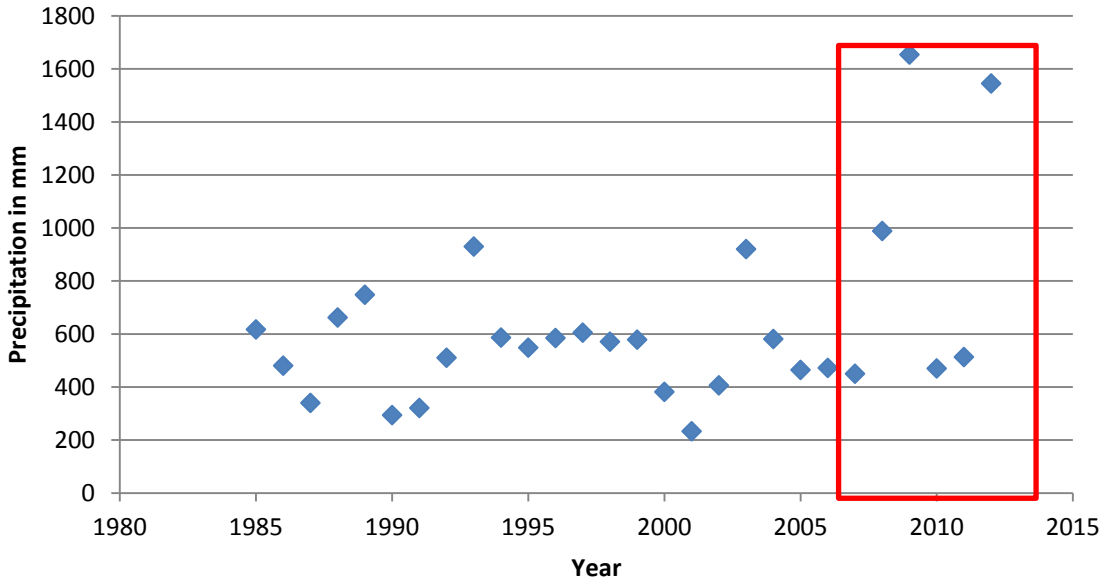

Figure 4.2 Fluctuation of precipitation trend between 1986 and 2012 in Damour

This disturbance in precipitation trend affects potential evapotranspiration (PET) since it is its main component. As **Figure 4.3** shows, years between 1986 and 2006 show a constant trend of PET where years between 2007 and 2012 show fluctuations; implying changes in climatic conditions that might alter forest fire regimes.

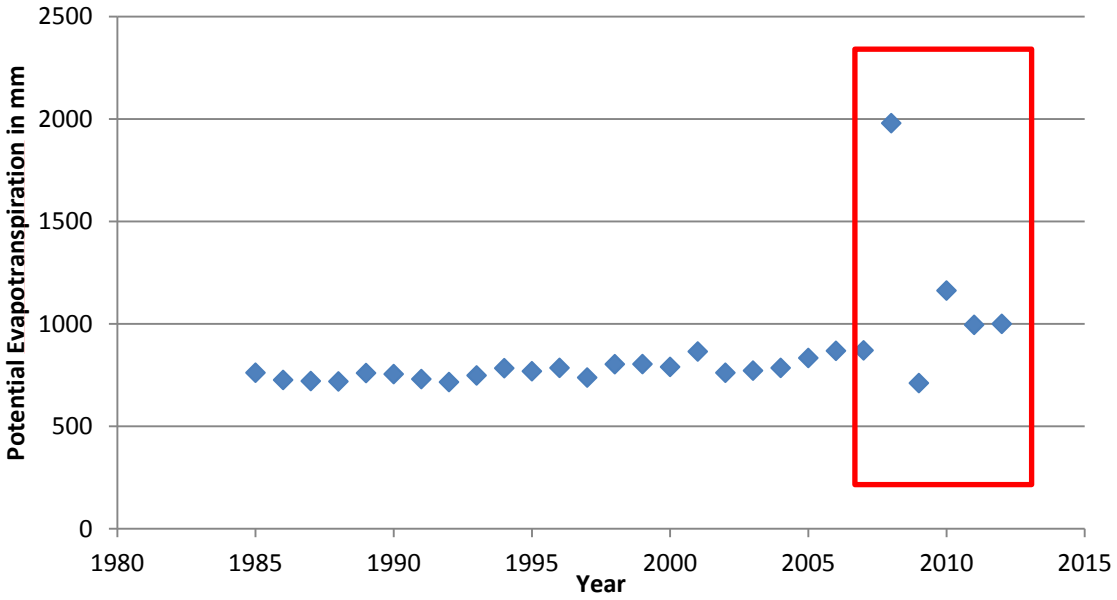

Figure 4.3 Increasing Potential Evapotranspiration (PET) of Damour watershed from year 1985 to 2012

On the hand,the developed time series include annual RDI_{st} values. In order to identify the role of climatic variability, the Reconnaissance Drought Index was calculated for the period 1984-2012 using **Equations 10 and 11**. It has been noticed that between 1984 and 1999 values showed a fairly constant trend with only three years of drought in 15 years. Values between 2000 and 2012 show a more fluctuating trend with 6 years of drought in 12 years. Moreover, years between 2008 and 2012 witnessed progressively extreme events of very wet and extremely dry years. A point should be mentioned that the "Near Normal" ranges vary between -0.99 which is almost "Moderately dry" and 0.99 which is almost "Moderately wet" meaning that while observing the RDI_{st} values, one should assess the actual values. Overall, RDI_{st} has a decreasing trendline towards more dry years as shown in **Figure 4.4**.

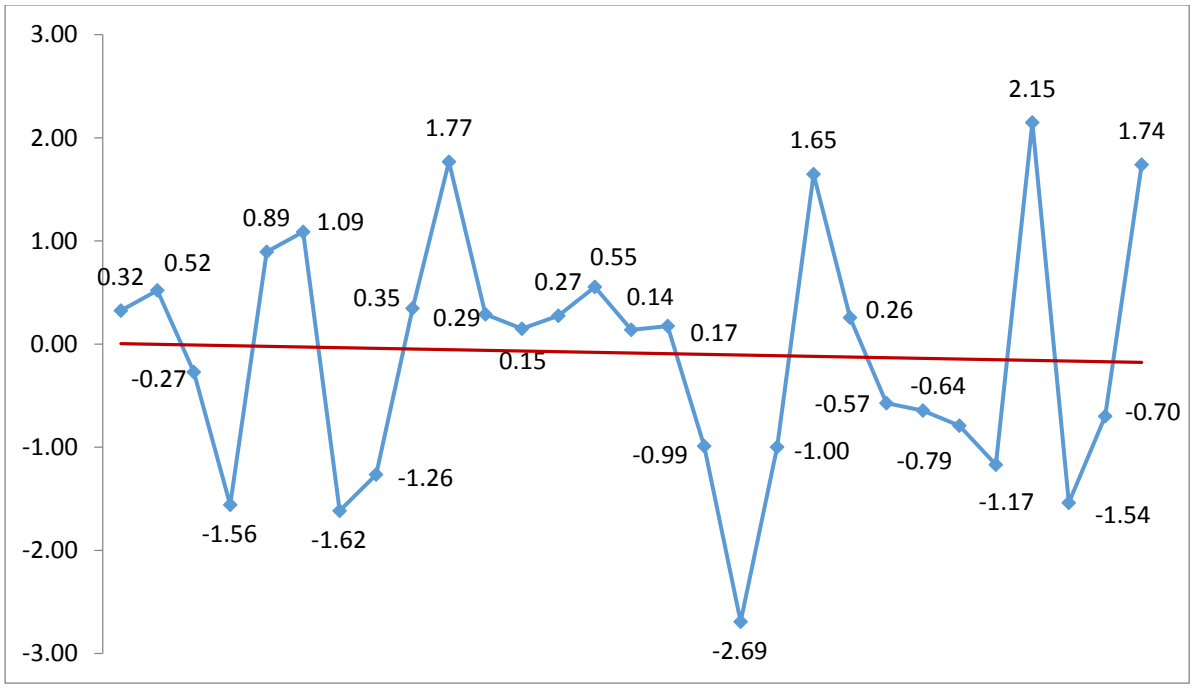

Figure 4.4 Decreasing Standardized Reconnaissance Drought Index (RDIst) trendline (in red) implying a tendency towards increased drought severity

In later discussions, values of RDI_{st} that were used in comparison with NBR values were chosen to match the processed Landsat images in order to study a potential correlation , hence to assess the potential impact of RDI_{st} on NBR.

In addition to drought, various factors including other fire-weather conditions ,such as solar radiation and wind speed which were not included in this study due to the lack of this specific data, vegetation type and land-use also determine forest fire activity (Zumbrunnen et al., 2008; Littell et al., 2009).

4.3.2 Monitoring land use variation using NDVI

For the NDVI images, changes between non-vegetated and vegetated lands were identified. **Figure 4.5** shows the land cover change images using the outputs of the unclassified supervision classification technique of the Landsat images dating from 1984 till 2012 and the area coverage for the three classes respectively. NDVI change rate was minimal between 1984 and 1999. According to **Figure 4.6**, vegetation cover seems to have a decreasing linear trendline meaning that maximum NDVI values representing vegetated areas tend to decline whereas minimum values representing non vegetated areas tend to increase between 1984 and 2012. Moreover, in years 1984, 1986, 1987, 1992, 1998 and 1999 NDVI values were somewhat stable with 0.69, 0.78, 0.56, 0.563, 0.564, and 0.541 respectively. But in years stretching over the last decade 2002-2012, maximum NDVI trend started to fluctuate more frequently between 0.164, 0.321, 0.362, 0.767, 0.317, 0.489 and 0.515 for the years 2002, 2006, 2008, 2009, 2010, 2011, 2012 respectively. Moreover, land cover map of Damour of 1984 was compared to 2012. **Table 4.2** shows the cross-tabulation matrix for the areas changed from one NDVI class to another by percentage. In 1984, Medium NDVI occupied almost the entire area (85.5%) while High NDVI occupied 12.3% of the area and fewer extentions of Low NDVI (2.2%). In 2012, the reclamation accelerated and urban sprawl expanded. Consequently, a shift in NDVI classes was observed; medium NDVI areas decreased by 19.8% and high NDVI areas also decreased by 4.6%. This indicates that around 24.4% of the area was transformed to Low NDVI hence bare and urban land and water bodies. In order to verify the quality of the Remotely-Sensed NDVI maps that were derived, an Overlay Analysis was performed using ArcGIS (9.3) Intersect Tool to compare the RS NDVI with the field investigated land use map that was produced by the National Center of Scientific Research (NCSR) in 2010. The results showed an overlap of 83% between the two maps as shown in the **Figure 4.7** below.

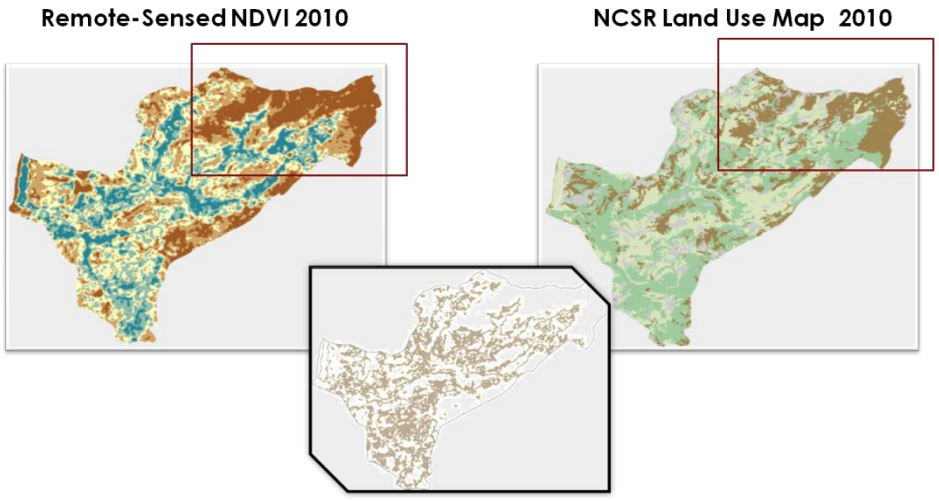

Figure 4.7 Overlay Analysis between Remotely Sensed NDVI and NCSR Land Use Map 2010

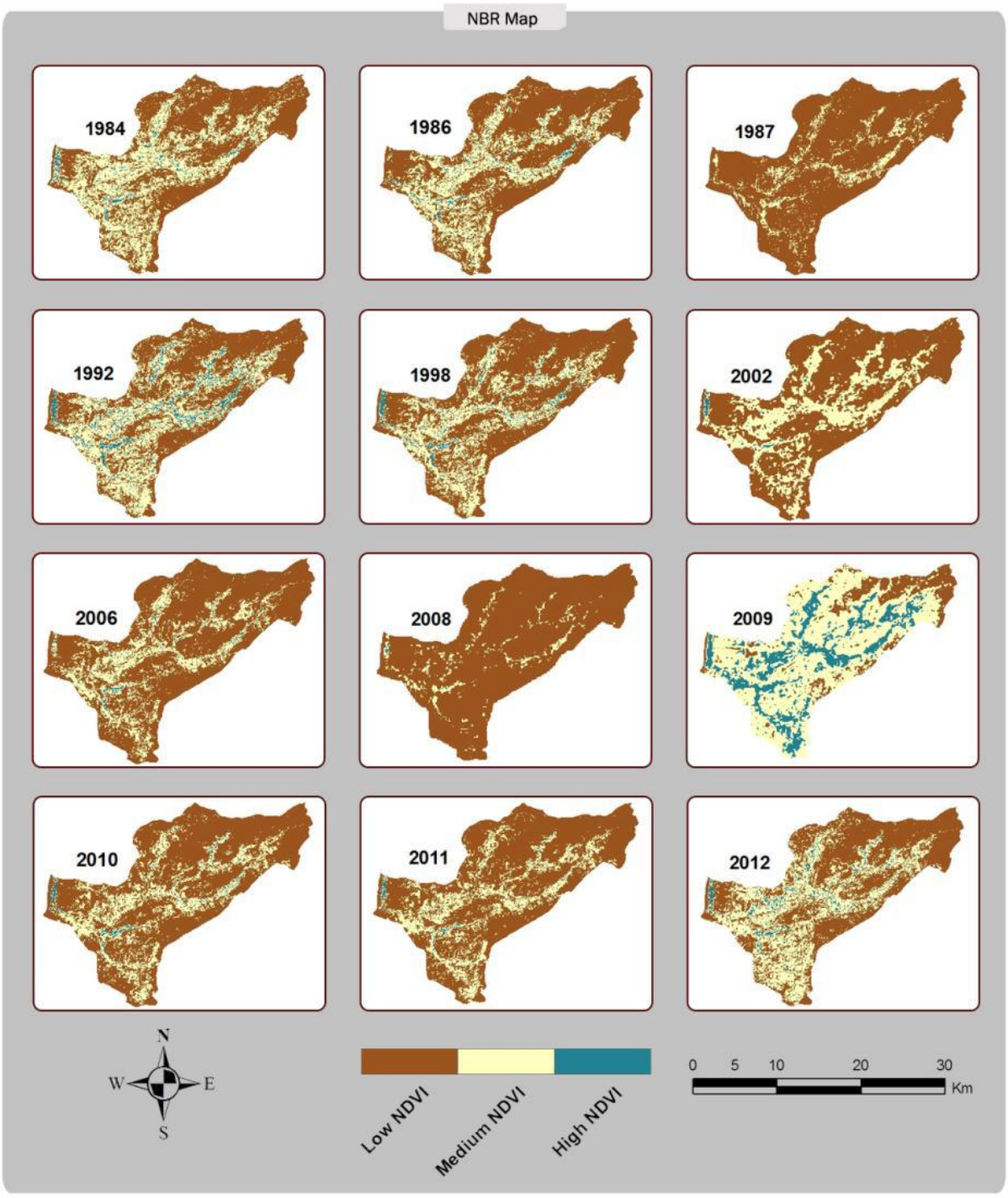

Figure 4.5 Normalized Difference Vegetation Index (NDVI) variation maps in Damour watershed showing the progression of burn severity from 1984-2012

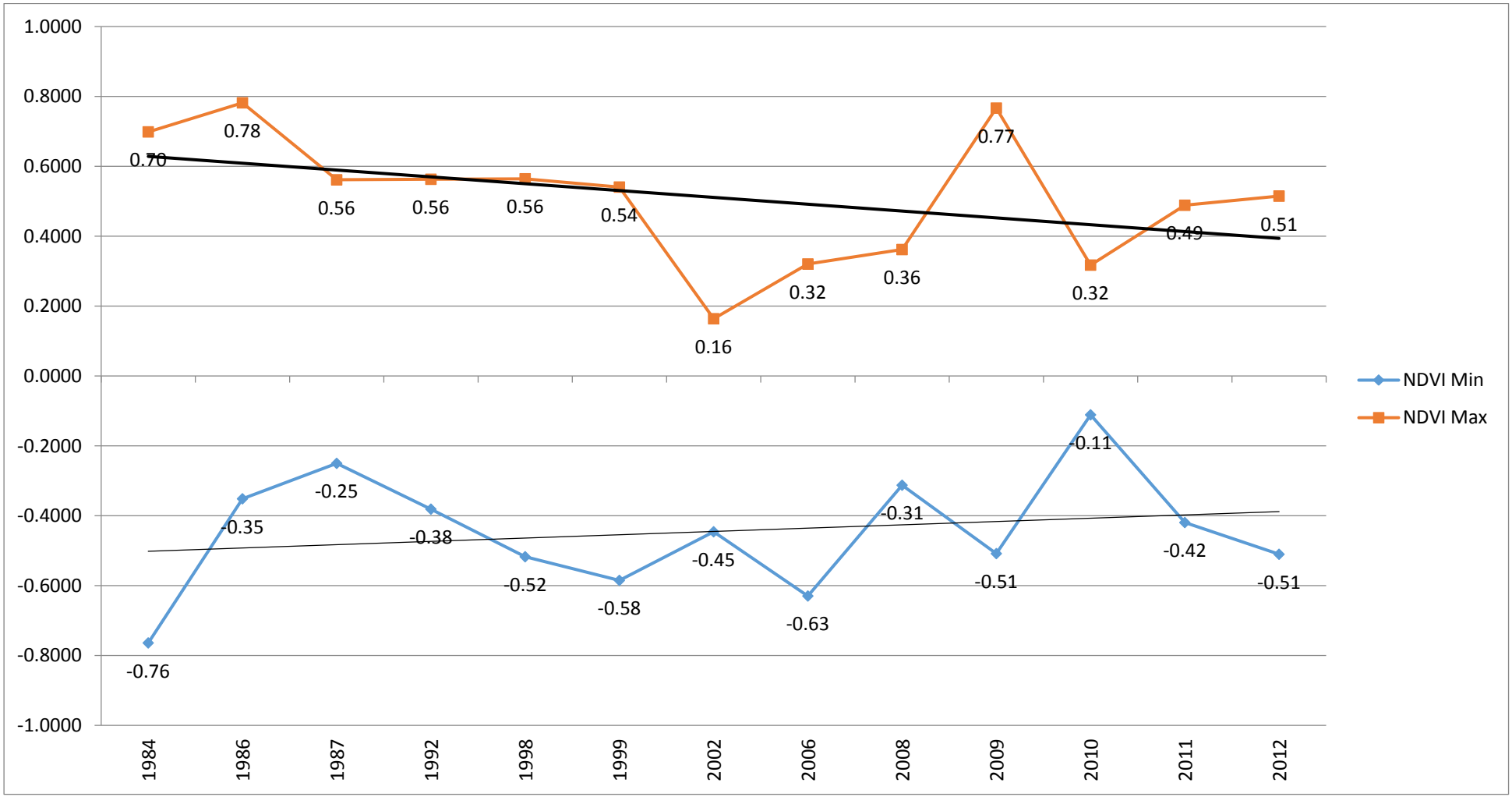

Figure 4.6 Normalized Difference Vegetation Index maximum (NDVImax) and minimum (NDVImin) values showing an increasing trendline in NDVImax values insinuating a decreased vegetation cover and increased NDVImin

Table 4.2 Comparison of Land cover maps of 1984 and 2012

Damour Land Cover	Low NDVI	Medium NDVI	High NDVI	Total Percentage (%)
NDVI_84	2.2	85.5	12.3	100
NDVI_12	26.6	65.7	7.7	100

4.3.3 Analysis results of forest fire burn severity variation through Normalized burn ratio

Landsat-derived NBR maps were produced according to **Equation 2**. Recurrence of forest fires in certain areas of the watershed enhances the development of increased burn severity. According to **Figure 4.7**, maximum NBR (NBR_{max}) values tend to have a positive linear trendline. This implies that areas affected by forest fire tend to undergo increased burn severity. NBR_{max} values have been somewhat constant between 1984 and 1998. Values varied between 0.355 and 0.496. However values representing years between 2002 and 2012 showed a more varied fluctuation with increased NBR_{max} values ranging between 0.371 and 0.688.

Moreover, it has been noticed that variations in NBR maps between low, moderate and high severity can be linked to RDI_{st} values .Map of 1987 demonstrates moderate and high severity areas as compared to 1984. When compared to RDI_{st}, it was a severely dry year with a value of -1.55. Similarly, map of 2002 was a moderately dry year with a value of 0.99 and was preceded by two years of severely and extremely dry years of 2000 and 2002. Moreover, years of 2008, 2010 and 2011 which were classified as moderately and severely dry years with values -1.17, -1.54 and -0.7 respectively also show moderate and high burn severity areas.

Even though year 2006 was a near normal year preceded by wet and near normal years of 2003, 2004 and 2005, its NBR exhibits moderate and high burn severity. This can be related to the 2006 war (Israel war on Lebanon) which witnessed various bombing caused fires. On the other hand, and despite the fact that the years 2009 and 2012 were very wet years with RDI_{st} values of 2.14 and 1.74 respectively, the corresponding NBR maps show traces of moderate burn severity substantiating the fact that forest fire burn severity is not solely affected by climatic variations.

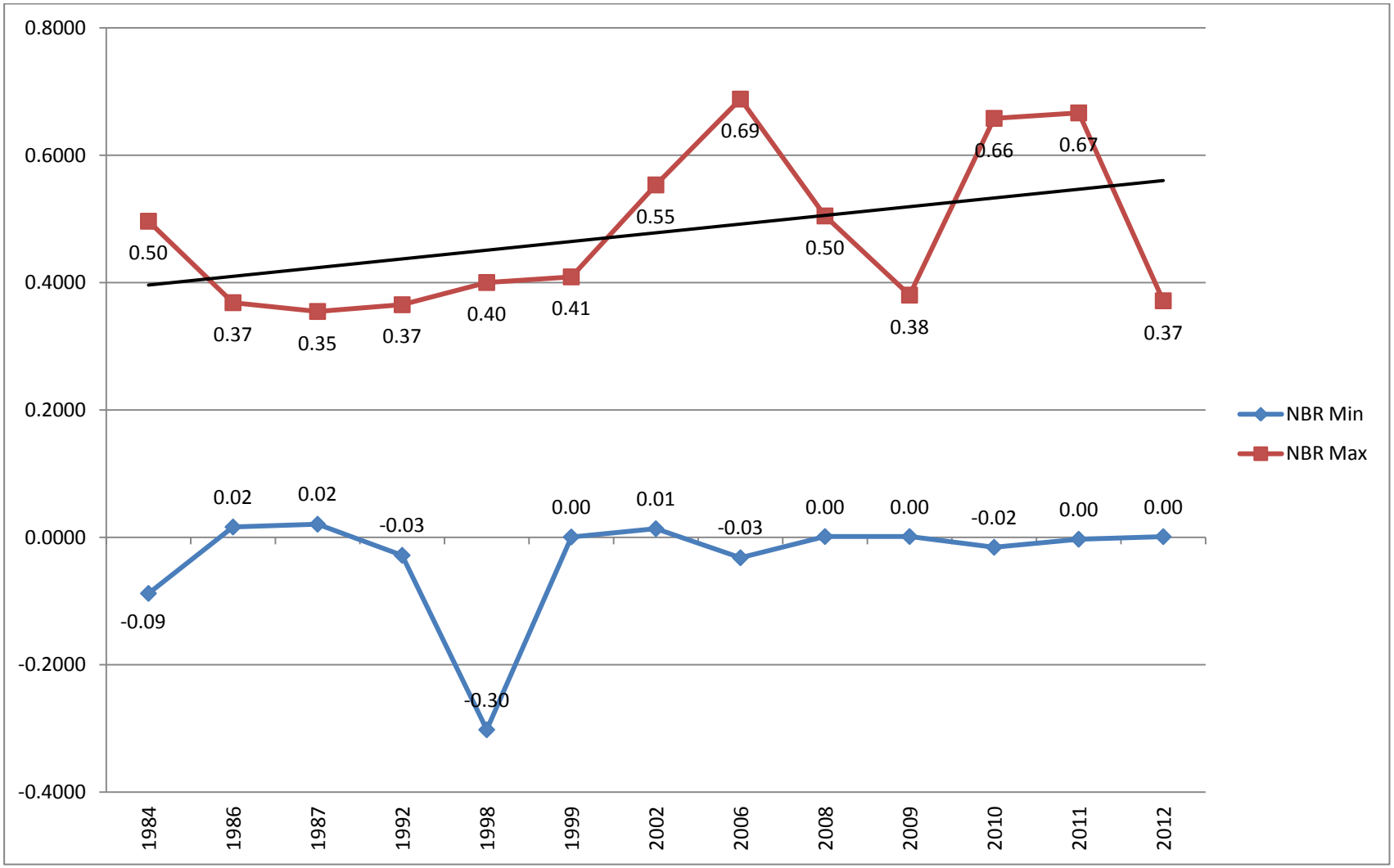

Figure 4.8 Normalized Burn Ratio maximum (NBR_{max}) and minimum (NBR_{min}) values showing an increasing trendline in NBR_{max} values insinuating an increased burn severity

4.4 Correlation between Forest fire burn severity and impacting factors

The association between forest fire burn severity, climate or land cover change has been discussed through many studies. Some have concluded that climatic variation will affect fire frequency and severity saying that evidence is already accumulating from records of fire that recent changes have coincided with increases in both extent and intensity of fires in several regions (Pausas, 2004; Flannigan et al., 2005; Running, 2006, Tymstra et al., 2007; Koutsias et al., 2012; Yang et al., 2011). Others have concluded that while natural ignition occurs relatively infrequently on a global scale, human ignition associated with land use is widespread (Hely et al., 2001; Csiszar et al., 2004; Aráoz and Grau, 2010; San-Miguel-Ayanz et al., 2012). In order to get a better understanding of the relative contributions of climate and human activities in driving forest fire burn severity in our study area, the interactions and association between NBR and NDVI on one hand and NBR and RDI_{st} on the other, indices values were explored and compared and a statistical correlation was calculated using Pearson Correlation Coefficient (*r*). The quantity r, called the linear correlation coefficient, measures the strength and the direction of a linear relationship between two variables (x and y).

$$r = \frac{n\sum xy - (\sum x)(\sum y)}{\sqrt{\sqrt{n(\sum x^2)}(\sum x)^2}\sqrt{n(\sum y^2)}(\sum y)^2} \quad (14)$$

A correlation greater than 0.8 is generally described as strong, whereas a correlation less than 0.5 is generally described as weak.

This combined analyses provided an approach to identify the dynamics of forest fire burn severity. It is quite obvious that the NDVI and NBR have inverse trends (**Figure 4.7**) As NDVI decreases, meaning a minor difference between red and NIR hence less photosynthetic activity, NBR increases meaning increased burn severity. Both indices' fluctuation increased between 2002 and 2012 as compared to years between 1984 and 1999 where NBR values were somewhat stable.

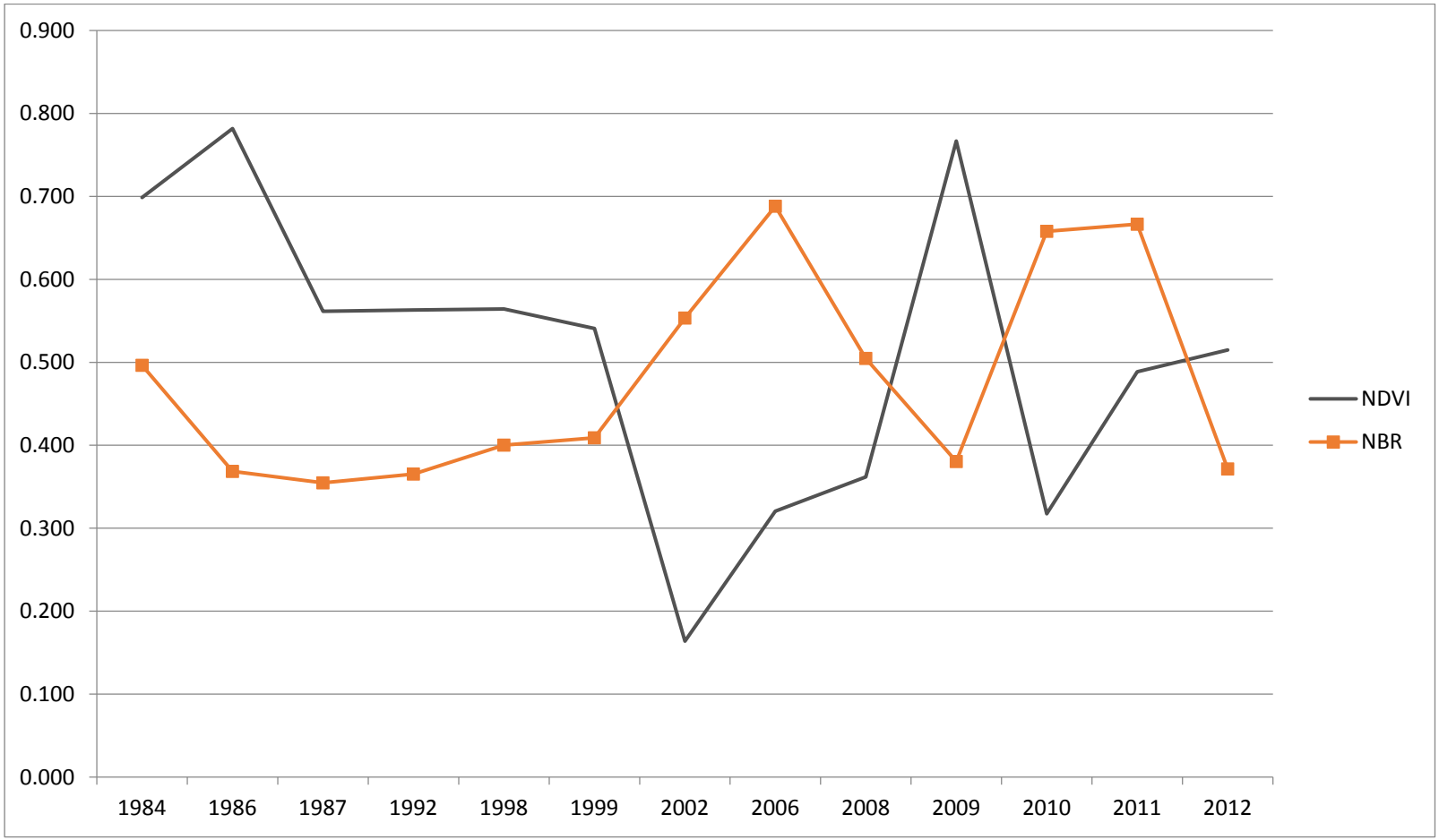

Figure 3.9 Comparing Normalized Burn Ratio (NBR) to Normalized Difference Vegetation Index (NDVI)

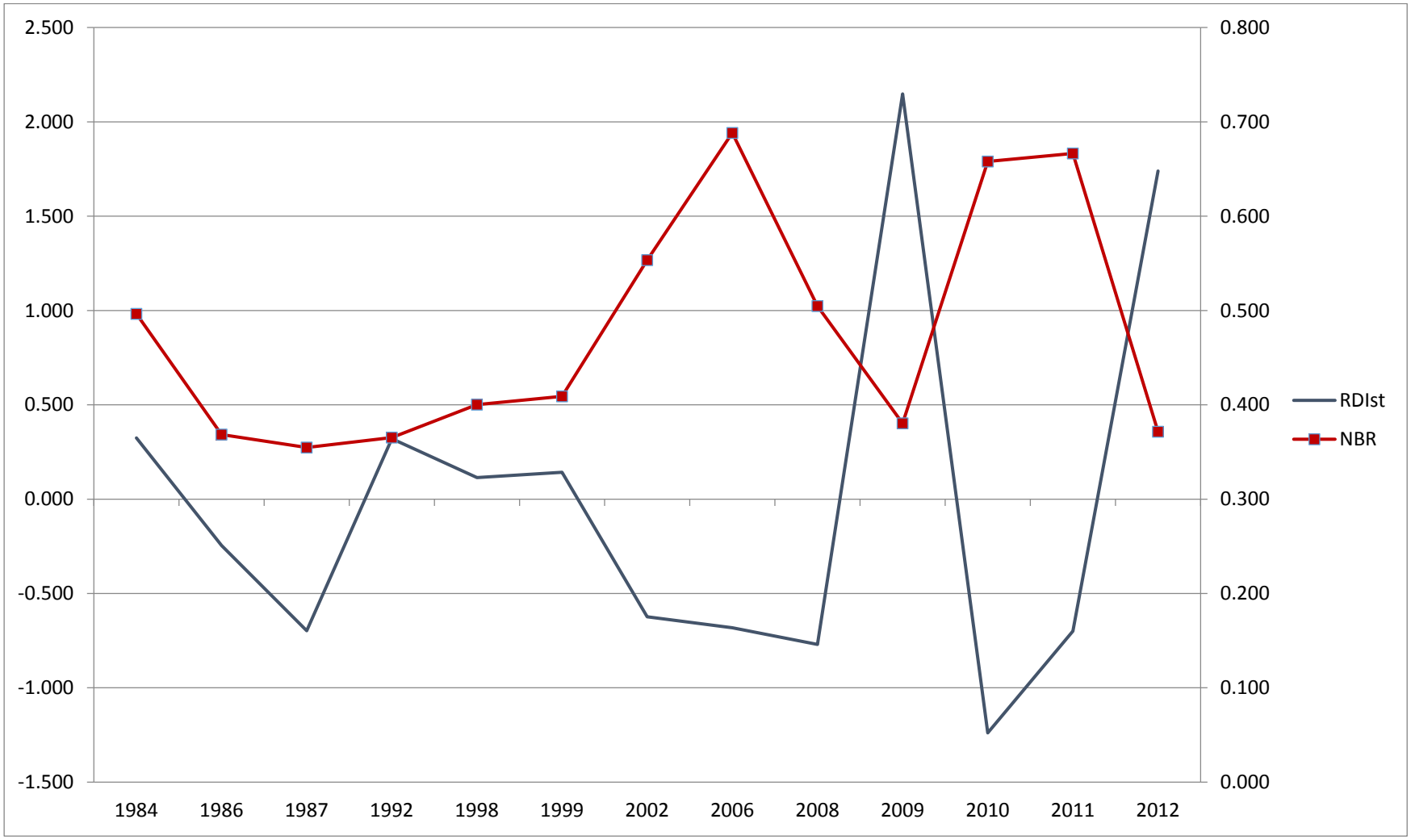

Figure 4.10 Comparing Normalized Burn Ratio (NBR) to Standardized Reconnaissance Drought Index (RDIst) trendline showing negative correlation

On the other hand, The NBR was compared to RDI_{st} values which represent the impact of climatic variations on NBR values. As seen in **Figure 4.9**, RDI_{st} and NBR trends are also somewhat inversely parallel. When RDI_{st} increases suggesting a wet year, NBR values decrease because of less fuel availability. However, less significant negative statistical correlation (R= -0.59) was established. It is important to note that the climatic data covers 28 years but the years that were chosen to be represented in the curve match the processed Landsat images' dates.

Results showed a moderate negative correlation R= -0.65 between NBR and NDVI. $NDVI_{max}$ and a lower inverse correlation R= -0.59 between NBR_{max} and RDI_{st} .These results substantiate the relationship between NBR forest fire severity and NDVI on one hand and RDI_{st} on the other.

It can be concluded that forest fire burn severity depends on the interactions among climate and land use rather than being the result of a sole factor. Such associations play a significant part in mitigating climate change and land-use through their potential roles to assessing changes in responses between terrestrial ecosystems and climate, mediated by forest fires. Moreover, such comparisons help in land management and mass movement mitigation planning at various geographical scales after its inducing factor's drivers have been thouroughly studied.

Conclusion

The type of work done in this thesis is the first of its sort in Lebanon on the topic of potential impact of forest fire on mass movement occurrence under the influence of climatic fluctuation and land use change using remote sensing and GIS techniques. The implemented methodologies can also be used as research necessities in other Mediterranean countries with similar geo-environmental characteristics.

Diverse types of mass movements (MM) were detected and delineated using aerial and satellite images. Similarily, forest fire inventory was established using remote sensing in addition to input from public organizations and Nongovernmental agencies. Using Infoval, a bivariate relationship between MM occurrence and its preconditioning factors and forest fire burn severity as an inducing factor was established, MM susceptibility Map (MMSM) of the study area was produced and the impact of forest fire on MM was identified as the second most influential factor.

Due to this high relevancy, forest fire potential triggering factors were investigated in order to attain a comprehension of fire regime dynamics. This will serve as an important conception to MM occurrence and help in putting into practice sustainable mitigation plans for Lebanon as a whole and the study area in particular.

The findings obtained in this thesis can be divided into four main parts:

A. Mass movement and forest fire detection and delineation using Remote Sensing

Aerial photos, Ikonos satellite images and Google Earth timeline were used for Mass movement and forest fire inventory compilation. Ikonos images were draped over 10m accuracy DEM in order to enhance visual interpretation. Similarly, and the 3D terrain of Google Earth facilitated the geomorphic analysis and verification of previous MM and FF occurrence. **Results showed that MM events increased by 47% between 1956 and 2005 and by 21% between 2005 and 2008** in addition to the field investigation that was carried on in 2102 for validation of MM and forest fire inventory maps. Forest fire on the other hand proved to be recurrent in various locations, intensifying there probable effects on MM.

B. ***Analysis of associations between mass movement, preconditioning and inducing factors***

In order to recognize factors that are instigating this constant increase in MM occurrence, GIS was exploited through InfoVal, a bivariate statistical analysis method, to assess the relationship between MM and its preconditioning factors on one hand (Rock Type, Soil, Land use, Slope degree, Slope

aspect and mean annual precipitation) and the investigated inducing factor Forest fire burn severity since FF has also emerged as an important natural hazard destroying over 25% of Lebanon's forests in less than 40 years. **In Damour, preceded by soil (84) and tied with rock type (67), forest fire burn severity represented by Normalized burn ratio (67) extracted from LANDSAT images proved to have the second highest weight factor on MM occurrence.**

C. *Mass movement susceptibility mapping*

Using GIS and depending on the weight factors obtained through InfoVAL, a M ass Movement Susceptibility Map (MMSM) was generated with four susceptibility levels: High, moderate, low and no susceptibility. This map was validated using an independent set of MM events that were a subset of the produced inventory. An accuracy of **78% of the existing mass movements** occur in the **predicted high- and moderate-susceptibility** zones in Damour watershed. Moreover, **21% of the mass movements** occur **in no- or low-susceptibility** zones, which comprise 61.9% of the total area. In order to establish the impact of Forest fire on mass movement, NBR was removed from the MMSM and another susceptibility map was generated. The percentage of mass movements **decreased by 16% in high-susceptibility areas**, increased by **18% in moderate-susceptibility areas, increased by 21% in low-susceptibility areas, and increased by 12% in no-susceptibility.**

D. Investigating the causes that control forest fire system

Due to its proved high impact on MM occurrence, it is only logical to investigate further on the factors that potentially influence forest fire burn severity. Climatic variations represented through the Standardized Reconnaissance Drought Index (RDI_{st}) and land use changes through the Normalized Difference Vegetation Index (NDVI) were considered as inducing factors. Results showed a moderate negative correlation **R= -0.65 between NBR and NDVI.** $NDVI_{max}$ and a lower inverse **correlation R= -0.59 between NBR_{max} and RDI_{st}** .These results substantiate the relationship between NBR forest fire severity and NDVI on one hand and RDI_{st} on the other. **It can be concluded that forest fire burn severity depends on the interactions among climate and land use rather than being the result of a sole factor.**

Perspectives and Recommendations

The work done in this thesis can be further enhanced, developed and expanded through integrating new remote sensing and GIS techniques and/or through gathering more field and climatic data to increase result accuracies and stronger correlations. Below are some recommendations to be exploited:

- Mass movement inventories can be improved and updated using current and soon launched satellite sensors. Recent literature of these sensors shows that the most promising approaches will be exploiting VHR optical (Worldview 3, GeoEye 2, Pleiades 1-2, Sentinel 2, Spot 6 and Spot 7) and Radar (Sentinel 1, Palsar 2, Tandem-L). Not only will they provide much better spatial resolution but also higher temporal resolution which can reach up to 1 day recurrence with the Pleiades and 3-6 days recurrence with Sentinel 2A and 2B. Even though LiDAR sensors are the most used for surface topography analysis through providing a highly detailed terrain, some optical images have stereo capabilities of providing a 1m DEM (ex: Pleiades).
- A more extensive field investigation for MM and forest fire inventory validation covering more locations and obtaining more infiltometer measurements for a more accurate post fire soil water repellency status.
- Mass movement susceptibility model can enclose more preconditioning parameters such as drainage system and detailed faulting system. Moreover, more inducing factors such as floods and intensity rainfall events can be individually investigated for their impact on MM occurrence.
- Uncertainty is associated with each stage of climate variation impact assessment hence data should be as credible and accurate as possible. In this context, climatic data used for drought assessment and correlation with forest fire burn severity was yearly records. Monthly and even daily records could have produced a sharper correlation but this kind of data is not available for all Lebanese watersheds.
- It is important to note that the climatic data covers 28 years but the years that were chosen to be represented in the curve match the processed Landsat images' dates. Firther investigation could aim to incorporate a larger number of satellite images for a more sharper correlation between drought hence climate and forest fire regime.

A total of three articles and a book chapter were prepared throughout this thesis corresponding to chapters one, two and three through 3.

- Abdallah, C., **Ziade, R**., Baghdadi,N., Al Kafri, AM. (2012). Climate Change Impacts on Land Stability; El Damour. *In Hydrometeorological Disasters and Climate Change*. Taylor and Francis. **Accepted**
- **Ziade, R**., Abdallah, C., Baghdadi, N. (2014) *The effect of forest fire on mass movement in Lebanese mountainous areas. International Journal of Wildland Fire*. **23**, 845–859
- Ziade, R., Abdallah, C., Baghdadi, N.(2014) *Forest Fire burn severity between climatic variation and land use change*. Submitted to *Mitigation and Adaptation Strategies for Global Change*.
- **Ziade, R**., Abdallah, C., Baghdadi, N., Berger, F. (2014). Mass Movement: A Review on applied monitotoring and Modeling Techniques. **Submitted** to Bulletin of Engineerig Gelology and the Environement.

In addition to these publications, oral communications and posters of the thesis work were presented in international conferences:

1. Ziade R., Abdallah C., and Baghdadi N., 2012. Mass Movement Hazards in the Mediterranean; A review on applied techniques and methodologies. European Geosciences Union General Assembly (EGU), Vienna, Austria, 22-27 avril, Geophysical Research abstract, vol. 14, EGU2012-6226.
2. Ziade R., Abdallah C., and Baghdadi N., 2012. Impact of forest fire and intensity rainfall on mass movement occurrence in Lebanon. *ForestSAT 2012*, Corvallis, Oregon USA, 11-14 September 2012.
3. Abdallah C., Ziade R., Baghdadi N., and Al kafri A.M., 2013. Climate Change Impacts on Land Stability; El Damour Basin (Lebanon) Case Study, Poster. Secondes journées Franco-Libanaises, Avancées de la Recherche et des ses applications, 22 au 25 octobre 2013, Université du Tittoral Côte d'Opale, Dunkerque, France.
4. Abdallah, C., **Ziade, R**., Khater, C., 2014. Forest Fire Impact on Landslides. Medpine 5, Solosona ,Spain, 22-26 September

References

Abdallah, C., Chorowicz, J., Boukheir, R., Dhont, D. (2007). Comparative use of processed satellite images in remote sensing of mass movements: Lebanon as a case study. International Journal of Remote Sensing, 28(19),1 - 20.

Abdallah, C. (2010). Spatial distribution of block falls using volumetric GIS–decision-tree models. International Journal of Applied Earth Observation and Geoinformation, 12(5), 393-403.

Abdallah, C. (2012). Assessment of erosion, mass movements and flood risk in Lebanon. In H. Kouyoumjian & M. Hamze (Eds.), Review and Perspective of Environmental Studies in Lebanon (pp. 225-246). Beirut: INCAM-EU-CNRS Lebanon.

Abdallah, C., Chorowicz, J., Bou Kheir, R., & Khawlie, M. (2005). Detecting major terrain parameters relating to mass movements' occurrence using GIS, remote sensing and statistical correlations, case study Lebanon. Remote Sensing of Environment, 99(4), 448-461. doi: http://dx.doi.org/10.1016/j.rse.2005.09.014

Afify, A. (2011). Evaluation of change detection techniques for monitoring land-cover changes: A case study in new Burg El-Arab area. Alexandria Engineering Journal, 50(2), 187-195. doi: http://dx.doi.org/10.1016/j.aej.2011.06.001

Ahmadi, H., & Fooladmand, R. (2008). Spatially distributed monthly reference evapotranspiration derived from the calibration of Thornthwaite equation: a case study, South of Iran. Irrigation Science, 26(4), 303-312. doi: 10.1007/s00271-007-0094-8

Akbarimehr, M., Motagh, M., & Haghshenas-Haghighi, M.. (2013). Slope Stability Assessment of the Sarcheshmeh Landslide, Northeast Iran, Investigated Using InSAR and GPS Observations. Remote Sensing, 5(8), 3681-3700.

Akgun, A. (2012). A comparison of landslide susceptibility maps produced by logistic regression, multicriteria decision and likelihood ratio methods: case study at Izmir, Turkey. Landslides, 93–106.

Aleotti, P., & Chowdhury, R. (1999). Landslide hazard assessment: summary review and new perspectives. Bulletin of Engineering Geology and the Environment, 58(1), 21-44. doi: 10.1007/s100640050066

Alexander, D.E. (1991). Natural disasters: a framework for research and teaching. Disasters, 15, 209-226.

Alexandrian, D., Esnault, F., & Calabri, G. (1999). Forest Fire in Mediterranean Areas. Unasylva, 50(197), 35-41.

Ali, A., de Bie, C.A.J.M., Skidmore, A.K., Scarrott, R.G., Hamad, A., Venus, V., & Lymberakis, P. (2013). Mapping land cover gradients through analysis of hyper-temporal NDVI imagery. International Journal of Applied Earth Observation and Geoinformation, 23(0), 301-312. doi: http://dx.doi.org/10.1016/j.jag.2012.10.001

Alkevli, T., & Ercanoglu, M.. (2011). Assessment of ASTER satellite images in landslide inventory mapping: Yenice-Gökçebey (Western Black Sea Region, Turkey). Bulletin of Engineering Geology and the Environment, 70(4), 607-617. doi: 10.1007/s10064-011-0353-z

Alonso-Sarria, F., & Lopez-Bermudez, F. (1994). Rainfall time and space variability during short storms in south-east Spain. Geookodynamik Band, 261-278.

Alphan, H., & Derse, Ali. (2012). Change detection in Southern Turkey using normalized difference vegetation index (NDVI). Journal of Environmental Engineering and Landscape Management, 21(1), 12-18. doi: 10.3846/16486897.2012.663091

Althuwaynee, F., Pradhan, B., Park, H.J., & Lee, J.H. (2014). A novel ensemble bivariate statistical evidential belief function with knowledge-based analytical hierarchy process and multivariate statistical logistic regression for landslide susceptibility mapping. CATENA, 114(0), 21-36. doi: http://dx.doi.org/10.1016/j.catena.2013.10.011

Alves Júnior, J., Folegatti, V., Silva, R., Silva, J. A., & Evangelista, W.P. (2011). Response of young 'Tahiti' lime trees to different irrigation levels. Engenharia Agrícola, 31, 303-314.

Alvioli, M., Guzzetti, F., & Rossi, M.. (2014). Scaling properties of rainfall induced landslides predicted by a physically based model. Geomorphology, 213(0), 38-47. doi: http://dx.doi.org/10.1016/j.geomorph.2013.12.039

Ambraseys, N. N., & Barazangi, M.. (1989). The 1759 Earthquake in the Bekaa Valley: Implications for earthquake hazard assessment in the Eastern Mediterranean Region. Journal of Geophysical Research: Solid Earth, 94(B4), 4007-4013. doi: 10.1029/JB094iB04p04007

Améztegui, A., Brotons, L., & Coll, L. (2010). Land-use changes as major drivers of mountain pine (Pinus uncinata Ram.) expansion in the Pyrenees. Global Ecology and Biogeography, 19(5), 632-641. doi: 10.1111/j.1466-8238.2010.00550.x

Amor, L.G., Carrasco, A., & Ibáñez, J.C. (2009). Using and Testing Drought Indicators. In Ana Iglesias, Antonino Cancelliere, DonaldA Wilhite, Luis Garrote & Francisco Cubillo (Eds.), Coping with Drought Risk in Agriculture and Water Supply Systems (Vol. 26, pp. 257-272): Springer Netherlands.

Anderson, M. G., Holcombe, L., & Renaud, J. P. (2007). Assessing slope stability in unplanned settlements in developing countries. Journal of Environmental Management, 85(1), 101-111. doi: 10.1016/j.jenvman.2006.08.005

Anderson, R. , Hardy, E., Roach, T., & Witmer, E. (1976). A land use and land cover classification system for use with remote sensor data (Vol. 964): USGS

Anderson, S., & Sitar, N. (1995). Analysis of Rainfall-Induced Debris Flows. Journal of Geotechnical Engineering, 121(7), 544-552. doi: doi:10.1061/(ASCE)0733-9410(1995)121:7(544)

Antonarakis, A. S., Richards, K. S., & Brasington, J. (2008). Object-based land cover classification using airborne LiDAR. Remote Sensing of Environment, 112(6), 2988-2998. doi: http://dx.doi.org/10.1016/j.rse.2008.02.004

Antonello, G., Casagli, N., Farina, P., Leva, D., Nico, G., Sieber, A. J., & Tarchi, D. (2004). Ground-based SAR interferometry for monitoring mass movements. Landslides, 1(1), 21-28. doi: 10.1007/s10346-003-0009-6

Antonini, G., Ardizzone, F., Cardinali, M., Galli, M., Guzzetti, F., & Reichenbach, P. (2002). Surface deposits and landslide inventory map of the area affected by the 1997 Umbria–Marche earthquakes. Bollettino della Societa Geologica Italiana, 121(2), 843–853.

Aráoz, E., & Grau, R.. (2010). Fire-Mediated Forest Encroachment in Response to Climatic and Land-Use Change in Subtropical Andean Treelines. Ecosystems, 13(7), 992-1005. doi: 10.1007/s10021-010-9369-7

Arcenegui, V., Mataix-Solera, J., Guerrero, C., Zornoza, R., Mataix-Beneyto, J., & García-Orenes, F. (2008). Immediate effects of wildfires on water repellency and aggregate stability in Mediterranean calcareous soils. CATENA, 74(3), 219-226. doi: http://dx.doi.org/10.1016/j.catena.2007.12.008

Ardizzone, F., Cardinali, M., Galli, M., Guzzetti, F., & Reichenbach, P. (2007). Identification and mapping of recent rainfall-induced landslides using elevation data collected by airborne Lidar. Natural Hazard Earth Systems Science, 7(6), 637–650.

Ardizzone, F., Fiorucci, F., Santangelo, M., Cardinali, M., Mondini, A.C., Rossi, M., . . . Guzzetti, F. (2013). Very-High Resolution Stereoscopic Satellite Images for Landslide Mapping. In Claudio Margottini, Paolo Canuti & Kyoji Sassa (Eds.), Landslide Science and Practice (pp. 95-101): Springer Berlin Heidelberg.

Asadi Zarch, M.A., Malekinezhad, H., Mobin, M.H., Dastorani, M.T., & Kousari, M.R. (2011). Drought Monitoring by Reconnaissance Drought Index (RDI) in Iran. Water Resources Management, 25(13), 3485-3504. doi: 10.1007/s11269-011-9867-1

Asner, P., & Warner, S. (2003). Canopy shadow in IKONOS satellite observations of tropical forests and savannas. Remote Sensing of Environment, 87(4), 521-533. doi: http://dx.doi.org/10.1016/j.rse.2003.08.006

Assouline, S., & Ben-Hur, M. (2006). Effects of rainfall intensity and slope gradient on the dynamics of interrill erosion during soil surface sealing. CATENA, 66(3), 211-220. doi: http://dx.doi.org/10.1016/j.catena.2006.02.005

Atkinson, P. M., & Massari, R. (1998). Generalised linear modelling of susceptibility to landsliding in the central apennines, italy. Computers & Geosciences, 24(4), 373-385. doi: http://dx.doi.org/10.1016/S0098-3004(97)00117-9

Aubert, M., Baghdadi, N., Zribi, M., Douaoui, A., Loumagne, C., Baup, F., . . . Garrigues, S. (2011). Analysis of TerraSAR-X data sensitivity to bare soil moisture, roughness, composition and soil crust. Remote Sensing of Environment, 115(8), 1801-1810. doi: http://dx.doi.org/10.1016/j.rse.2011.02.021

Avery, T., & Berlin, L. (1992). Fundamentals of Remote Sensing and Airphoto Interpretation New Jersey: Prentice Hall.

Badia, A., Saurı, D., Cerdan, R., . . . Llurdés, J.C. (2002). Causality and management of forest fires in Mediterranean environments: an example from Catalonia. Global Environmental Change Part B: Environmental Hazards, 4(1), 23-32. doi: http://dx.doi.org/10.1016/S1464-2867(02)00014-1

Baghdadi, N., Aubert, M., & Zribi, M. (2012). Use of TerraSAR-X Data to Retrieve Soil Moisture Over Bare Soil Agricultural Fields. Geoscience and Remote Sensing Letters, IEEE, 9(3), 512-516. doi: 10.1109/LGRS.2011.2173155

Bai, S., Lü, G., Wang, J., Zhou, P., & Ding, L. (2011). GIS-based rare events logistic regression for landslide-susceptibility mapping of Lianyungang, China. Environmental Earth Sciences, 62(1), 139-149. doi: 10.1007/s12665-010-0509-3

Bajocco, S., Pezzatti, B., Mazzoleni, S., & Ricotta, C. (2010). Wildfire seasonality and land use: when do wildfires prefer to burn? Environmental Monitoring and Assessment, 164(1-4), 445-452. doi: 10.1007/s10661-009-0905-x

Bakr, N., Weindorf, D. C., Bahnassy, M. H., Marei, S. M., & El-Badawi, M. M. (2010). Monitoring land cover changes in a newly reclaimed area of Egypt using multi-temporal Landsat data. Applied Geography, 30(4), 592-605. doi: http://dx.doi.org/10.1016/j.apgeog.2009.10.008

Baldo, M., Bicocchi, C., Chiocchini, U., Giordan, D., & Lollino, G.. (2009). LIDAR monitoring of mass wasting processes: The Radicofani landslide, Province of Siena, Central Italy. Geomorphology, 105(3–4), 193-201. doi: http://dx.doi.org/10.1016/j.geomorph.2008.09.015

Ballais, J. L. , & Bosc, M. C. (1994). The ignifracts of the Sainte-Victoire mountain (Lower Provence, France). Paper presented at the Soil erosion and degradation as a consequence of forest fires

International conference, Logrono, Spain.

Bălteanu, D., Chendeş, V., Sima, M., & Enciu, P.. (2010). A country-wide spatial assessment of landslide susceptibility in Romania. Geomorphology, 124(3–4), 102-112. doi: http://dx.doi.org/10.1016/j.geomorph.2010.03.005

Barbero, M., Bonin, G., Loisel, R., & Quézel, P. (1990). Changes and disturbances of forest ecosystems caused by human activities in the western part of the mediterranean basin. Vegetatio, 87(2), 151-173. doi: 10.1007/BF00042952

Barlow, J., Franklin, S., & Martin, Y. (2006). High Spatial Resolution Satellite Imagery, DEM Derivatives, and Image Segmentation for the Detection of Mass Wasting Processes. Photogrammetric Engineering and Remote Sensing, 72(6), 687-692.

Baumgartl, T., & Horn, R. (1991). Effect of aggregate stability on soil compaction. Soil and Tillage Research, 19(2–3), 203-213. doi: http://dx.doi.org/10.1016/0167-1987(91)90088-F

Beatty, M., & Smith, E. (2013). Dynamic soil water repellency and infiltration in post-wildfire soils. Geoderma, 192(0), 160-172. doi: http://dx.doi.org/10.1016/j.geoderma.2012.08.012

Bento-Gonçalves, A., Vieira, A., Úbeda, X., & Martin, D. (2012). Fire and soils: Key concepts and recent advances. Geoderma, 191(0), 3-13. doi: http://dx.doi.org/10.1016/j.geoderma.2012.01.004

Benz, U.C., Hofmann, P., Willhauck, G., Lingenfelder, I., & Markus, H. (2004). Multi-resolution, object-oriented fuzzy analysis of remote sensing data for GIS-ready information. ISPRS, 58, 239–258.

Berardino, P., Fornaro, G., Lanari, R., & Sansosti, E. (2002). A new algorithm for surface deformation monitoring based on small baseline differential SAR interferograms. Geoscience and Remote Sensing, IEEE Transactions on, 40(11), 2375-2383. doi: 10.1109/TGRS.2002.803792

Bindschadler, A., Scambos, A., Choi, H., & Haran, M. (2010). Ice sheet change detection by satellite image differencing. Remote Sensing of Environment, 114(7), 1353-1362. doi: http://dx.doi.org/10.1016/j.rse.2010.01.014

Blaschke, T. (2010). Object oriented image analysis for remote sensing. ISPRS, 65(1), 2–16.

Bonano, M., Manunta, M., Pepe, A., Paglia, L., & Lanari, R. (2013). From previous C-band to new X-band SAR systems: Assessment of the DInSAR mapping improvement for deformation time-series retrieval in urban areas. IEEE.

Booij, M. J. (2005). Impact of climate change on river flooding assessed with different spatial model resolutions. Journal of Hydrology, 303(1–4), 176-198. doi: http://dx.doi.org/10.1016/j.jhydrol.2004.07.013

Booth, M., Roering, J., & Perron, T. (2009). Automated landslide mapping using spectral analysis and high-resolution topographic data: Puget Sound lowlands, Washington, and Portland Hills, Oregon. Geomorphology, 109(3–4), 132-147. doi: http://dx.doi.org/10.1016/j.geomorph.2009.02.027

Borghuis, A. M., Chang, K., & Lee, H. Y. (2007). Comparison between automated and manual mapping of typhoon-triggered landslides from SPOT-5 imagery. International Journal of Remote Sensing, 28(8), 1843-1856. doi: 10.1080/01431160600935638

Bottari, C., & Sepe, V. (2013). The role of earthquakes, landslides and climate changes in the abandonment of the Roman Carsulae site (Tevere basin – Central Italy). Quaternary International, 308–309(0), 105-111. doi: http://dx.doi.org/10.1016/j.quaint.2012.10.053

Bou Kheir, R., Abdallah, C., & Khawlie, M. (2008). Assessing soil erosion in Mediterranean karst landscapes of Lebanon using remote sensing and GIS. Engineering Geology, 99(3–4), 239-254. doi: http://dx.doi.org/10.1016/j.enggeo.2007.11.012

Bovenga, F., Wasowski, J., Nitti, D.O., Nutricato, R., & Chiaradia, M.T. (2012). Using COSMO/SkyMed X-band and ENVISAT C-band SAR interferometry for landslides analysis. Remote Sensing of Environment, 119(C), 272–285.

Bozzano, F., Cipriani, I., Mazzanti, P., & Prestininzi, A. (2011). Displacement patterns of a landslide affected by human activities: insights from ground-based InSAR monitoring. Natural Hazards, 59(3), 1377-1396. doi: 10.1007/s11069-011-9840-6

Breidenbach, J., Ortiz, M., & Reich, M. (2010). Forest monitoring with TerraSAR-X: first results. European Journal of Forest Research, 129(5), 813-823. doi: 10.1007/s10342-009-0318-y

Brenner, R.P. , Tam, H.K. , & Brand, E.W. . (1985). Field stress path simulation of rain-induced slope failure. Paper presented at the 11th International Conference on Soil Mechanics and Foundation Engineering, San Fransisco.

Broncano, M.J., & Retana, J. (2004). Topography and pre-fire vegetation affecting the spatial heterogeneity generated after a large forest wildfire in the Mediterranean Basin. International Journal of Wildland Fire 13, 209-216.

Brown, T., Hall, L., & Westerling, A.L. (2004). The Impact of Twenty-First Century Climate Change on Wildland Fire Danger in the Western United States: An Applications Perspective. Climatic Change, 62(1-3), 365-388. doi: 10.1023/B:CLIM.0000013680.07783.de

Buma, J., & Dehn, M. (1998). A method for predicting the impact of climate change on slope stability. Environmental Geology, 35(2-3), 190-196. doi: 10.1007/s002540050305

Burn, H., & Hesch, M. (2007). Trends in evaporation for the Canadian Prairies. Journal of Hydrology, 336(1–2), 61-73. doi: http://dx.doi.org/10.1016/j.jhydrol.2006.12.011

Calò, F., Ardizzone, F., Castaldo, R., Lollino, P., Tizzani, P., Guzzetti, F., . . . Manunta, M. (2014). Enhanced landslide investigations through advanced DInSAR techniques: The Ivancich case study, Assisi, Italy. Remote Sensing of Environment, 142, 69-82. doi: http://dx.doi.org/10.1016/j.rse.2013.11.003

Campo, J., Andreu, V., Gimeno-García, E., González, O., & Rubio, J. L. (2006). Occurrence of soil erosion after repeated experimental fires in a Mediterranean environment. Geomorphology, 82(3–4), 376-387. doi: http://dx.doi.org/10.1016/j.geomorph.2006.05.014

Cannon, H., & Reneau, L. (2000). Conditions for generation of fire-related debris flows, Capulin Canyon, New Mexico. Earth Surface Processes and Landforms, 25(10), 1103-1121. doi: 10.1002/1096-9837(200009)25:10<1103::AID-ESP120>3.0.CO;2-H

Cardinali, M. , Antonini, G. , Reichenbach, P., & Guzzetti, F. (Cartographer). (2001). Photogeological and landslide inventory map for the Upper Tiber River basin.

Carere, K., Ratto, S., & Zanolini, F. (2001). Prevention des mouvements de versants et des instabilites de falaises, Confrontation des m ethodes d'etudes des eboulements rocheux dans l'arc alpin.

Carmi, G., & Berliner, P. (2008). The effect of soil crust on the generation of runoff on small plots in an arid environment. CATENA, 74(1), 37-42. doi: http://dx.doi.org/10.1016/j.catena.2008.02.002

Carrara, A., Guzzetti, F., Cardinali, M., & Reichenbach, P. (1999). Use of GIS Technology in the Prediction and Monitoring of Landslide Hazard. Natural Hazards, 20(2-3), 117-135. doi: 10.1023/A:1008097111310

Carro, M., De Amicis, M., Luzi, L., & Marzorati, S. (2003). The application of predictive modeling techniques to landslides induced by earthquakes: the case study of the 26 September 1997 Umbria–Marche earthquake (Italy). Engineering Geology, 69(1–2), 139-159. doi: http://dx.doi.org/10.1016/S0013-7952(02)00277-6

Carter, B.J. , & Ciolkosz, E.J. . (1991). Slope gradienr and aspect effects on soils developed from sandstone in Pennsylvania. Geoderma, 49, 199-121.

Cascini, L., Fornaro, G., & Peduto, D. . (2009). Analysis at medium scale of low-resolution DInSAR data in slow-moving landslide-affected areas. ISPRS, 64, 598–611.

Cascini, L., Fornaro, G., & Peduto, D. (2010). Advanced low- and full-resolution DInSAR map generation for slow-moving landslide analysis at different scales. Engineering Geology, 112(1–4), 29-42. doi: http://dx.doi.org/10.1016/j.enggeo.2010.01.003

Castellnou, M., & M., Miralles. (2010). The great fire changes in the Mediterranean—the example of Catalonia, Spain. Crisis Response, 5, 56–57.

Cendrero, A. , & Dramis, F. (1996). The contribution of landslides to landscape evolution in Europe,. Geomorphology, 15(3-4), 191-211.

Certini, G. (2005). Effects of fire on properties of forest soils: a review. Oecologia, 143, 1-10.

Çevik, E., & Topal, T. (2003). GIS-based landslide susceptibility mapping for a problematic segment of the natural gas pipeline, Hendek (Turkey). Environmental Geology, 44(8), 949-962. doi: 10.1007/s00254-003-0838-6

Chander, G., & Markham, B. (2003). Revised Landsat-5 TM radiometric calibration procedures and postcalibration dynamic ranges. Geoscience and Remote Sensing, IEEE Transactions on, 41(11), 2674-2677. doi: 10.1109/TGRS.2003.818464

Chaplot, V.A.M. , & Le Bissonnais, Y. . (2003). Runoff features for interrill erosion at different rainfall intensities, slope lengths, and gradients in an agricultural loessial hillslope. Soil Science Society of America Journal, 67(3), 844-851.

Chauhan, S., Sharma, M., Arora, M. K., & Gupta, N. K. (2010). Landslide Susceptibility Zonation through ratings derived from Artificial Neural Network. International Journal of Applied Earth Observation and Geoinformation, 12(5), 340-350. doi: http://dx.doi.org/10.1016/j.jag.2010.04.006

Che, V. B., Kervyn, M., Suh, C. E., Fontijn, K., Ernst, G. G. J., del Marmol, M. A., . . . Jacobs, P. (2012). Landslide susceptibility assessment in Limbe (SW Cameroon): A field calibrated seed cell and information value method. CATENA, 92(0), 83-98. doi: http://dx.doi.org/10.1016/j.catena.2011.11.014

Chebbani, R., Djilli, K., & Roose, E. (1999). Etude des risques d'érosion dans le bassin versant de l'isser, Algérie. Bulletin Réseau Erosion, 19, 85-95.

Chen, C.Y., & Huang, W.L.. (2013). Land use change and landslide characteristics analysis for community-based disaster mitigation. Environmental Monitoring and Assessment, 185(5), 4125-4139. doi: 10.1007/s10661-012-2855-y

Chen, G., Hay, G.J. , Carvalho, L.M.T., & Wulder, M.A. (2012). Object-based change detection. International Journal for Remote Sensing, 33, 4434–4457.

Cheng, K. S., Wei, C., & Chang, S. C. (2004). Locating landslides using multi-temporal satellite images. Advances in Space Research, 33(3), 296-301. doi: http://dx.doi.org/10.1016/S0273-1177(03)00471-X

Choi, J., Oh, H.J., Lee, H.J., Lee, C., & Lee, S. (2012). Combining landslide susceptibility maps obtained from frequency ratio, logistic regression, and artificial neural network models using ASTER images and GIS. Engineering Geology, 124(0), 12-23. doi: http://dx.doi.org/10.1016/j.enggeo.2011.09.011

Chorowicz, J., & Deroin, J.P. (2003). La télédétection et la cartographie géomorphologique et géologique. Paris: Contemporary Publishing International.

Ciappa, A., Pietranera, L., & Battazza, F.. (2010). Perito Moreno Glacier (Argentina) flow estimation by COSMO SkyMed sequence of high-resolution SAR-X imagery. Remote Sensing of Environment, 114(9), 2088-2096. doi: citeulike-article-id:7267379

doi: 10.1016/j.rse.2010.04.014

Cifuentes, P., Malpica, J.A, & González-Matesanz, F.J. (2008). Change Detection with SPOT-5 and FORMOSAT-2 Imageries. In George Bebis, Richard Boyle, Bahram Parvin, Darko Koracin, Paolo Remagnino, Fatih Porikli, Jörg Peters, James Klosowski, Laura Arns, YuKa Chun, Theresa-Marie Rhyne & Laura Monroe (Eds.), Advances in Visual Computing (Vol. 5359, pp. 1186-1195): Springer Berlin Heidelberg.

Cigna, F., Del Ventisette, C., Liguori, V., & Casagli, N. (2011). Advanced radar-interpretation of InSAR time series for mapping and characterization of geological processes. Nat. Hazards Earth Syst. Sci., 11(3), 865-881. doi: 10.5194/nhess-11-865-2011

Coates, D.R. (1977). Landslides. Engineering Geology, 3, 1-278.

Colesanti, C., & Wasowski, J. (2006). Investigating landslides with space-borne Synthetic Aperture Radar (SAR) interferometry. Engineering Geology, 88(3–4), 173-199. doi: http://dx.doi.org/10.1016/j.enggeo.2006.09.013

Conforti, M., Pascale, S., Robustelli, G., & Sdao, F. (2014). Evaluation of prediction capability of the artificial neural networks for mapping landslide susceptibility in the Turbolo River catchment (northern Calabria, Italy). CATENA, 113(0), 236-250. doi: http://dx.doi.org/10.1016/j.catena.2013.08.006

Conoscenti, C., Di Maggio, C. , & Rotigliano, E. (2008). GIS analysis to assess landslide susceptibility in a fluvial basin of NW Sicily (Italy). Geomorphology, 94, 325–339.

Corominas, J., Westen, C., Frattini, P., Cascini, L., Malet, J. P., Fotopoulou, S., . . . Smith, J. T. (2014). Recommendations for the quantitative analysis of landslide risk. Bulletin of Engineering Geology and the Environment, 73(2), 209-263. doi: 10.1007/s10064-013-0538-8

Corsini, A., Cervi, F., Daehne, A., Ronchetti, F., & Borgatti, L. (2009). Coupling geomorphic field observation and LiDAR derivatives to map complex landslides. In J.P. Malet, A. Remaître & T. Bogaard (Eds.), Landslides Processes — From Geomorphologic Mapping to Dynamic Modelling (pp. 15-18). Strasbourg: CERG Editions.

Corti, T., Muccione, V., Köllner-Heck, P., Bresch, D., & Seneviratne, S. I. (2009). Simulating past droughts and associated building damages in France. Hydrol. Earth Syst. Sci., 13(9), 1739-1747. doi: 10.5194/hess-13-1739-2009

Crozier, M. (1986). Climatic triggering of landslide episodes. Landslide, Croom Helm(169-192).

Cruden, D.M., & Varnes, D.J. . (1996). Landslide Types and Processes. In A.K. Turner & R.L. Schuster (Eds.), Landslides. Investigation and Mitigation (Vol. 3). Washington D.C.: Transport Research Board, National Research Council.

Csiszar, I., Justice, C. O., McGuire, A. D., Cochrane, M. A., Roy, D. P., Brown, F., . . . Verbyla, D. L. (2004). Land Use and Fires. In Garik Gutman, AnthonyC Janetos, ChristopherO Justice, EmilioF Moran, JohnF Mustard, RonaldR Rindfuss, David Skole, BillyLee Turner, II & MarkA Cochrane (Eds.), Land Change Science (Vol. 6, pp. 329-350): Springer Netherlands.

Cumming, SG. (2001). Forest type and wildfire in the Alberta boreal mixedwood: What do fires burn? Ecological Applications, 11, 97–110.

Czuchlewski, K.R., Weissel, J.K., & Kim, Y. (2003). Polarimetric synthetic aperture radar study of the Tsaoling landslide generated by the 1999 Chi-Chi earthquake, Taiwan. Journal of Geophysical Research: Earth Surface, 108(F1), 6006. doi: 10.1029/2003JF000037

Dahal, R., Hasegawa, S., Nonomura, A., Yamanaka, M., Masuda, T., & Nishino, K. (2009). Failure characteristics of rainfall-induced shallow landslides in granitic terrains of Shikoku Island of Japan. Environmental Geology, 56(7), 1295-1310.

Dahal, R.K., Hasegawa, S., Nonomura, A., Yamanaka, M., Dhakal, S., & Paudyal, P. (2008). Predictive modelling of rainfall-induced landslide hazard in the Lesser Himalaya of Nepal based on weights-of-evidence. Geomorphology, 102(3–4), 496-510. doi: http://dx.doi.org/10.1016/j.geomorph.2008.05.041

Dai, F. C., & Lee, C. F. (2001). Frequency–volume relation and prediction of rainfall-induced landslides. Engineering Geology, 59(3–4), 253-266. doi: http://dx.doi.org/10.1016/S0013-7952(00)00077-6

Dai, F. C., & Lee, C. F. (2002). Landslide characteristics and slope instability modeling using GIS, Lantau Island, Hong Kong. Geomorphology, 42(3–4), 213-228. doi: http://dx.doi.org/10.1016/S0169-555X(01)00087-3

Darwich, T. (1988). Particularités régionales de la pédogenèse en Méditerranée orientale. Lebanese Science Bulletin, 4(2), 65-74.

Darwish, T. M., & Zurayk, R. A. (1997). Distribution and nature of Red Mediterranean soils in Lebanon along an altitudinal sequence. CATENA, 28(3–4), 191-202. doi: http://dx.doi.org/10.1016/S0341-8162(96)00037-9

Datta, P.S., & Schack-Kirchner, H. (2010). Erosion Relevant Topographical Parameters Derived from Different DEMs—A Comparative Study from the Indian Lesser Himalayas. Remote Sensing, 2(8), 1941-1961.

De Santis, A., Asner, G.P., Vaughan, P.J., & Knapp, D.E. (2010). Mapping burn severity and burning efficiency in California using simulation models and Landsat imagery. Remote Sensing of Environment, 114(7), 1535-1545. doi: http://dx.doi.org/10.1016/j.rse.2010.02.008

DeBano, L. F. (2000). The role of fire and soil heating on water repellency in wildland environments: a review. Journal of Hydrology, 231–232(0), 195-206. doi: http://dx.doi.org/10.1016/S0022-1694(00)00194-3

Del Gaudio, V., & Wasowski, J. (2004). Time probabilistic evaluation of seismically induced landslide hazard in Irpinia (Southern Italy). Soil Dynamics and Earthquake Engineering, 24(12), 915-928. doi: http://dx.doi.org/10.1016/j.soildyn.2004.06.019

Del Ventisette, C., Righini, G., Moretti, S., & Casagli, N. (2014). Multitemporal landslides inventory map updating using spaceborne SAR analysis. International Journal of Applied Earth Observation and Geoinformation, 30(0), 238-246. doi: http://dx.doi.org/10.1016/j.jag.2014.02.008

Delacourt, C., Allemand, P., Casson, B., & Vadon, H. (2004). Velocity field of the "La Clapière" landslide measured by the correlation of aerial and QuickBird satellite images. Geophysical Research Letters, 31(15), L15619. doi: 10.1029/2004GL020193

Delgado, J., Vicente, F., García-Tortosa, F., Alfaro, P., Estévez, A., Lopez-Sanchez, J. M., . . . Mallorquí, J. J. (2011). A deep seated compound rotational rock slide and rock spread in SE Spain: Structural control and DInSAR monitoring. Geomorphology, 129(3–4), 252-262. doi: http://dx.doi.org/10.1016/j.geomorph.2011.02.019

Deng, J. S. , Wang, K. , Deng, Y. H. , & Qi, G. J. . (2008). PCA-based land-use change detection and analysis using multitemporal and multisensor satellite data. International Journal for Remote Sensing, 29, 4823-4838.

Derron, M. H., & Jaboyedoff, M. (2010). Preface "LIDAR and DEM techniques for landslides monitoring and characterization". Nat. Hazards Earth Syst. Sci., 10(9), 1877-1879. doi: 10.5194/nhess-10-1877-2010

Decon Devices. (2012). Mini Disk Infiltrometer User's Manual. In Inc. Decagon Devices (Ed.). Pullman, WA.

Diodato, N., Bellocchi, G., Romano, N., & Chirico, G.B. (2011). How the aggressiveness of rainfalls in the Mediterranean lands is enhanced by climate change. Climatic Change, 108(3), 591-599. doi: 10.1007/s10584-011-0216-4

Dixon, N., & Brook, E.. (2007). Impact of predicted climate change on landslide reactivation: case study of Mam Tor, UK. Landslides, 4(2), 137-147. doi: 10.1007/s10346-006-0071-y

Doerr, S.H., Blake, W.H., Shakesby, R.A., Stagnitti, F., Vuurens, S.H., Humphreys, G.S., & Wallbrink, P. (2004). Heating effects on water repellency in Australian eucalypt forest soils and their value in estimating wildfire soil temperatures. International Journal of Wildland Fire, 13(2), 157-163. doi: http://dx.doi.org/10.1071/WF03051

Doerr, S. H., Shakesby, R. A., & Walsh, R. P. D. (2000). Soil water repellency: its causes, characteristics and hydro-geomorphological significance. Earth-Science Reviews, 51(1–4), 33-65. doi: http://dx.doi.org/10.1016/S0012-8252(00)00011-8

Dong, J.J., Tung, Y.H., Chen, C.C., Liao, J.J., & Pan, Y.W. (2009). Discriminant analysis of the geomorphic characteristics and stability of landslide dams. Geomorphology, 110(3–4), 162-171. doi: http://dx.doi.org/10.1016/j.geomorph.2009.04.004

Dong, J.J., Tung, Y.H., Chen, C.C., Liao, J.J., & Pan, Y.W. (2011). Logistic regression model for predicting the failure probability of a landslide dam. Engineering Geology, 117(1–2), 52-61. doi: http://dx.doi.org/10.1016/j.enggeo.2010.10.004

Dubertret, L. (Cartographer). (1945). Cartes géologiques à l'échelle de 1/50 000.

Duman, T.Y., Çan, T., Emre, Ö. , Keçer, M., Doğan, A., Şerafettin, A. , & Serap, D. (2005). Landslide inventory of northwestern Anatolia, Turkey. Engineering Geology, 77(1-2), 99–114.

Dunjó, G., Pardini, G., & Gispert, M. (2003). Land use change effects on abandoned terraced soils in a Mediterranean catchment, NE Spain. CATENA, 52(1), 23-37. doi: http://dx.doi.org/10.1016/S0341-8162(02)00148-0

Dunning, S. A., Mitchell, W. A., Rosser, N. J., & Petley, D. N. (2007). The Hattian Bala rock avalanche and associated landslides triggered by the Kashmir Earthquake of 8 October 2005. Engineering Geology, 93(3–4), 130-144. doi: http://dx.doi.org/10.1016/j.enggeo.2007.07.003

Easterling, D.R., Wallis, W. R., Lawrimore, J.H., & Heim, R.R. (2007). Effects of temperature and precipitation trends on U.S. drought. Geophysical Research Letters, 34(20), L20709. doi: 10.1029/2007GL031541

EC. (2010). Forest Fire in Europe 2009. European Commission Joint Research Center. http://effis.jrc.ec.europa.eu/effis-news/89-forest-fires-in-europe-2009

Eisbacher, G.H., & Clague, J.J. (1984). Destructive mass movements in the high mountains: hazard and management. Geologic Survey Canada, 84(16), 229.

Eisenbies, M.A., Aust, W.M., Burger, J.A., & Adams, M.B. (2007). Forest operations, extreme flooding events, and considerations for hydrologic modeling in the Appalachians--A review. Forest Ecology and Management, 242, 77-98.

El Kenawy, A., López-Moreno, J.I., & Vicente-Serrano, S.M. (2012). Trend and variability of surface air temperature in northeastern Spain (1920–2006): Linkage to atmospheric circulation. Atmospheric Research, 106(0), 159-180. doi: http://dx.doi.org/10.1016/j.atmosres.2011.12.006

EM-DAT. (2010). The OFDA/CRED International Disaster Database. from http://www.emdat.be/

Epting, J., Verbyla, D., & Sorbel, B. (2005). Evaluation of remotely sensed indices for assessing burn severity in interior Alaska using Landsat TM and ETM+. Remote Sensing of Environment, 96(3–4), 328-339. doi: http://dx.doi.org/10.1016/j.rse.2005.03.002

Ercanoglu, M., Gokceoglu, C., & Van Asch, Th W. J. (2004). Landslide Susceptibility Zoning North of Yenice (NW Turkey) by Multivariate Statistical Techniques. Natural Hazards, 32(1), 1-23. doi: 10.1023/B:NHAZ.0000026786.85589.4a

FAO. (1998). Forest fires in the Mediterranean area. from http://www.fao.org/docrep/x1880e/x1880e07.htm

Fard, M. (2001, 16-19 September). Slope stability – Study of a real landslide in Tabriz. Paper presented at the 54th Canadian Geotechnical Conference, 2nd Joint IAH and CGS Groundwater Conference, Calgary, Alberta, Canada.

Farina, P., Colombo, D., Fumagalli, A., Marks, F., & Moretti, S. (2006). Permanent Scatterers for landslide investigations: outcomes from the ESA-SLAM project. Engineering Geology, 88(3–4), 200-217. doi: http://dx.doi.org/10.1016/j.enggeo.2006.09.007

Farjalla, N., **& Ziade, R.** (2009). Drought Frequency under a changing climate in the easterm Mediterranean: Beqaa Valley, Lebanon. Paper presented at the EGU, Vienna.

Favis-Mortlock, D., & Boardman, J. (1995). Nonlinear responses of soil erosion to climate change: a modelling study on the UK South Downs. CATENA, 25(1–4), 365-387. doi: http://dx.doi.org/10.1016/0341-8162(95)00018-N

Fell, R., Corominas, J., Bonnard, C., Cascini, L., Leroi, E., & Savage, Z. (2008). Guidelines for landslide susceptibility, hazard and risk zoning for land use planning. Engineering Geology, 102(3–4), 85-98. doi: http://dx.doi.org/10.1016/j.enggeo.2008.03.022

Fiorucci, F., Cardinali, M., Carlà, R., Rossi, M., Mondini, A. C., Santurri, L., . . . Guzzetti, F. (2011). Seasonal landslide mapping and estimation of landslide mobilization rates using aerial and satellite images. Geomorphology, 129(1–2), 59-70. doi: http://dx.doi.org/10.1016/j.geomorph.2011.01.013

FIREMON. (2004). The Normalized Burn Ratio-Brief outline of processing steps: USDA.

Flannigan, M. D., Amiro, B. D., Logan, K. A., Stocks, B. J., & Wotton, B. M. (2006). Forest Fires and Climate Change in the 21ST Century. Mitigation and Adaptation Strategies for Global Change, 11(4), 847-859. doi: 10.1007/s11027-005-9020-7

Florinsky, I.V. (2012). Digital Terrain Analysis in Soil Science and Geology. Russia: Elsevier.

Fried, J.S., Torn, M.S., & Mills, E. (2004). The Impact of Climate Change on Wildfire Severity: A Regional Forecast for Northern California. Climatic Change, 64(1-2), 169-191. doi: 10.1023/B:CLIM.0000024667.89579.ed

Fröhlich, B., Bach, E., Walde, I., Hese, S. , Schmullius, C., & Denzler, J. (2013). Land cover classification of satellite images using contextual information. ISPRS, II-3/W1, 1-6.

Galli, M., Ardizzone, F., Cardinali, M., Guzzetti, F., & Reichenbach, P. (2008). Comparing landslide inventory maps. Geomorphology, 94, 268–289.

Ganteaume, A., Camia, A., Jappiot, M., San-Miguel-Ayanz, J., Long-Fournel, M., & Lampin, C. (2013). A Review of the Main Driving Factors of Forest Fire Ignition Over Europe. Environmental Management, 51(3), 651-662. doi: 10.1007/s00267-012-9961-z

García-Davalillo, J.C., Herrera, G., Notti, D., Strozzi, T., & Álvarez-Fernández, I. (2014). DInSAR analysis of ALOS PALSAR images for the assessment of very slow landslides: the Tena Valley case study. Landslides, 11(2), 225-246. doi: 10.1007/s10346-012-0379-8

García-Rodríguez, M. J., Malpica, J. A., Benito, B., & Díaz, M. (2008). Susceptibility assessment of earthquake-triggered landslides in El Salvador using logistic regression. Geomorphology, 95(3–4), 172-191. doi: http://dx.doi.org/10.1016/j.geomorph.2007.06.001

García-Ruiz, José M. (2010). The effects of land uses on soil erosion in Spain: A review. CATENA, 81(1), 1-11. doi: http://dx.doi.org/10.1016/j.catena.2010.01.001

García-Ruiz, José M., Arnáez, José, Gómez-Villar, Amelia, Ortigosa, Luis, & Lana-Renault, Noemí. (2013). Fire-related debris flows in the Iberian Range, Spain. Geomorphology, 196(0), 221-230. doi: http://dx.doi.org/10.1016/j.geomorph.2012.03.032

Gee, J. R., Masson, D.G., Watts, A.B., & Mitchell, N.C. (2001). Passage of debris flows and turbidity currents through a topographic constriction: seafloor erosion and deflection of flow pathways. Sedimentology, 48(6), 1389-1409. doi: 10.1046/j.1365-3091.2001.00427.x

Gèze, B. (Cartographer). (1956). Carte de reconnaissance des sols du Liban à l'échelle de 1/200 000.

Ghosh, S., van Westen, C.J., Carranza, E.J.M. , Jetten, V.G., Cardinali, M., Rossi, M., & Guzzetti, F. (2011). Generating event-based landslide maps in a data-scarce Himalayan environment for estimating temporal and magnitude probability. Engineering Geology, 128, 49–62.

Giddings, L., Soto, M., Rutherford, B. M., & Maarouf, A. (2005). Standardized Precipitation Index Zones for México. Atmósfera, 18, 33-56.

Gimmi, U., Wohlgemuth, T., Rigling, A., Hoffmann, C., & Bürgi, M. (2010). Land-use and climate change effects in forest compositional trajectories in a dry Central-Alpine valley. Annals of Forest Science, 67(7), 701-701. doi: 10.1051/forest/2010026

Giordan, D., Allasia, P., Manconi, A., Baldo, M., Santangelo, M., Cardinali, M., . . . Guzzetti, F. (2013). Morphological and kinematic evolution of a large earthflow: The Montaguto landslide, southern Italy. Geomorphology, 187(0), 61-79. doi: http://dx.doi.org/10.1016/j.geomorph.2012.12.035

Glade, T. (1998). Establishing the frequency and magnitude of landslide-triggering rainstorm events in New Zealand. Environmental Geology, 35((2-3)), 160–174.

Godt, J. W., Baum, R. L., Savage, W. Z., Salciarini, D., Schulz, W. H., & Harp, E. L. (2008). Transient deterministic shallow landslide modeling: Requirements for susceptibility and hazard assessments in a GIS framework. Engineering Geology, 102(3–4), 214-226. doi: http://dx.doi.org/10.1016/j.enggeo.2008.03.019

Gökceoglu, C., & Aksoy, H. (1996). Landslide susceptibility mapping of the slopes in the residual soils of the Mengen region (Turkey) by deterministic stability analyses and image processing

techniques. Engineering Geology, 44(1–4), 147-161. doi: http://dx.doi.org/10.1016/S0013-7952(97)81260-4

Gómez, H., & Kavzoglu, T. (2005). Assessment of shallow landslide susceptibility using artificial neural networks in Jabonosa River Basin, Venezuela. Engineering Geology, 78(1–2), 11-27. doi: http://dx.doi.org/10.1016/j.enggeo.2004.10.004

Gonzalez, P., Neilson, .P., Lenihan, .M., & Drapek, .J. (2010). Global patterns in the vulnerability of ecosystems to vegetation shifts due to climate change. Global Ecology and Biogeography, 19(6), 755-768. doi: 10.1111/j.1466-8238.2010.00558.x

Göransson, G., Norrman, J., Larson, M., Alén, C., & Rosén, L. (2014). A methodology for estimating risks associated with landslides of contaminated soil into rivers. Science of The Total Environment, 472(0), 481-495. doi: http://dx.doi.org/10.1016/j.scitotenv.2013.11.013

Gorum, T., Fan, X., van Westen, C.J., Huang, R.Q., Xu, Qi., Tang, C., & Wang, G. (2011). Distribution pattern of earthquake-induced landslides triggered by the 12 May 2008 Wenchuan earthquake. Geomorphology, 133(3–4), 152-167. doi: http://dx.doi.org/10.1016/j.geomorph.2010.12.030

Goswami, R., Mitchell, N.C., & Brocklehurst, S.H. (2011). Distribution and causes of landslides in the eastern Peloritani of NE Sicily and western Aspromonte of SW Calabria, Italy. Geomorphology, 132(3–4), 111-122. doi: http://dx.doi.org/10.1016/j.geomorph.2011.04.036

Granica, K., Almer, A., Hirschmugl, M., Proske, H., Wurm, M., Schnabel, T., . . . Schardt, M. (2007, 23-28 July 2007). Generation and webgis representation of landslide susceptibility maps using VHR satellite data. Paper presented at the Geoscience and Remote Sensing Symposium, 2007. IGARSS 2007. IEEE International.

Greco, R., Sorriso-Valvo, M., & Catalano, E. (2007). Logistic Regression analysis in the evaluation of mass movements susceptibility: The Aspromonte case study, Calabria, Italy. Engineering Geology, 89(1–2), 47-66. doi: http://dx.doi.org/10.1016/j.enggeo.2006.09.006

Griffiths, J.S., Mather, A.E., & Hart, A.B. (2002). Landslide susceptibility in the Rio Aguas catchment, SE Spain. Quaternary journal of engineering geology and hydrogeology, 35(1), 9-17.

Groisman, P.Y., Knight, R.W., Easterling, D.R., Karl, T.R., Hegerl, G.C., & Razuvaev, V.N. (2005). Trends in Intense Precipitation in the Climate Record. Journal of Climate, 18(9), 1326-1350. doi: 10.1175/JCLI3339.1

Gunzburger, Y., Merrien-Soukatchoff, V., & Guglielmi, Y. (2005). Influence of daily surface temperature fluctuations on rock slope stability: case study of the Rochers de Valabres slope (France). International Journal of Rock Mechanics and Mining Sciences, 42(3), 331-349. doi: http://dx.doi.org/10.1016/j.ijrmms.2004.11.003

Guzzetti, F. (2000). Landslide fatalities and the evaluation of landslide risk in Italy. Engineering Geology, 58(2), 89–107.

Guzzetti, F., Ardizzone, F., Cardinali, M. , Galli, M., & Reichenbach, P. (2008). Distribution of landslides in the Upper Tiber River basin, central Italy. Geomorphology, 96, 105–122.

Guzzetti, F. , Cardinali, M., Reichenbach, P., & Carrara, A. (2000). Comparing landslide maps: a case study in the upper Tiber River Basin, Central Italy. Environmental Management, 25(3), 247–363.

Guzzetti, F., Carrara, A., Cardinali, M., & Reichenbach, P.. (1999). Landslide hazard evaluation: a review of current techniques and their application in a multi-scale study, Central Italy. Geomorphology, 31(1–4), 181-216. doi: http://dx.doi.org/10.1016/S0169-555X(99)00078-1

Guzzetti, F., Mondini, C., Cardinali, M., Fiorucci, F., Santangelo, M., & Chang, K.T. (2012). Landslide inventory maps: New tools for an old problem. Earth-Science Reviews, 112(1–2), 42-66. doi: http://dx.doi.org/10.1016/j.earscirev.2012.02.001

Guzzetti, F., Reichenbach, P., Ardizzone, F., Cardinali, M., & Galli, M. (2006). Estimating the quality of landslide susceptibility models. Geomorphology, 81(1–2), 166-184. doi: http://dx.doi.org/10.1016/j.geomorph.2006.04.007

Guzzetti, F., Reichenbach, P., Cardinali, M., Galli, M., & Ardizzone, F. (2005). Probabilistic landslide hazard assessment at the basin scale. Geomorphology, 72(1–4), 272-299. doi: http://dx.doi.org/10.1016/j.geomorph.2005.06.002

Hack, R., Alkema, D., Kruse, A. M., Leenders, N., & Luzi, L. (2007). Influence of earthquakes on the stability of slopes. Engineering Geology, 91(1), 4-15. doi: http://dx.doi.org/10.1016/j.enggeo.2006.12.016

Hadji, R., Boumazbeur, A.E., Limani, Y., Baghem, M., Chouabi, A.M., & Demdoum, A. (2013). Geologic, topographic and climatic controls in landslide hazard assessment using GIS modeling: A case study of Souk Ahras region, NE Algeria. Quaternary International, 302(0), 224-237. doi: http://dx.doi.org/10.1016/j.quaint.2012.11.027

Haibo, L., Xiang, X., Jianchun, L., Jian, Z., Bo, L., & Yaqun, L.. (2011). Rock damage control in bedrock blasting excavation for a nuclear power plant. International Journal of Rock Mechanics and Mining Sciences, 48(2), 210-218. doi: http://dx.doi.org/10.1016/j.ijrmms.2010.11.016

Hansen, M. C., Egorov, A., Potapov, P. V., Stehman, S. V., Tyukavina, A., Turubanova, S. A., . . . Bents, T. (2014). Monitoring conterminous United States (CONUS) land cover change with Web-Enabled Landsat Data (WELD). Remote Sensing of Environment, 140(0), 466-484. doi: http://dx.doi.org/10.1016/j.rse.2013.08.014

Hanson, R. (1991). Evapotranspiration and Droughts. In R.W. Paulson, E.B. Chase, R.S. Roberts & D.W. Moody (Eds.), National Water Summary 1988-89: Hydrologic Events and Floods and Droughts (pp. 99-104): U.S. Geological Survey.

Harp, L., Keefer, K., Sato, P., & Yagi, H. (2011). Landslide inventories: The essential part of seismic landslide hazard analyses. Engineering Geology, 122(1–2), 9-21. doi: http://dx.doi.org/10.1016/j.enggeo.2010.06.013

Hashimoto, M., Enomoto, M., & Fukushima, Y. (2010). Coseismic Deformation from the 2008 Wenchuan, China, Earthquake Derived from ALOS/PALSAR Images. Tectonophysics, 491(1–4), 59-71. doi: http://dx.doi.org/10.1016/j.tecto.2009.08.034

Hayes, M. (2007). Drought indices. Intermountain West Climate Summary, 2-6.

He, S., Pan, P., Dai, L., Wang, H., & Liu, J. (2012). Application of kernel-based Fisher discriminant analysis to map landslide susceptibility in the Qinggan River delta, Three Gorges, China. Geomorphology, 171–172(0), 30-41. doi: http://dx.doi.org/10.1016/j.geomorph.2012.04.024

Hély, C., Flannigan, M.D., Bergeron, Y., & McRae, D.J. (2001). ole of vegetation and weather on fire behavior in the Canadian mixedwood boreal forest using two fire behavior prediction systems. Canadian Journal of forest research, 31, 430–441.

Herrera, G., Gutiérrez, F., García-Davalillo, J. C., Guerrero, J., Notti, D., Galve, J. P., . . . Cooksley, G. (2013). Multi-sensor advanced DInSAR monitoring of very slow landslides: The Tena Valley case

study (Central Spanish Pyrenees). Remote Sensing of Environment, 128(0), 31-43. doi: http://dx.doi.org/10.1016/j.rse.2012.09.020

Hervás, J., & Bobrowsky, P. (2009). Mapping: Inventories, Susceptibility, Hazard and Risk. In Kyoji Sassa & Paolo Canuti (Eds.), Landslides – Disaster Risk Reduction (pp. 321-349): Springer Berlin Heidelberg.

Hooper, A., Zebker, H., Segall, P., & Kampes, B. (2004). New method for measuring deformation on volcanoes and other natural terrains using InSAR persistent scatterers.

Hoque, R., Nakayama, D., Matsuyama, H., & Matsumoto, J. (2011). Flood monitoring, mapping and assessing capabilities using RADARSAT remote sensing, GIS and ground data for Bangladesh. Natural Hazards, 57(2), 525-548. doi: 10.1007/s11069-010-9638-y

Horváth, S., Szép, I. Jankó, M., László, M., János, Pajtók-Tari, I., & Utasi, Z. (2010). Effect of evapotranspiration parameterisation on the Palmer Drought Severity Index. Physics and Chemistry of the Earth, Parts A/B/C, 35(1–2), 11-18. doi: http://dx.doi.org/10.1016/j.pce.2010.03.015

Hu, H., Fernandez-Steeger, T. M., Dong, M., & Azzam, R. (2012). Numerical modeling of LiDAR-based geological model for landslide analysis. Automation in Construction, 24(0), 184-193. doi: http://dx.doi.org/10.1016/j.autcon.2012.03.001

Huang, A.B., Lee, J.T., Ho, Y.T., Chiu, Y.F., & Cheng, S.Y. (2012). Stability monitoring of rainfall-induced deep landslides through pore pressure profile measurements. Soils and Foundations, 52(4), 737-747. doi: http://dx.doi.org/10.1016/j.sandf.2012.07.013

Hungr, O., Evans, S.G., Bovis, M., & Hutchinson, J.N. (2001). Review of the classification of landslides of the flow type. Environmental and Engineering Geoscience, 7(221-238).

Ilanloo, M. (2011). A comparative study of fuzzy logic approach for landslide susceptibility mapping using GIS: An experience of Karaj dam basin in Iran. Procedia - Social and Behavioral Sciences, 19(1), 668-676.

Inbar, M., Tamir, M., & Wittenberg, L. (1998). Runoff and erosion processes after a forest fire in Mount Carmel, a Mediterranean area. Geomorphology, 24(1), 17-33. doi: http://dx.doi.org/10.1016/S0169-555X(97)00098-6

IPCC. (2007). Intergovernmental Pannel on Climate Change; Synthesis Report. In R.K. Pachauri & A. Reisinger (Eds.), Contribution of Working Groups I, II and III to the Fourth Assessment Report of the Intergovernmental Panel on Climate Change (pp. 104). Geneva, Switzerland.

Irigaray, C., FernaÂndez, T. , & ChacoÂn, J. (1996). Comparative analysis of methods for landslide susceptibility mapping. In J. ChacoÂn, C. Irigaray & T. FernaÂndez (Eds.), Landslides (pp. 373-384). Balkema, Rotterdam.

Jaboyedoff, M., Oppikofer, T., Abellán, A., Derron, M.H., Loye, A., Metzger, R., & Pedrazzini, A. (2012). Use of LIDAR in landslide investigations: a review. Natural Hazards, 61(1), 5-28. doi: 10.1007/s11069-010-9634-2

Jakob, M., & Lambert, S. (2009). Climate change effects on landslides along the southwest coast of British Columbia. Geomorphology, 107(3–4), 275-284. doi: http://dx.doi.org/10.1016/j.geomorph.2008.12.009

Jia, N., Mitani, Y., Xie, M., & Djamaluddin, I. (2012). Shallow landslide hazard assessment using a three-dimensional deterministic model in a mountainous area. Computers and Geotechnics, 45, 1-10. doi: http://dx.doi.org/10.1016/j.compgeo.2012.04.007

Jianyaa, G., Haiganga, S. , Guoruia, M., & Qimingb, Z. (2008). A Review of Multi-Temporal Remote Sensing Data Change Detection Algorithms. Paper presented at the ISPRS Congress, Beijing, China.

Jimenez Sanchez, M. , Farias, P., Rodrıguez, A., & Menendez Duarte, R.A. (1999). Landslide development in a coastal valley in northern Spain: conditioning factors and temporal occurrence. Geomorphology, 30, 115–123.

Johnson, EA. (1992). Fire and Vegetation Dynamics: Studies from the North American Boreal Forest. Cambridge: Cambridge University Press.

Julien, Y., Sobrino, J. A., Mattar, C., Ruescas, A.B., Jiménez-Muñoz, J.C., Sòria, G., . . . Cuenca, J. (2011). Temporal analysis of normalized difference vegetation index (NDVI) and land surface temperature (LST) parameters to detect changes in the Iberian land cover between 1981 and 2001. International Journal of Remote Sensing, 32(7), 2057-2068. doi: 10.1080/01431161003762363

Kamp, U., Growley, B. J., Khattak, G.A., & Owen, L.A. (2008). GIS-based landslide susceptibility mapping for the 2005 Kashmir earthquake region. Geomorphology, 101(4), 631-642. doi: http://dx.doi.org/10.1016/j.geomorph.2008.03.003

Kanellou, E.C, Spyropoulos, N.V, & Dalezios, N.R. (2012). Geoinformatic Intelligence Methodologies for Drought Spatiotemporal Variability in Greece. Water Resources Management, 26(5), 1089-1106. doi: 10.1007/s11269-011-9948-1

Kanungo, D. P., Arora, M. K., Gupta, R. P., & Sarkar, S. (2008). Landslide risk assessment using concepts of danger pixels and fuzzy set theory in Darjeeling Himalayas. Landslides, 5(4), 407-416. doi: 10.1007/s10346-008-0134-3

Karsli, F., Atasoy, M., Yalcin, A., Reis, S., Demir, O., & Gokceoglu, C. (2009). Effects of land-use changes on landslides in a landslide-prone area (Ardesen, Rize, NE Turkey). Environmental Monitoring and Assessment, 156(1-4), 241-255. doi: 10.1007/s10661-008-0481-5

Kassouk, Z., Thouret, J.C., Gupta, A., Solikhin, A., & Liew, S.C. Object-oriented classification of a high-spatial resolution SPOT5 image for mapping geology and landforms of active volcanoes: Semeru case study, Indonesia. Geomorphology(0). doi: http://dx.doi.org/10.1016/j.geomorph.2014.04.022

Kawabata, D., & Bandibas, J. (2009). Landslide susceptibility mapping using geological data, a DEM from ASTER images and an Artificial Neural Network (ANN). Geomorphology, 113(1–2), 97-109. doi: http://dx.doi.org/10.1016/j.geomorph.2009.06.006

Kayastha, P., Dhital, M. R., & De Smedt, F. (2013). Application of the analytical hierarchy process (AHP) for landslide susceptibility mapping: A case study from the Tinau watershed, west Nepal. Computers & Geosciences, 52(0), 398-408. doi: http://dx.doi.org/10.1016/j.cageo.2012.11.003

Keefer, D.K. (1994). The importance of earthquake-induced landslides to long-term slope erosion and slope-failure hazards in seismically active regions. In M. Morisawa (Ed.), Geomorphology and Natural Hazards (pp. 265-284). Amsterdam: Elsevier.

Keeley, J.E., Brennan, T., & Pfaff, A.H. (2008). Fire severity and ecosytem responses following crown fires in california shrublands. Ecological Applications, 18(6), 1530-1546. doi: 10.1890/07-0836.1

Kehew, A.E. (1995). Geology for engineers and environmental scientists (Vol. 2). New Jersey: Prentice Hall.

Key, C.H., & Benson, N.C. (2005). Landscape assessment: ground measure of severity, the Composite Burn Index; and remote sensing of severity, the Normalized Burn Ratio. In D.C. Lutes

(Ed.), FIREMON: Fire Effects Monitoring and Inventory System. Rocky Mountains: USDA Forest Service.

Khalili, D., Farnoud, T., Jamshidi, H., Kamgar-Haghighi, A., & Zand-Parsa, S. (2011). Comparability Analyses of the SPI and RDI Meteorological Drought Indices in Different Climatic Zones. Water Resources Management, 25(6), 1737-1757. doi: 10.1007/s11269-010-9772-z

Kharin, V.V., & Zwiers, F.W. (2005). Estimating Extremes in Transient Climate Change Simulations. Journal of Climate, 18(8), 1156-1173. doi: 10.1175/JCLI3320.1

Khawlie, M. (1992). Shaping the eastern Mediterranean coast by earthquakes: Lebanon. Geology Today, 8(2), 58-61.

Kilpeläinen, A., Kellomäki, S., Strandman, H., & Venäläinen, A. (2010). Climate change impacts on forest fire potential in boreal conditions in Finland. Climatic Change, 103(3-4), 383-398. doi: 10.1007/s10584-009-9788-7

Kim, J., Jeong, S., Park, S., & Sharma, J. (2004). Influence of rainfall-induced wetting on the stability of slopes in weathered soils. Engineering Geology, 75(3–4), 251-262. doi: http://dx.doi.org/10.1016/j.enggeo.2004.06.017

Kim, M., Madden, M., & Warner, T. (2008). Estimation of optimal image object size for the segmentation of forest stands with multispectral IKONOS imagery. In Thomas Blaschke, Stefan Lang & GeoffreyJ Hay (Eds.), Object-Based Image Analysis (pp. 291-307): Springer Berlin Heidelberg.

Kjekstad, O., & Highland, L. (2009). Economic and Social Impacts of Landslides. In Kyoji Sassa & Paolo Canuti (Eds.), Landslides – Disaster Risk Reduction (pp. 573-587): Springer Berlin Heidelberg.

Koutsias, N., Mallinis, G., & Karteris, M. (2009). A forward/backward principal component analysis of Landsat-7 ETM+ data to enhance the spectral signal of burnt surfaces. ISPRS Journal of Photogrammetry and Remote Sensing, 64(1), 37-46. doi: http://dx.doi.org/10.1016/j.isprsjprs.2008.06.004

Koutsias, N., Xanthopoulos, G., Founda, D., Xystrakis, F., Nioti, F., Pleniou, M., . . . Arianoutsou, M. (2013). On the relationships between forest fires and weather conditions in Greece from long-term national observations (1894–2010). International Journal of Wildland Fire, 22(4), 493-507. doi: http://dx.doi.org/10.1071/WF12003

Kundu, S. , Sharma, D.C., Saha, A.K., Pant, C.C. , & Mathew, J. (2012). IS-based Statistical Landslide Susceptibility Zonation: A Case Study in Ganeshganga Watershed, The Himalayas. ArcIndia News, 6(1), 26-31.

Kuzu, C., & Ergin, H. (2005). An assessment of environmental impacts of quarry-blasting operation: a case study in Istanbul, Turkey. Environmental Geology, 48(2), 211-217. doi: 10.1007/s00254-005-1291-5

Lal, R. (2001). Soil degradation by erosion. Land Degradation & Development, 12(6), 519-539. doi: 10.1002/ldr.472

Lan, H., Martin, C.D., Zhou, C., & Lim, C.H. (2010). Rockfall hazard analysis using LiDAR and spatial modeling. Geomorphology, 118(1–2), 213-223. doi: http://dx.doi.org/10.1016/j.geomorph.2010.01.002

Langford, M., & Bell, W. (1997). Land cover mapping in a tropical hillsides environment: A case study in the Cauca region of Colombia. International Journal of Remote Sensing, 18(6), 1289-1306. doi: 10.1080/014311697218421

Larsen, J., Montgomery, R., & Korup, O. (2010). Landslide erosion controlled by hillslope material. Nature Geoscience, 3(4), 247- 251.

Larsen, J., Pederson, L., & Schmidt, C. (2006). Geologic versus wildfire controls on hillslope processes and debris flow initiation in the Green River canyons of Dinosaur National Monument. Geomorphology, 81(1–2), 114-127. doi: http://dx.doi.org/10.1016/j.geomorph.2006.04.002

Lee, S. , Chwaea, U., Min, K. (2002). Landslide susceptibility mapping by correlation between topography and geological structure: the Janghung area, Korea. Geomorphology, 149–162.

Lee, S. (2004). Application of likelihood ratio and logistic regression models to landslide susceptibility mapping using GIS. Environmental Management, 34(2), 223-232.

Lee, S. (2007). Application and verification of fuzzy algebraic operators to landslide susceptibility mapping. Environmental Geology, 52(4), 615-623.

Lee, S., & Pradhan, B. (2007). Landslide hazard mapping at Selangor, Malaysia using frequency ratio and logistic regression models. Landslides, 4(1), 33-41. doi: 10.1007/s10346-006-0047-y

Lee, Y.F., & Chi, Y.Y. (2011). Rainfall-induced landslide risk at Lushan, Taiwan. Engineering Geology, 123(1–2), 113-121. doi: http://dx.doi.org/10.1016/j.enggeo.2011.03.006

Lewis, A., Wu, Q., & Robichaud, R. (2006). Assessing burn severity and comparing soil water repellency, Hayman Fire, Colorado. Hydrological Processes, 20(1), 1-16. doi: 10.1002/hyp.5880

Lewis, S.M., Barfield, B.J. , Storm, D.E. , & Ormsbee, L.E. . (2004). PRORIL-An erosion model using probability distributions for rill flow and density. Trans. ASAE, 37, 115–123.

Lhermitte, S., Verbesselt, J., Jonckheere, I., Nackaerts, K., van Aardt, J.A.N., Verstraeten, W.W., & Coppin, P. (2008). Hierarchical image segmentation based on similarity of NDVI time series. Remote Sensing of Environment, 112(2), 506-521. doi: http://dx.doi.org/10.1016/j.rse.2007.05.018

Li, A., Jiang, J., Bian, J., & Deng, W. (2012). Combining the matter element model with the associated function of probability transformation for multi-source remote sensing data classification in mountainous regions. ISPRS Journal of Photogrammetry and Remote Sensing, 67(0), 80-92. doi: http://dx.doi.org/10.1016/j.isprsjprs.2011.10.008

Littell, J.S., McKenzie, D., Peterson, D.L., & Westerling, A.L. (2009). Climate and wildfire area burned in western U.S. ecoprovinces, 1916–2003. Ecological Applications, 19(4), 1003-1021. doi: 10.1890/07-1183.1

Liu, Y., Goodrick, S., & Heilman, W.. (2014). Wildland fire emissions, carbon, and climate: Wildfire–climate interactions. Forest Ecology and Management, 317(0), 80-96. doi: http://dx.doi.org/10.1016/j.foreco.2013.02.020

Lloret, F., Peñuelas, J., Prieto, P., Llorens, L. , & Estiarte, M. (2009). Plant community changes induced by experimental climate change: seedling and adult species composition. Perspectives in Plant Ecology, Evolution and Systematics, 11, 53-63.

LNCSR-LMoA (Cartographer). (2010). Land cover/use map of Lebanon at a scale of 1:20,000.

Loáiciga, A., Pedreros, D., & Roberts, D. (2001). Wildfire-streamflow interactions in a chaparral watershed. Advances in Environmental Research, 5(3), 295-305. doi: http://dx.doi.org/10.1016/S1093-0191(00)00064-2

López-Vicente, M., Navas, A., & Machín, J. (2008). Identifying erosive periods by using RUSLE factors in mountain fields of the Central Spanish Pyrenees. Hydrol. Earth Syst. Sci., 12(2), 523-535. doi: 10.5194/hess-12-523-2008

Lu, D., Mausel, P., Batistella, M., & Moran, E. (2005). Land-cover binary change detection methods for use in the moist tropical region of the Amazon: a comparative study. International Journal of Remote Sensing, 26(1), 101-114. doi: 10.1080/01431160410001720748

Lu, D., Mausel, P. , Brondízio, E., & Moran, E. (2004). Change detection techniques. International Journal of Remote Sensing, 25, 2365–2401.

Lucà, F., Conforti, M., & Robustelli, G. (2011). Comparison of GIS-based gullying susceptibility mapping using bivariate and multivariate statistics: Northern Calabria, South Italy. Geomorphology, 134(3–4), 297-308. doi: http://dx.doi.org/10.1016/j.geomorph.2011.07.006

Lunetta, S., Knight, F., Ediriwickrema, J., Lyon, J.G., & Worthy, L.D. (2006). Land-cover change detection using multi-temporal MODIS NDVI data. Remote Sensing of Environment, 105(2), 142-154. doi: http://dx.doi.org/10.1016/j.rse.2006.06.018

Mahdavifar, R., Solaymani, S., & Jafari, K. (2006). Landslides triggered by the Avaj, Iran earthquake of June 22, 2002. Engineering Geology, 86(2–3), 166-182. doi: http://dx.doi.org/10.1016/j.enggeo.2006.02.016

Majumdar, T. J., Bhattacharyya, R., & Chatterjee, S. (2007). On the utilization of ENVISAT AATSR data for geological/hydrological applications. Acta Astronautica, 60(10–11), 899-905. doi: http://dx.doi.org/10.1016/j.actaastro.2006.11.006

Malamud, B.D., Turcotte, D.L., Guzzetti, F., & Reichenbach, P. (2004). Landslide inventories and their statistical properties. Earth Surface Processes and Landforms, 29(6), 687–711.

Malkinson, D., & Wittenberg, L. (2011). Post fire induced soil water repellency—Modeling short and long-term processes. Geomorphology, 125(1), 186-192. doi: http://dx.doi.org/10.1016/j.geomorph.2010.09.014

Marcelino, E.V., Formaggio, A.R., & Maeda, E.E. (2009). Landslide inventory using fusion technique in Brazil. International Journal of Applied Earth Observation and Geoinformation, 11, 181–191.

Marshak, S. (2001). Earth: Portrait of a planet New York: Norton & Company Inc.

Martha, R. (2011). Detecting Landslides by Object Oriented Image Analysis. Enschede, Netherlands: ITC.

Martha, R., Kerle, N., Jetten, V., van Westen, C.J., & Kumar, Vinod. (2010). Characterising spectral, spatial and morphometric properties of landslides for semi-automatic detection using object-oriented methods. Geomorphology, 116(1–2), 24-36. doi: http://dx.doi.org/10.1016/j.geomorph.2009.10.004

Martínez-Casasnovas, J. A., & Concepción Ramos, M. (2009). Soil alteration due to erosion, ploughing and levelling of vineyards in north east Spain. Soil Use and Management, 25(2), 183-192. doi: 10.1111/j.1475-2743.2009.00215.x

Martínez-Casasnovas, J. A., Ramos, M. C., & Ribes-Dasi, M. (2002). Soil erosion caused by extreme rainfall events: mapping and quantification in agricultural plots from very detailed digital elevation models. Geoderma, 105(1–2), 125-140. doi: http://dx.doi.org/10.1016/S0016-7061(01)00096-9

Mas, J. F. (1999). Monitoring land-cover changes: A comparison of change detection techniques. International Journal of Remote Sensing, 20(1), 139-152. doi: 10.1080/014311699213659

Mastrandrea, M.D, Tebaldi, C., Snyder, C.W., & Schneider, S.H. (2011). Current and future impacts of extreme events in California. Climatic Change, 109(1), 43-70. doi: 10.1007/s10584-011-0311-6

Matsushita B., Yang W., Chen J., Onda Y., Qiu G. (2007) Sensitivity of the Enhanced Vegetation Index (EVI) and Normalized Difference Vegetation Index (NDVI) to Topographic Effects: A Case Study in High-density Cypress. Forest Sensors 7:2636-2651

Mayor, A. G., Bautista, S., Llovet, J., & Bellot, J. (2007). Post-fire hydrological and erosional responses of a Mediterranean landscpe: Seven years of catchment-scale dynamics. CATENA, 71(1), 68-75. doi: http://dx.doi.org/10.1016/j.catena.2006.10.006

McDonald, H.C., & Grubbs, R.C. (1975). Landsat imagery analysis: an aid for predicting landslide prone areas for highway construction. Paper presented at the NASA Earth resource survey symposium, Huston, Texas.

Meijer, A. D., Heitman, J. L., White, J. G., & Austin, R. E. (2013). Measuring erosion in long-term tillage plots using ground-based lidar. Soil and Tillage Research, 126(0), 1-10. doi: http://dx.doi.org/10.1016/j.still.2012.07.002

Meng, Q., & Meentemeyer, K. (2011). Modeling of multi-strata forest fire severity using Landsat TM Data. International Journal of Applied Earth Observation and Geoinformation, 13(1), 120-126. doi: http://dx.doi.org/10.1016/j.jag.2010.08.002

Meusburger, K., Bänninger, D., & Alewell, C. (2010). Estimating vegetation parameter for soil erosion assessment in an alpine catchment by means of QuickBird imagery. International Journal of Applied Earth Observation and Geoinformation, 12(3), 201-207. doi: http://dx.doi.org/10.1016/j.jag.2010.02.009

Mitri, G. (2010). Lebanon's National Forest Fire Management Strategy-Second Draft. Beirut: AFDC.

MoE. (2011). Lebanon's Second National Communication to the United Nations Framework Convention on

Climate Change. Beirut: UFCCC.

Moeyersons, J., Trefois, Ph, Nahimana, L., Ilunga, L., Vandecasteele, I., Byizigiro, V., & Sadiki, S. (2010). River and landslide dynamics on the western Tanganyika rift border, Uvira, D.R. Congo: diachronic observations and a GIS inventory of traces of extreme geomorphologic activity. Natural Hazards, 53(2), 291-311. doi: 10.1007/s11069-009-9430-z

Mondini, C., Chang, K.T., & Yin, H.Y. (2011). Combining multiple change detection indices for mapping landslides triggered by typhoons. Geomorphology, 134(3–4), 440-451. doi: http://dx.doi.org/10.1016/j.geomorph.2011.07.021

Montgomery, R., & Dietrich, E. (1994). A physically based model for the topographic control on shallow landsliding. Water Resources Research, 30(4), 1153-1171. doi: 10.1029/93WR02979

Moon, V., & Blackstock, H.. (2004). A Methodology for Assessing Landslide Hazard Using Deterministic Stability Models. Natural Hazards, 32(1), 111-134. doi: 10.1023/B:NHAZ.0000026793.49052.87

Morawitz, F., Blewett, M., Cohen, A., & Alberti, M. (2006). Using NDVI to Assess Vegetative Land Cover Change in Central Puget Sound. Environmental Monitoring and Assessment, 114(1-3), 85-106. doi: 10.1007/s10661-006-1679-z

Moreira, F., Catry, X., Rego, F., & Bacao, F. (2010). Size-dependent pattern of wildfire ignitions in Portugal: when do ignitions turn into big fires? Landscape Ecology, 25(9), 1405-1417. doi: 10.1007/s10980-010-9491-0

Moreira, F., Viedma, O., Arianoutsou, M., Curt, T., Koutsias, N., Rigolot, E., . . . Bilgili, E. (2011). Landscape – wildfire interactions in southern Europe: Implications for landscape management.

Journal of Environmental Management, 92(10), 2389-2402. doi: http://dx.doi.org/10.1016/j.jenvman.2011.06.028

Mori, S., & Johnson, A. (2013). Assessing possible shifts in wildfire regimes under a changing climate in mountainous landscapes. Forest Ecology and Management, 310(0), 875-886. doi: http://dx.doi.org/10.1016/j.foreco.2013.09.036

Mugagga, F., Kakembo, V., & Buyinza, M. (2012). Land use changes on the slopes of Mount Elgon and the implications for the occurrence of landslides. CATENA, 90(0), 39-46. doi: http://dx.doi.org/10.1016/j.catena.2011.11.004

Nandi, A., & Shakoor, A. (2010). A GIS-based landslide susceptibility evaluation using bivariate and multivariate statistical analyses. Engineering Geology, 110(1–2), 11-20. doi: http://dx.doi.org/10.1016/j.enggeo.2009.10.001

Navratil, O., Liébault, F., Bellot, H., Travaglini, E., Theule, J., Chambon, G., & Laigle, D. (2013). High-frequency monitoring of debris-flow propagation along the Réal Torrent, Southern French Prealps. Geomorphology, 201(0), 157-171. doi: http://dx.doi.org/10.1016/j.geomorph.2013.06.017

Nearing, M.A., Pruski, F.F., & O'Neal, M.R. (2004). Expected climate change impacts on soil erosion rates: A review. Journal of Soil and Water Conservation, 59(1), 43-50.

Nefeslioglu, H.A., Gokceoglu, C., & Sonmez, H. (2008). An assessment on the use of logistic regression and artificial neural networks with different sampling strategies for the preparation of landslide susceptibility maps. Engineering Geology, 97(3–4), 171-191. doi: http://dx.doi.org/10.1016/j.enggeo.2008.01.004

Nefeslioglu, H.A., San, B.T., Gokceoglu, C., & Duman, T.Y. (2012). An assessment on the use of Terra ASTER L3A data in landslide susceptibility mapping. International Journal of Applied Earth Observation and Geoinformation, 14(1), 40-60. doi: http://dx.doi.org/10.1016/j.jag.2011.08.005

Nemčok, A., Pašek, J., & Rybář, J. (1972). Classification of landslides and other mass movements. Rock mechanics, 4(2), 71-78. doi: 10.1007/BF01239137

Nichol, J., Man Sing, Wong, & Shaker, A. (2009, 20-22 May 2009). Application of high-resolution satellite images to detailed landslide hazard assessment. Paper presented at the Urban Remote Sensing Event, 2009 Joint.

Nichol, J., & Wong, M. S. (2005). Satellite remote sensing for detailed landslide inventories using change detection and image fusion. International Journal of Remote Sensing, 26(9), 1913-1926. doi: 10.1080/01431160512331314047

Nichol, E., Shaker, A., & Wong, M.S. (2006). Application of high-resolution stereo satellite images to detailed landslide hazard assessment. Geomorphology, 76(1–2), 68-75. doi: http://dx.doi.org/10.1016/j.geomorph.2005.10.001

Niemeyer, S. (2008). New Drought Indices. Paper presented at the 1st International Conference on drought Management: Scientific and Technological Innovations, Zaragoza. http://www.iamz.ciheam.org/medroplan/zaragoza2008/Sequia2008/Session3/S.Niemeyer.pdf

NOAA. (2011). Human-caused climate change a major factor in more frequent Mediterranean droughts. Retrieved March, 2014, from http://www.noaanews.noaa.gov/stories2011/20111027_drought.html

Noferini, L., Pieraccini, M., Mecatti, D., Macaluso, G., Atzeni, C., Mantovani, M., Marcato, G., Pasuto, A., Silvano,S., Tagliavini, F. (2007). Using GB-SAR technique to monitor slow moving landslide. Engineering Geology, 95, 88-98.

Nunes, C.S., Vasconcelos, M.J., Pereira, J.M.C., Dasgupta, N., Alldredge, R.J., & Rego, F.C. (2005). Land Cover Type and Fire in Portugal: Do Fires Burn Land Cover Selectively? Landscape Ecology, 20(6), 661-673. doi: 10.1007/s10980-005-0070-8

Owen, L.A., Kamp, U., Khattak, A., Harp, L., Keefer, K., & Bauer, A. (2008). Landslides triggered by the 8 October 2005 Kashmir earthquake. Geomorphology, 94(1–2), 1-9. doi: http://dx.doi.org/10.1016/j.geomorph.2007.04.007

Ozdemir, A., & Altural, T. (2013). A comparative study of frequency ratio, weights of evidence and logistic regression methods for landslide susceptibility mapping: Sultan Mountains, SW Turkey. Journal of Asian Earth Sciences, 64(0), 180-197. doi: http://dx.doi.org/10.1016/j.jseaes.2012.12.014

Özhan, Süleyman, Gökbulak, Ferhat, Serengil, Yusuf, & Özcan, Mehmet. (2010). Evapotranspiration from a Mixed Deciduous Forest Ecosystem. Water Resources Management, 24(10), 2353-2363. doi: 10.1007/s11269-009-9555-6

Oztekin, B., & Topal, T. (2005). GIS-based detachment susceptibility analyses of a cut slope in limestone, Ankara—Turkey. Environmental Geology, 49(1), 124-132. doi: 10.1007/s00254-005-0071-6

Pal, S., Kaynia, M., Bhasin, K., & Paul, D.K. (2012). Earthquake Stability Analysis of Rock Slopes: a Case Study. Rock Mechanics and Rock Engineering, 45(2), 205-215. doi: 10.1007/s00603-011-0145-6

Park, S.E., Bartsch, A., Sabel, D., Wagner, W., Naeimi, V., & Yamaguchi, Y. (2011). Monitoring freeze/thaw cycles using ENVISAT ASAR Global Mode. Remote Sensing of Environment, 115(12), 3457-3467. doi: http://dx.doi.org/10.1016/j.rse.2011.08.009

Parker, R.N., Densmore, A.L., Rosser, N.J., de Michele, M. , Li, Y., Huang, R., . . . Petley, D.N. (2011). Mass wasting triggered by the 2008 Wenchuan earthquake is greater than orogenic growth. Nature Geoscience, 4(7), 449–452.

Parsakhoo, A., Hosseini, S.A., Lotfalian, M., & Jalilvand, H. (2009). Soil loss and displacement by heavy equipment in forest road subgrading projects. International Journal of Sediment Research, 24(2), 227-235. doi: http://dx.doi.org/10.1016/S1001-6279(09)60029-9

Parson, A., Robichaud, Peter R., Lewis, Sarah A., Napper, Carolyn, & Clark, Jess T. (2011). Field guide for mapping post-fire soil burn severity General Technical Report (GTR) (Vol. Gen. Tech. Rep. RMRS-GTR-243, pp. 49). Rocky Mountain Research Station: U.S. Department of Agriculture, Forest Service.

Paula, S., & Ojeda, F. (2006). Resistance of three co-occurring resprouter Erica species to highly frequent disturbance. Plant Ecology, 183(2), 329-336. doi: 10.1007/s11258-005-9043-x

Pausas, JG. (2004). Changes in fire and climate in the eastern Iberian penninsula (Mediterranean Basin). Climatic Change, 63, 337–350.

Pausas, J.G, & Fernández-Muñoz, S. (2012). Fire regime changes in the Western Mediterranean Basin: from fuel-limited to drought-driven fire regime. Climatic Change, 110(1-2), 215-226. doi: 10.1007/s10584-011-0060-6

Pausas, J.G., & Bradstock, A. (2007). Fire persistence traits of plants along a productivity and disturbance gradient in mediterranean shrublands of south-east Australia. Global Ecology and Biogeography, 16(3), 330-340. doi: 10.1111/j.1466-8238.2006.00283.x

Pausas, J. G., Llovet, J., Rodrigo, A., & Vallejo, R. (2008). Are wildfires a disaster in the Mediterranean basin? – A review. International Journal of Wildland Fire, 17(6), 713-723. doi: http://dx.doi.org/10.1071/WF07151

Pechony, O., & Shindell, D. T. (2010). Driving forces of global wildfires over the past millennium and the forthcoming century. Proceedings of the National Academy of Sciences. doi: 10.1073/pnas.1003669107

Pellegrini, B., & Surian, N. (1996). Geomorphological study of the Fadalto landslide, Venetian Prealps, Italy. Geomorphology, 15(3–4), 337-350. doi: http://dx.doi.org/10.1016/0169-555X(95)00079-K

Peruccacci, S., Brunetti, M.T., Luciani, S., Vennari, C., & Guzzetti, F. (2012). Lithological and seasonal control on rainfall thresholds for the possible initiation of landslides in central Italy. Geomorphology, 139–140(0), 79-90. doi: http://dx.doi.org/10.1016/j.geomorph.2011.10.005

Petan, S., Rusjan, S., Vidmar, A., & Mikoš, M.. (2010). The rainfall kinetic energy–intensity relationship for rainfall erosivity estimation in the mediterranean part of Slovenia. Journal of Hydrology, 391(3–4), 314-321. doi: http://dx.doi.org/10.1016/j.jhydrol.2010.07.031

Piacentini, D., Troiani, F., Soldati, M., Notarnicola, C., Savelli, D., Schneiderbauer, S., & Strada, C. (2012). Statistical analysis for assessing shallow-landslide susceptibility in South Tyrol (south-eastern Alps, Italy). Geomorphology, 151–152(0), 196-206. doi: http://dx.doi.org/10.1016/j.geomorph.2012.02.003

Pike, J. (1988). The geometric signature: Quantifying landslide-terrain types from digital elevation models. Mathematical Geology, 20(5), 491-511. doi: 10.1007/BF00890333

Pitman, A. J., Narisma, G. T., & McAneney, J. (2007). The impact of climate change on the risk of forest and grassland fires in Australia. Climatic Change, 84(3-4), 383-401. doi: 10.1007/s10584-007-9243-6

Planton, S., Déqué, M., Douville, H., & Spagnoli, B. (2005). Impact du réchauffement climatique sur le cycle hydrologique. Comptes Rendus Geoscience, 337(1–2), 193-202. doi: http://dx.doi.org/10.1016/j.crte.2004.10.003

Plassard, J. (Cartographer). (1971). Carte pluviométrique du Liban à l'échelle de 1/200 000.

Platt, V. (2014). Wildfire hazard in the home ignition zone: An object-oriented analysis integrating LiDAR and VHR satellite imagery. Applied Geography, 51(0), 108-117. doi: http://dx.doi.org/10.1016/j.apgeog.2014.03.011

Poesen, J., & Hooke, J.M. (1997). Erosion, flooding and channel management in Mediterranean environments of southern Europe. Progress in Physical Geography 21(2), 157–199.

Poiraud, A. (2014). Landslide susceptibility–certainty mapping by a multi-method approach: A case study in the Tertiary basin of Puy-en-Velay (Massif central, France). Geomorphology, 216(0), 208-224. doi: http://dx.doi.org/10.1016/j.geomorph.2014.04.001

Pourghasemi, R., Mohammady, M., & Pradhan, B. (2012). Landslide susceptibility mapping using index of entropy and conditional probability models in GIS: Safarood Basin, Iran. CATENA, 97(0), 71-84. doi: http://dx.doi.org/10.1016/j.catena.2012.05.005

Pradhan, B., & Lee, S. (2010). Landslide susceptibility assessment and factor effect analysis: backpropagation artificial neural networks and their comparison with frequency ratio and bivariate logistic regression modelling. Environmental Modelling & Software, 25(6), 747-759. doi: http://dx.doi.org/10.1016/j.envsoft.2009.10.016

Pradhan, B., Lee, S., & Buchroithner, F. (2010). A GIS-based back-propagation neural network model and its cross-application and validation for landslide susceptibility analyses. Computers, Environment and Urban Systems, 34(3), 216-235. doi: http://dx.doi.org/10.1016/j.compenvurbsys.2009.12.004

Pradhan, B., Singh, R. P., & Buchroithner, M. F. (2006). Estimation of stress and its use in evaluation of landslide prone regions using remote sensing data. Advances in Space Research, 37(4), 698-709. doi: http://dx.doi.org/10.1016/j.asr.2005.03.137

Pulvirenti, L., Pierdicca, N., Chini, M., & Guerriero, L. (2011). An algorithm for operational flood mapping from Synthetic Aperture Radar (SAR) data using fuzzy logic. Nat. Hazards Earth Syst. Sci., 11(2), 529-540. doi: 10.5194/nhess-11-529-2011

Qi, S., Xu, Q., Lan, H., Zhang, B., & Liu, J. (2010). Spatial distribution analysis of landslides triggered by 2008.5.12 Wenchuan Earthquake, China. Engineering Geology, 116(1–2), 95-108. doi: http://dx.doi.org/10.1016/j.enggeo.2010.07.011

Rachman, A., Anderson, S. H., Gantzer, C. J., & Thompson, A. L. (2003). Influence of Long-term Cropping Systems on Soil Physical Properties Related to Soil Erodibility Contribution from the Center for Soil and Agroclimate Research, Indonesia and the Missouri Agricultural Experiment Station. Soil Sci. Soc. Am. J., 67(2), 637-644. doi: 10.2136/sssaj2003.6370

Ramos, M. C., & Martínez-Casasnovas, J. A. (2006). Trends in Precipitation Concentration and Extremes in the Mediterranean Penedès-Anoia Region, Ne Spain. Climatic Change, 74(4), 457-474. doi: 10.1007/s10584-006-3458-9

Rapolla, A., Paoletti, V., & Secomandi, M. (2010). Seismically-induced landslide susceptibility evaluation: Application of a new procedure to the island of Ischia, Campania Region, Southern Italy. Engineering Geology, 114(1–2), 10-25. doi: http://dx.doi.org/10.1016/j.enggeo.2010.03.006

Raucoules, D., de Michele, M., Malet, J. P., & Ulrich, P. (2013). Time-variable 3D ground displacements from high-resolution synthetic aperture radar (SAR). application to La Valette landslide (South French Alps). Remote Sensing of Environment, 139(0), 198-204. doi: http://dx.doi.org/10.1016/j.rse.2013.08.006

Razak, K.A., Straatsma, M.W., van Westen, C.J., Malet, J.-P., & de Jong, S.M. (2011). Air-borne laser scanning of forested landslides characterization: terrain model quality and visualization. Geomorphology, 126, 186–200.

Refice, A., & Capolongo, D. (2002). Probabilistic modeling of uncertainties in earthquake-induced landslide hazard assessment. Computers & Geosciences, 28(6), 735-749. doi: http://dx.doi.org/10.1016/S0098-3004(01)00104-2

Regmi, R., Giardino, R., & Vitek, D. (2010). Modeling susceptibility to landslides using the weight of evidence approach: Western Colorado, USA. Geomorphology, 115(1–2), 172-187. doi: http://dx.doi.org/10.1016/j.geomorph.2009.10.002

Rodríguez, C. E., Bommer, J. J., & Chandler, R. J. (1999). Earthquake-induced landslides: 1980–1997. Soil Dynamics and Earthquake Engineering, 18(5), 325-346. doi: http://dx.doi.org/10.1016/S0267-7261(99)00012-3

Rodríguez-Alleres, M., Varela, M. E., & Benito, E. (2012). Natural severity of water repellency in pine forest soils from NW Spain and influence of wildfire severity on its persistence. Geoderma, 191(0), 125-131. doi: http://dx.doi.org/10.1016/j.geoderma.2012.02.006

Roy, D. P., Boschetti, L., & Trigg, S. N. (2006). Remote sensing of fire severity: assessing the performance of the normalized burn ratio. Geoscience and Remote Sensing Letters, IEEE, 3(1), 112-116. doi: 10.1109/LGRS.2005.858485

Rucci, A., Ferretti, A., Monti Guarnieri, A., & Rocca, F. (2012). Sentinel 1 SAR interferometry applications: The outlook for sub millimeter measurements. Remote Sensing of Environment, 120(0), 156-163. doi: http://dx.doi.org/10.1016/j.rse.2011.09.030

Ruff, M., & Czurda, K. (2008). Landslide susceptibility analysis with a heuristic approach in the Eastern Alps (Vorarlberg, Austria). Geomorphology, 94(3–4), 314-324. doi: http://dx.doi.org/10.1016/j.geomorph.2006.10.032

Ruiz-Leo, A. M., Hernández, E., Queralt, S., & Maqueda, G. (2013). Convective and stratiform precipitation trends in the Spanish Mediterranean coast. Atmospheric Research, 119(0), 46-55. doi: http://dx.doi.org/10.1016/j.atmosres.2011.07.019

Running, SW. (2006). Is global warming causing more larger wildfires? Science, 313, 927–928.

Saba, Bahar, van der M., Mark, & van der Werff, H. (2010). Spatiotemporal landslide detection for the 2005 Kashmir earthquake region. Geomorphology, 124(1–2), 17-25. doi: http://dx.doi.org/10.1016/j.geomorph.2010.07.026

Saboya Jr, F., da Glória A., Maria, & Dias Pinto, W. (2006). Assessment of failure susceptibility of soil slopes using fuzzy logic. Engineering Geology, 86(4), 211-224. doi: http://dx.doi.org/10.1016/j.enggeo.2006.05.001

Saha, K, Gupta, P, Sarkar, I., Arora, K, & Csaplovics, E. (2005). An approach for GIS-based statistical landslide susceptibility zonation—with a case study in the Himalayas. Landslides, 2(1), 61-69. doi: 10.1007/s10346-004-0039-8

Saito, H., Nakayama, D., & Matsuyama, H. (2009). Comparison of landslide susceptibility based on a decision-tree model and actual landslide occurrence: The Akaishi Mountains, Japan. Geomorphology, 109(3–4), 108-121. doi: http://dx.doi.org/10.1016/j.geomorph.2009.02.026

Salis, M., Ager, A, Finney, A, Arca, B., & Spano, D. (2014). Analyzing spatiotemporal changes in wildfire regime and exposure across a Mediterranean fire-prone area. Natural Hazards, 71(3), 1389-1418. doi: 10.1007/s11069-013-0951-0

Salvati, P., Balducci, V., Bianchi, C., Guzzetti, F., & Tonelli, G. (2009). A WebGIS for the dissemination of information on historical landslides and floods in Umbria, Italy. GeoInformatica, 13, 305–322.

San-Miguel-Ayanz, J., Rodrigues, M., Oliveira, S., Pacheco, K., Moreira, F., Duguy, B., & Camia, A. (2012). Land Cover Change and Fire Regime in the European Mediterranean Region. In Francisco Moreira, Margarita Arianoutsou, Piermaria Corona & Jorge De las Heras (Eds.), Post-Fire Management and Restoration of Southern European Forests (Vol. 24, pp. 21-43): Springer Netherlands.

Santangelo, M. , Marchesini, I. , Bucci, F., Cardinali , M. , Rossi, M. , Taylor, F.E. , . . . Guzzetti, F. (2013). A new approach to reduce the mapping error of landslide inventory maps. Paper presented at the EGU General Assembly, Vienna.

Sato, P., Hasegawa, H., Fujiwara, S., Tobita, M., Koarai, M., Une, H., & Iwahashi, J. (2007). Interpretation of landslide distribution triggered by the 2005 Northern Pakistan earthquake using SPOT 5 imagery. Landslides, 4(2), 113-122. doi: 10.1007/s10346-006-0069-5

Sato, H.P., Hasegawa, H., Fujiwara, S., Tobita, M., Koarai,M., Une,H., Iwahashi, J. (2007). Interpretation of landslide distribution triggered by the 2005 Northern Pakistan earthquake using SPOT 5 imagery Landslide, 4, 113-122.

Sato, H. P., & Harp, E. L. (2009). Interpretation of earthquake-induced landslides triggered by the 12 May 2008, M7.9 Wenchuan earthquake in the Beichuan area, Sichuan Province, China using satellite imagery and Google Earth. Landslides, 6(2), 153-159. doi: 10.1007/s10346-009-0147-6

Schicker, R., & Moon, V.. (2012). Comparison of bivariate and multivariate statistical approaches in landslide susceptibility mapping at a regional scale. Geomorphology, 161–162(0), 40-57. doi: http://dx.doi.org/10.1016/j.geomorph.2012.03.036

Schulz, H. (2007). Landslide susceptibility revealed by LIDAR imagery and historical records, Seattle, Washington. Engineering Geology, 89(1–2), 67-87. doi: http://dx.doi.org/10.1016/j.enggeo.2006.09.019

Schumacher, S., Reineking, B., Sibold, J., & Bugmann, H. (2006). Modeling the Impact of Climate and Vegetation on Fire Regimes in Mountain Landscapes. Landscape Ecology, 21(4), 539-554. doi: 10.1007/s10980-005-2165-7

Schuster, R.L. , & Hihland, L.M. (2007). The third Hans Cloos Lecture. Urban landslides: socioeconomic impacts and overview of mitigative strategies. Bulletin of Engineering Geoogy for thel Environemnt, 66, 1–27.

Shakesby, R.A. (2011). Post-wildfire soil erosion in the Mediterranean: Review and future research directions. Earth-Science Reviews, 105, 71-100.

Shakesby, R. A., & Doerr, S. H. (2006). Wildfire as a hydrological and geomorphological agent. Earth-Science Reviews, 74(3–4), 269-307. doi: http://dx.doi.org/10.1016/j.earscirev.2005.10.006

Short, N.M. (1982) The Landsat tutorial workbook: basics of satellite remote sensing. NASA reference publication.1078, vol viii, 553 p. National Aeronautics and Space Administration, Scientific and Technical Information Branch ; For sale by the Supt. of Docs., U.S. Govt. Print. Off., Washington, D.C. : [Springfield, Va.

Shroder, J. F. (2013). 3.2 Ground, Aerial, and Satellite Photography for Geomorphology and Geomorphic Change. In John F. Shroder (Ed.), Treatise on Geomorphology (pp. 25-42). San Diego: Academic Press.

Simonetti, E., Simonetti, D., Preatoni, D. (2014) Phenology-based land cover classification using Landsat 8 time series. European Commission- Joint Research Centre- Institute for Environment and Sustainability, Luxembourg. doi:10.2788/15561

Singh, K. (2010). Bioengineering techniques of slope stabilization and landslide mitigation. Disaster Prevention and Management, 19(3), 384 - 397.

Singh, S. M. (1988). Simulation of solar zenith angle effect on global vegetation index (GVI) data. International Journal of Remote Sensing, 9(2), 237-248. doi: 10.1080/01431168808954848

Singhroy, V., Molch, K. (2004). Characterizing and monitoring rockslides from SAR techniques. Advances in Space Research, 33(3), 290-295. doi: http://dx.doi.org/10.1016/S0273-1177(03)00470-8

Soverel, O., Perrakis, D. B., & Coops, C. (2010). Estimating burn severity from Landsat dNBR and RdNBR indices across western Canada. Remote Sensing of Environment, 114(9), 1896-1909. doi: http://dx.doi.org/10.1016/j.rse.2010.03.013

Sterlacchini, S., Ballabio, C., Blahut, J., Masetti, M., & Sorichetta, A. (2011). Spatial agreement of predicted patterns in landslide susceptibility maps. Geomorphology, 125(1), 51-61. doi: http://dx.doi.org/10.1016/j.geomorph.2010.09.004

Stine, M.B. (2013). Fire as a Geomorphic Agent. In D.R. Butler, Hupp, C.R (Ed.), Treatise on Geomorphology (Vol. 12, pp. 236-251). San Diego, CA: Academic Press.

Strozzi, T., Farina, P., Corsini, A., Ambrosi, C., Thüring, M., Zilger, J., . . . Werner, C. (2005). Survey and monitoring of landslide displacements by means of L-band satellite SAR interferometry. Landslides, 2(3), 193-201. doi: 10.1007/s10346-005-0003-2

Stumpf, A., Malet, J. P., Allemand, P., & Ulrich, P. (2014). Surface reconstruction and landslide displacement measurements with Pléiades satellite images. ISPRS Journal of Photogrammetry and Remote Sensing, 95(0), 1-12. doi: http://dx.doi.org/10.1016/j.isprsjprs.2014.05.008

Tarolli, P., Sofia, G., & Dalla F., Giancarlo. (2012). Geomorphic features extraction from high-resolution topography: landslide crowns and bank erosion. Natural Hazards, 61(1), 65-83. doi: 10.1007/s11069-010-9695-2

Thornes, J. (1995). Global environmental change and regional response: the European Mediterranean. Transaction Institute British Geographers, 20, 357–367.

Thornthwaite, CW. (1948). An Approach toward a Rational Classification of Climate (Vol. 38, pp. 55-94): American Geographical Society.

Tien Bui, D., Pradhan, B., Lofman, O., Revhaug, I., & Dick, B. (2012). Spatial prediction of landslide hazards in Hoa Binh province (Vietnam): A comparative assessment of the efficacy of evidential belief functions and fuzzy logic models. CATENA, 96(0), 28-40. doi: http://dx.doi.org/10.1016/j.catena.2012.04.001

Tittebrand, A., Spank, U., & Bernhofer, C. H. (2009). Comparison of satellite- and ground-based NDVI above different land-use types. Theoretical and Applied Climatology, 98(1-2), 171-186. doi: 10.1007/s00704-009-0103-3

Tolomei, C., Taramelli, A., Moro, M., Saroli, M., Aringoli, D., & Salvi, S. (2013). Analysis of the deep-seated gravitational slope deformations over Mt. Frascare (Central Italy) with geomorphological assessment and DInSAR approaches. Geomorphology, 201(0), 281-292. doi: http://dx.doi.org/10.1016/j.geomorph.2013.07.002

Trabaud, L. (1987). Dynamics after fire of sclerophyllous plant communities in the Mediterranean basin. Ecologia Mediterranea, 13, 25-37.

Trigila, A., Iadanza, C., & Spizzichino, D.. (2010). Quality assessment of the Italian Landslide Inventory using GIS processing. Landslides, 7(4), 455-470. doi: 10.1007/s10346-010-0213-0

Tsakiris, G., Pangalou, D., & Vangelis, H. (2007). Regional Drought Assessment Based on the Reconnaissance Drought Index (RDI). Water Resources Management, 21(5), 821-833. doi: 10.1007/s11269-006-9105-4

Tsakiris, G., & Vangelis, H. (2005). Establishing a drought index incorporating evapotrasnpiration. European Water 9(10), 3-11.

Tsitsoni, T. (1997). Conditions determining natural regeneration after wildfires in the Pinus halepensis (Miller, 1768) forests of Kassandra Peninsula (North Greece). Forest Ecology Management, 92, 199-208.

Turcotte, D.L., Malamud, B.D. , Guzzetti, F. , & Reichenbach, P. (Eds.). (2002). Self-organization, the cascade model and natural hazards (Vol. 99): Preceedings of the National Academy of Science.

Tymstra, C., Flannigan, M. D., Armitage, O. B., & Logan, K. (2007). Impact of climate change on area burned in Alberta's boreal forest. International Journal of Wildland Fire, 16(2), 153-160. doi: http://dx.doi.org/10.1071/WF06084

USGS. (2013). SLC-off Products: Background. http://landsat.usgs.gov/products_slcoffbackground.php

Vahidnia, H., Alesheikh, A., Alimohammadi, A., & Hosseinali, F. (2010). A GIS-based neuro-fuzzy procedure for integrating knowledge and data in landslide susceptibility mapping. Computers & Geosciences, 36(9), 1101-1114. doi: http://dx.doi.org/10.1016/j.cageo.2010.04.004

van Asch, Th W. J., Hendriks, M. R., Hessel, R., & Rappange, F. E. (1996). Hydrological triggering conditions of landslides in varved clays in the French Alps. Engineering Geology, 42(4), 239-251. doi: http://dx.doi.org/10.1016/0013-7952(95)00082-8

van Asselen, S., & Seijmonsbergen, A. C. (2006). Expert-driven semi-automated geomorphological mapping for a mountainous area using a laser DTM. Geomorphology, 78(3–4), 309-320. doi: http://dx.doi.org/10.1016/j.geomorph.2006.01.037

Van Beek, L. P. H., & Van Asch, Th W. J. (2004). Regional Assessment of the Effects of Land-Use Change on Landslide Hazard By Means of Physically Based Modelling. Natural Hazards, 31(1), 289-304. doi: 10.1023/B:NHAZ.0000020267.39691.39

Van Den Eeckhaut, M., & Hervás, J. (2012). State of the art of national landslide databases in Europe and their potential for assessing landslide susceptibility, hazard and risk. Geomorphology, 139–140(0), 545-558. doi: http://dx.doi.org/10.1016/j.geomorph.2011.12.006

van Westen, C.J., Castellanos, E., & Kuriakose, L. (2008). Spatial data for landslide susceptibility, hazard, and vulnerability assessment: An overview. Engineering Geology, 102(3–4), 112-131. doi: http://dx.doi.org/10.1016/j.enggeo.2008.03.010

van Westen, C. J., Rengers, N., & Soeters, R. (2003). Use of Geomorphological Information in Indirect Landslide Susceptibility Assessment. Natural Hazards, 30(3), 399-419. doi: 10.1023/B:NHAZ.0000007097.42735.9e

van Westen, C. J., van Asch, T. W. J., & Soeters, R. (2006). Landslide hazard and risk zonation—why is it still so difficult? Bulletin of Engineering Geology and the Environment, 65(2), 167-184. doi: 10.1007/s10064-005-0023-0

Vangelis, H., Tigkas, D., & Tsakiris, G. (2013). The effect of PET method on Reconnaissance Drought Index (RDI) calculation. Journal of Arid Environments, 88(0), 130-140. doi: http://dx.doi.org/10.1016/j.jaridenv.2012.07.020

Varnes, D.J. (1974). Landslide hazard zonation: a review of principles and practice. Paris: UNESCO Press.

Veraverbeke, S., Lhermitte, S., Verstraeten, W.W., & Goossens, R. (2010). The temporal dimension of differenced Normalized Burn Ratio (dNBR) fire/burn severity studies: the case of the large 2007 Peloponnese wildfires in Greece. Remote Sensing of Environment, 114, 2548-2563.

Verbyla, D., Kasischke, E., Hoy, E. (2008) Seasonal and topographic effects on estimating fire severity from Landsat TM/ETM+ data International Journal of Wildland Fire 17:527–534

Verhoef, W., Menenti, M., & Azzali, S. (1996). Cover A colour composite of NOAA-AVHRR-NDVI based on time series analysis (1981-1992). International Journal of Remote Sensing, 17(2), 231-235. doi: 10.1080/01431169608949001

Vijith, H., Rejith, P. G., & Madhu, G. (2009). Using InfoVal method and GIS techniques for the spatial modelling of landslide susceptibility in the upper catchment of river Meenachil in Kerala. Journal of the Indian Society of Remote Sensing, 37(2), 241-250. doi: 10.1007/s12524-009-0028-4

Vilén, T., & Fernandes, M. (2011). Forest Fires in Mediterranean Countries: CO2 Emissions and Mitigation Possibilities Through Prescribed Burning. Environmental Management, 48(3), 558-567. doi: 10.1007/s00267-011-9681-9

Wainwright, J. (1996). Infiltration, runoff and erosion characteristics of agricultural land in extreme storm events, SE France. Catena, 26, 24–47.

Wang, L.J., Sawada, K., & Moriguchi, S. (2013). Landslide susceptibility analysis with logistic regression model based on FCM sampling strategy. Computers & Geosciences, 57(0), 81-92. doi: http://dx.doi.org/10.1016/j.cageo.2013.04.006

Wastl, C., Schunk, C., Leuchner, M., Pezzatti, G.B., & Menzel, A. (2012). Recent climate change: Long-term trends in meteorological forest fire danger in the Alps. Agricultural and Forest Meteorology, 162–163(0), 1-13. doi: http://dx.doi.org/10.1016/j.agrformet.2012.04.001

Watts, C.F. (2001). Cause versus trigger in rockfalls and rockslides: implications in cases of property damage and personal injury. Retrieved April 6, 2012, from http://gsa.confex.com/gsa/2001SE/finalprogram/abstract_4818.htm

Wegmüller, U., Santoro, M., Werner, C., Strozzi, T., Wiesmann, A., & Lengert, W.. (2009). DEM generation using ERS–ENVISAT interferometry. Journal of Applied Geophysics, 69(1), 51-58. doi: http://dx.doi.org/10.1016/j.jappgeo.2009.04.002

Weirich, F., & Blesius, L.. (2007). Comparison of satellite and air photo based landslide susceptibility maps. Geomorphology, 87(4), 352-364. doi: http://dx.doi.org/10.1016/j.geomorph.2006.10.003

Wen-Yen, C., Chih-Tien, W., Chih-Yuan, C., & Jyun-Ru, K. (2012). Mapping Geo-Hazard by Satellite Radar Interferometry. Proceedings of the IEEE, 100(10), 2835-2850. doi: 10.1109/JPROC.2012.2194629

Westerling, A. L., & Bryant, B. P. (2008). Climate change and wildfire in California. Climatic Change, 87(1), 231-249. doi: 10.1007/s10584-007-9363-z

Westerling, A. L., Hidalgo, H. G., Cayan, D. R., & Swetnam, T. W. (2006). Warming and Earlier Spring Increase Western U.S. Forest Wildfire Activity. Science, 313(5789), 940-943. doi: 10.1126/science.1128834

Whitlock, C., Shafer, L., & Marlon, J.. (2003). The role of climate and vegetation change in shaping past and future fire regimes in the northwestern US and the implications for ecosystem management.

Forest Ecology and Management, 178(1–2), 5-21. doi: http://dx.doi.org/10.1016/S0378-1127(03)00051-3

Wieczorek, G.F. , Mandrone, G., & DeColla, L. (1997). The influence of hill-slope shape on debris-flow initiation. In C.L. Chen (Ed.), Debris-Flow Hazards Mitigation: Mechanics, Prediction, and Assessment (pp. 21-31). New York: American Society of Civil Engineers.

Witten, I. H. , & Frank, E. . (2005). Data Mining—Practical Machine Learning Tools and Techniques (Vol. 2nd edition). Amsterdam, The Netherlands: Elsevier.

Wright, K, Beurs, M, & Henebry, M. (2012). Combined analysis of land cover change and NDVI trends in the Northern Eurasian grain belt. Frontiers of Earth Science, 6(2), 177-187. doi: 10.1007/s11707-012-0327-x

Wu, Y., Chen, L., Cheng, C., Yin, K., & Török, Á. (2014). GIS-based landslide hazard predicting system and its real-time test during a typhoon, Zhejiang Province, Southeast China. Engineering Geology, 175(0), 9-21. doi: http://dx.doi.org/10.1016/j.enggeo.2014.03.005

Xu, C., & Xu, X. (2012). Comment on "Spatial distribution analysis of landslides triggered by 2008.5.12 Wenchuan Earthquake, China" by Shengwen Qi, Qiang Xu, Hengxing Lan, Bing Zhang, Jianyou Liu [Engineering Geology 116 (2010) 95–108]. Engineering Geology, 133–134(0), 40-42. doi: http://dx.doi.org/10.1016/j.enggeo.2012.02.017

Xu, C., Xu, X., Lee, Y.H., Tan, X., Yu, G., & Dai, F. (2012). The 2010 Yushu earthquake triggered landslide hazard mapping using GIS and weight of evidence modeling. Environmental Earth Sciences, 66(6), 1603-1616. doi: 10.1007/s12665-012-1624-0

Yalcin, A., & Bulut, F. (2007). Landslide susceptibility mapping using GIS and digital photogrammetric techniques: a case study from Ardesen (NE-Turkey). Natural Hazards, 41(1), 201-226. doi: 10.1007/s11069-006-9030-0

Yalcin, A., Reis, S., Aydinoglu, A. C., & Yomralioglu, T. (2011). A GIS-based comparative study of frequency ratio, analytical hierarchy process, bivariate statistics and logistics regression methods for landslide susceptibility mapping in Trabzon, NE Turkey. CATENA, 85(3), 274-287. doi: http://dx.doi.org/10.1016/j.catena.2011.01.014

Yang, C., Everitt, H., & Murden, D. (2011). Evaluating high resolution SPOT 5 satellite imagery for crop identification. Computers and Electronics in Agriculture, 75(2), 347-354. doi: http://dx.doi.org/10.1016/j.compag.2010.12.012

Yang, G., Di, X.Y., Guo, Q.Xi, Shu, Z., Zeng, T., Yu, H.Z., & Wang, C. (2011). The impact of climate change on forest fire danger rating in China's boreal forest. Journal of Forestry Research, 22(2), 249-257. doi: 10.1007/s11676-011-0158-8

Yeon, Y.K., Han, J.G., & Ryu, K.H. (2010). Landslide susceptibility mapping in Injae, Korea, using a decision tree. Engineering Geology, 116(3–4), 274-283. doi: http://dx.doi.org/10.1016/j.enggeo.2010.09.009

Yesilnacar, E., & Topal, T. (2005). Landslide susceptibility mapping: A comparison of logistic regression and neural networks methods in a medium scale study, Hendek region (Turkey). Engineering Geology, 79(3–4), 251-266. doi: http://dx.doi.org/10.1016/j.enggeo.2005.02.002

Yilmaz, I. (2010). The effect of the sampling strategies on the landslide susceptibility mapping by conditional probability and artificial neural networks. Environmental Earth Sciences, 60(3), 505-519.

Yin, K.L., & Yan, T.Z. (1988). Statistical prediction models for slope instability of metamorphosed rocks. Paper presented at the Proc 5th International Symposium on Landslides, Lausanne, Switzerland.

Záruba, Q., & Mencl, V. . (1984). Landslides and their control. International Journal of Rock Mechanics and Mining Sciences & Geomechanics Abstracts, 21(4), 151.

Zezere, J.L. (2002). Landslide susceptibility assessment considering landslide typology. A case study in area north of Lisbon (Portugal). Natural Hazards and Earth Natural Hazards and Earth, 2, 73-82.

Zhang, Y.G. , Nearing, M.A. , Zhang, X.C. , Xie, Y. , & Wei, H. (2010). Projected rainfall erosivity changes under climate change from multimodel and multiscenario projections in Northeast China. Journal of Hydrology, 384(1-2), 97-106.

Zhao, C., Lu, Z., Zhang, Q., & de la Fuente, J. (2012). Large-area landslide detection and monitoring with ALOS/PALSAR imagery data over Northern California and Southern Oregon, USA. Remote Sensing of Environment, 124(0), 348-359. doi: http://dx.doi.org/10.1016/j.rse.2012.05.025

Zhu, Xing, Wang, R., Qiao, J., Qin, C.Z., Chen, Y., Liu, J., . . . Zhu, T. (2014). An expert knowledge-based approach to landslide susceptibility mapping using GIS and fuzzy logic. Geomorphology, 214(0), 128-138. doi: http://dx.doi.org/10.1016/j.geomorph.2014.02.003

Zhu, X., Liu, D., & Chen, J. (2012). A new geostatistical approach for filling gaps in Landsat ETM+ SLC-off images. Remote Sensing of Environment, 124(0), 49-60. doi: http://dx.doi.org/10.1016/j.rse.2012.04.019

Zinck, A., López, J., Metternicht, I., Shrestha, P., & Vázquez-Selem, L. (2001). Mapping and modelling mass movements and gullies in mountainous areas using remote sensing and GIS techniques. International Journal of Applied Earth Observation and Geoinformation, 3(1), 43-53. doi: http://dx.doi.org/10.1016/S0303-2434(01)85020-0

Zumbrunnen, T., Bugmann, H., Conedera, M., & Bürgi, M. (2009). Linking Forest Fire Regimes and Climate—A Historical Analysis in a Dry Inner Alpine Valley. Ecosystems, 12(1), 73-86. doi: 10.1007/s10021-008-9207-3

Zumbrunnen, T., Menéndez, P., Bugmann, H., Conedera, M., Gimmi, U., & Bürgi, M. (2012). Human impacts on fire occurrence: a case study of hundred years of forest fires in a dry alpine valley in Switzerland. Regional Environmental Change, 12(4), 935-949. doi: 10.1007/s10113-012-0307-4

ANNEX

Annex 1 Preconditioning and inducing parameters affecting MM Occurrence (3:Restricted to this technique, 2=Mainly from this technique, 1:Supplementary)

Parameter	Description	Relevance	Techniques Used	
			Remote Sensing	Ground Truthing
Topograph	Portrays the elevation and shape of the land	Aspect (control hydraulic conductivity), gradient (mass wasting initiation and hydraulic direction) and slope curvature (flow divergence and convergence affects the amount of sediment loss)	3	NA
Geology	Rock type, structure and texture	The physical properties of slope-forming materials such as fractures fissures and rock strength that are involved in the mass wasting are related to the geology	2	1
Hydrogeology	Porosity, hydraulic conductivity, percolation, infiltration	Impact of the relationship between porosity and premeability on pore pressure	NA	2
Soil	Structural stability	Soil degradation mainly involves destruction of soil structure	NA	2
Land Cover	Change in Land Cover	Land cover change cause large alterations in the hydrological and morphological function of slopes	2	1
Neotectonics	Major or minor subsidence, faulting, jointing and earthquakes	Slope Fragility and Instability	1	1
Rainfall	Rainfall intensity	Precipitation acquires an erosive characteristic represented by an aggressive mechanism that targets soil deterioration and reduction of shear strength between its particles	1	2

Parameter	Description	Relevance	Techniques Used	
			Remote Sensing	Ground Truthing
Flooding	Flow event that exceeds the normal banks of a river or stream	Land instability with respect to mass wasting	1	1
Forest Fire	Combustion of vegetation has important implications for post-fire hydrological response	Loss of biodiversity, MM and desertification	3	1
Manmade excavation, road	Development built on steep slopes ,road construction	Blasting excavation, rock inducing weakness and vulnerability to failure	2	1
Construction, Unplanned urbanism	Removes the forest vegetation	Disturbs forest floor, and damages soil structure	2	1
Climatic Variation	Change in Temperature and Rainfall patterns	Climate parameters affecting groundwater and pore pressure fluctuations	1	2

Annex 2 Optical satellite images used in MM detection and delineation

Satellite Imagery	Image Resolution	Available Spectral Band	Stereo Capabilities	Revisit Time	Achieved Dates	Articles dealing with MM and ancillary data using the corresponding Imagery
LANDSAT (1,2,3,4,5,7) (ETM+)	15 - 90m	RGB (Red, Green, Blue) NIR (Near Infra-Red) MIR (Middle Infra-Red) FIR (Far Infra-Red) PAN (Panchromatic)	NO	16-18 days	1972-present	Singh 1988 Abdallah et al. 2007 Koutsias et al. 2009 Meng & Meentemeyer 2011 Hansen et al. 2014
SPOT (1-2-3-4) SPOT 5 SPOT 6-7	10m-20m 2.5m-5m 1.8m	Red NIR SWIR (Short Wave Infra-Red)	YES	2-3 days	1986-present	Abdallah et al. 2007 Sato et al. 2007 Pradhan and Lee 2010 Yang et al. 2011
IRS	PAN: 5.8m G , R, NIR : 23m (LISS) SWIR: 70m (LISS)	Red, Green NIR SWIR	YES	5 days	1988-present	Lee 2004 Pradhan et al. 2006
ASTER	15m-90m	Red, Green NIR SWIR TIR (Thermal Infra-Red)	YES	4-16 days	1999-Present	Kawabata et al. 2009 Alkevli and Ercanoglu 2011 Nefeslioglu et al. 2012

Satellite Imagery	Image Resolution	Available Spectral Band	Stereo Capabilities	Revisit Time	Achieved Dates	Articles dealing with MM and ancillary data using the corresponding Imagery
Ikonos	1m-4m	RGB IR (Infra-Red) PAN	YES	3-days	2000-present	Asner and Warner 2003 Nichol et al 2006 Moeyersons et al. 2011
QuickBird	Multi-spectral: 2.44m-2.88m Panchromatic: 60cm-70cm	RGB NIR PAN	YES	1-3.5 days	2001	Delacourt et al. 2004 Granica et al. 2007 Meusburger et al. 2010
FORMOSAT-2	PAN: 2m Multi-spectral: 8m	RGB NIR PAN	YES	Daily	2004	Cifuentes et al. 2008 Mondini et al. 2011
WorldView-1 WorldView-2 WorldView-3	0.5m 0.31m	PAN RGB CB (Coastal Band) YB (Yellow Band) NIR2 (Near Infra-Red 2) RE (Red Edge)	YES	1.7-5.9 days	2007 2009 mid-2014	

Satellite Imagery	Image Resolution	Available Spectral Band	Stereo Capabilities	Revisit Time	Achieved Dates	Articles dealing with MM and ancillary data using the corresponding Imagery
GeoEye-1 GeoEye-2	PAN: 0.41m Multispectral: 1.65m 0.34m	RGB PAN NIR	YES	2.1-8.3 days	2008 Launch date expected in 2016	
Pleiades-1 Pleiades-2	PAN: 0.5m Multispectral: 2m	RGB NIR		Daily	2011-Present End of 2012	Stumpfet al. 2014
Sentinel -2	10-60m	Mutli-spectral Instrument with 13 spectral bands in VIR, NIR and SWIR		5 days	2014	

Annex3 Radar satellite images used in MM detection and delineation

Satellite Imagery	Image Resolution	Available Bands	Revisit Interval	Achieved Dates	Articles dealing with MM and ancillary data using the corresponding Imagery
ERS-1/2	25m	C-band	3 days	1991-2000 1995-2011	Wegmüller et al. 2009 Calò et al. 2014 Del Ventisette et al. 2014
RADARSAT -1 RADARSAT -2	8m-100m 3m-100m	C-Band	24 days	1995-Present 2007	Singhroy et al. 2004 Hoque et al. 2011
ASAR/ENVISAT	25m-1000m	C-band	3 days	2002- May 2012	Majumdar et al. 2007 Park et al. 2011
PALSAR/ALOS	7-100m	L -band	46 days	2006-2011	Abdallah et al. 2010 Hashimoto et al. 2010 Zhao et al. 2012
PALASAR-2/ALOS	1-3m	L-band	14 days	2013	
CosmoSkyMed (1,2,3,4)	1-100m	X-band	4 days	2007	Ciappa et al. 2010 Pulvirenti et al. 2011 Bovenga et al. 2012

Satellite Imagery	**Image Resolution**	**Available Bands**	**Revisit Interval**	**Achieved Dates**	**Articles dealing with MM and ancillary data using the corresponding Imagery**
TerraSAR-X	1m-16m	X-band	11 days	2007	Breidenbach et al. 2010 Aubert et al. 2011 Baghdadi et al. 2012
TanDEM-X TanDEM-L	1m-16m 3m-10m	X-band L-band	11 days 7 days	2010 2019	
Sentinel-1	5m-40m	C-band	3-6 days Europe 6-12 days Globe	1A-2nd quarter of 2013 1B-1st quarter of 2015	

Annex 4 Mass Movement susceptibility assessment methods

Mass Movement Susceptibility Assessment Method	Pros	Cons	Formula	Terms Defined	References
Qualitative					
Distribution Analysis	-Depicts direct location of MM -Simple and objective -Shows distribution & magnitude of recent MM by the number and size of MM	-Provide no information on MM -potential of areas	Descriptive/GIS		Abdallah et al. 2007 Qi et al. 2010 Xu and Xu 2012
Heuristic Approach	-Appropriate for small scale regional surveys -Suits investigation phases	-Relies heavily on the professional experience of the expert - Subjectivity in attributing weighted value to each parameter	Descriptive/GIS		Aleotti and Chowdhury 1999 Ruff and Czurda, 2008

Mass Movement Susceptibility Assessment Method	Pros	Cons	Formula	Terms Defined	References
Quantitative					
Factor Overlay	- Highlights the degree of spatial coincidence between MM occurrence and specific factors - Particularly suited to raster GIS where factors are mapped either as discrete or continuous data - Computer processing and manipulation is fast & algorithmically simple	- Grid-cell limits do not bear any relation to the geological, geomorphological or other environmental boundaries	GIS application		Carrara et al. 1999 Guzzetti et al. 1999
Bivariate Statistical Techniques					
Information Value Method (Info Val)	- Consider each individual thematic map in terms of MM distribution - High predictive power	- Assumes that MMs will happen under influence of the same combination of factors	$W_i = \ln \frac{(Densclass)}{(Densmap)}$ $N_{pix(Si)} / N_{pix(Ni)}$ $\ln \frac{\sum_{i=1}^{n} N_{pix(Si)} / \sum_{i=1}^{n} N_{pix(Ni)}}{}$	*Wi:* is the weight given in the ith class of particular thematic layer *Denclass:* is the MM density within the thematic class *Densmap:* is the MM density within the entire thematic layer *Npix(Si):* the number of MM pixel in a certain thematic class *Npix(Ni:)* is the total number of MM pixel in a certain thematic class *n:* is the number of classes in a thematic map	Vivith et al. 2009 Che et al. 2012

Mass Movement Susceptibility Assessment Method	Pros	Cons	Formula	Terms Defined	References
Weight of Evidence	- Assigning weights is objective and almost independent by choices of the observer - Weights are calculated separately for each study area	- Probabilities are very low if the area is distinguished by exceptional events - Necessitates the supposition that input maps are temporarily independent	$W+ = \ln \frac{P\left(\frac{B}{D}\right)}{P\left(\frac{B}{\overline{D}}\right)}$ $W- = \ln \frac{P\left(\frac{\overline{B}}{D}\right)}{P\left(\frac{\overline{B}}{\overline{D}}\right)}$	*P :* is probability of occurrence *B: Controlling factor* *D: training point MM* *W+: level of positive correlation between presence of B and D* *W-: level of negative correlation between presence of B and D*	Dahal et al. 2008 Regmi et al. 2010 Piacentini et al. 2012
Frequency Ratio Method	- Simple through displaying correlation between MM and associated factors - Good Results for rigorous accuracy	- all the factors causing MM are assumed to be included in the database - all the events of instability have been identified and included in the analysis	$LSi = \sum F_i$	F_i: rating of each factor or range	Abdallah et al. 2005 Lee and Pradhan 2007 Regmi et al. 2010 Ozdemir and Altural, 2013
Multivariate Statistical Techniques					
Logistic Regression	- The variables may be either continuous or discrete or any combination of both types - Permits one to type a multivariate regression relationship between a dependent variable and numerous independent variables	- Requires a large dataset to aquire stable predictions - Mixture of continuous and categorical factors may lead to incorrect solution - Requires conversion to ASCII or other formats and another conversion to grid format	$Y = \log it(p)$ $= \ln\left(\frac{p}{1-p}\right)$ $= C_0 + C_1X_1 + C_2X_2$ $+ \cdots + C_nX_n$	*v = the discriminant coeffi cient or weight for that variable* *ce n'est pas v mais vi et pareil pour Xi* *X = respondent's score for that variable* *a = a constant* *i = the number of predictor variables*	Bai et al. 2011 Dong et al. 2011 Wang et al. 2013

Mass Movement Susceptibility Assessment Method	Pros	Cons	Formula	Terms Defined	References
Discriminant Analysis	- Converts a multivariate problem into a univariate contingency-table analysis	- Mixture of continuous and categorical factors may lead to incorrect solution	$D = v_1X_1 + v_2X_2 + v_3X_3 = \cdots v_iX_i + a$	*M:* susceptibility coefficient *X1 ….Xn:* are MM influencing factors *w1 ….Wn:* are weights of these factors	Donget al. 2009 He et al. 2012
Analytical Hierarchy Process	- Multi-objective/ Multi-criteria - Possibility to evaluate quantitative as well as qualitative criteria - Permitting a hierarchical structure of the criteria (provides better focus on specific criteria and sub-criteria when allocating the weights)	- Weighting and rating system developed by collecting questionnaires from expert opinions	$M = w_1X_1 + w_2X_2 + w_3X_3 + \cdots + w_nX_n$	*M:* susceptibility coefficient *X1 ….Xn:* are MM influencing factors *w1 ….Wn:* are weights of these factors	Kayastha et al. 2013 Althuwaynee et al. 2014

Mass Movement Susceptibility Assessment Method	Pros	Cons	Formula	Terms Defined	References
Distribution Free Methods					
Artificial Neural Network	- Ability to derive meaning from complicated or imprecise data - Handle imprecise and fuzzy data they can work with continuous, categorical and binary data	- Requires conversion to ASCII or other formats - Greater computational burden - Proneness to over fitting "Black box" approach where the adjusted weights are used to determine the outputs of each unknown data	$tansign(n) = \frac{e^n - e^{-n}}{e^n + e^{-n}}$	V being the set under study μA is called the membership function μA (x) is called the grad of membership of x w.r.t. A. μA (x) is also called the degree of truth of the proposition that x is an element of A.{x∈V: μA (x)>0} is called the support of A	Chauhan etal. 2010 Conforti et al. 2014
Fuzzy Logic	- Straightforward to understand and implement - Take into account the relationship among factors	- Requires tuning and simulation before operation -Requires a lot of data - Not generalizable and has to be run at every MM event	$\mu A: V \rightarrow [0,1]$	P(Y) the probability that an event Y will occur P(YX) the probability that events Y and X will both occur (Y and X), is equal to P(XY) P(Y|X) the probability that event A will occur if X occurs (Y given X), does not equal P(Y|X) P($\tilde{X}$) the probability that event X will not occur (not X), equals 1 - P(X)	Ilanloo 2011 Tien Bui et al. 2012 Zhu et al., 2014
Decision tree model	-Identify the most decisive variables - Handle data measured on different scales - Nonlinear relationships between parameters do not affect model	- Output attribute must be categorical - Instability where even a small change in input data can at times, cause large changes in the tree	$P(Y) = P(Y\|X)P(X) + P(Y\|\tilde{X})P(\tilde{X})$		Saito et al., 2009 Abdallah, 2010 Yeon et al. 2010

Mass Movement Susceptibility Assessment Method	Pros	Cons	Formula	Terms Defined	References
	performance				
Deterministic Method	Results can can then be used directly in the design of engineering works or in the quantification of risk - Permit quantitative factors of safety to be calculated	- Incompleteness of data may lead to oversimplification - Need of material data difficult to obtain over large areas	Physical laws and equations		Gokceoglu and Aksoy, 1996 Godt et al. 2008 Jia et al. 2012

Survey Date: ----/---/2012 Site Name:---------- Plot Size:----------

GPS readings: ---------- N Land Ownership Type:---------- Photo Number:----------
---------- E

Ground Cover:

☐ Bare Soil ☐ Sand ☐ Rocks (Cobbles & Boulders) ☐ Wood

☐ Litter ☐ Bedrock ☐ Other----------

Land Form:

☐ Alluvial Terrace ☐ Cliff ☐ Hills ☐ Mountain Valley ☐ Plain ☐ Plateau

Natural and Anthropogenic Disturbance:

☐ Logging ☐ Grazing ☐ Dumping ☐ Roads ☐ Vehicular Disturbance ☐ Agriculture

☐ Industrial Activity ☐ Urban Expansion ☐ Other Land Use ----------

Qualitative Assessment:

Structure

☐ Forest (Closed Tree Canopy) ☐ Wood (Closed Tree Canopy) ☐ Shrubland

☐ Herbaceous (<25% wooded Areas) ☐ Sparse Vegetation (<25% wooded Areas)

Forest Fire

Fire Severity

☐ Unburned (0.0)

☐ Scorched (1.0)

☐ Lightly Burned (1.5)

☐ Moderately Burned (2.0)

☐ Heavily Burned (3.0)

Mass Movement

MM Type

☐ Slide ☐ Topples

☐ Rills (1) ☐ Talus

☐ Gullies (3) ☐ Creep

☐ Rock/ Block Fall ☐ Slump

☐ Stable (0) ☐ Sheet (2)

Char Height

☐ No Effect (0m) ☐ Low Effect (1.8 m)

☐ Moderate (4 m) ☐ High (>7 m)

% Green

☐ No Effect (100%) ☐ Low Effect (80%)

☐ Moderate (30%) ☐ High (None)

% Living Resprout

☐ No Effect (100%) ☐ Low Effect (90%)

☐ Moderate (30%) ☐ High (>1%)

Annex 5 Mass Movement and Forest fire field survey sheet